University of Southampton

Faculty of Engineering and the Environment

The feasibility of using torsional guided wave for corrosion detection in buried steel gas pipes (with a diameter less than 5 cm)

By

Bahareh Zaghari

A dissertation submitted for degree of MSc in Advanced Mechanical Engineering (Mechatronics)

University of Southampton

Faculty of Engineering and the Environment

The feasibility of using torsional guided wave for corrosion detection in buried steel gas pipes (with a diameter less than 5 cm)

Abstract

Corrosion is one of the major issues for a wide range of industries, hence effective, rapid and low cost methods of pipeline inspection are needed. Compared with existing methods, the ultrasonic guided wave method has been found as an attractive alternative for the inspection of pipelines. However, there is a clear need to support different pipe sizes in a long range without excavation. In this project, small pipes (with a diameter less than 5 cm) are considered due to a request by Scotia Gas Network Ltd. The aim of the work presented here is to investigate the feasibility of torsional guided waves for inspecting buried pipes with a small diameter. In order to understand wave propagation, the wave displacement on plates and pipes (described theoretically) is used to generate MATLAB scripts. These scripts find the phase and group velocity dispersion curves for plates and pipes of varying size and thickness. The pipe is considered to be lossless, and the effect of attenuation was ignored in the calculations for this project. Upon finding the theoretical guided wave characteristics, real world analyses were conducted to see if the aim could be achieved in an experimental scenario. Experimental questions addressed in this report include: “How can the transducers be clamped to the plate and to the pipe?”; “What is the best propagation frequency?”; and “How can the wave velocities and appropriate transducer positions be found?”. Once these were answered, work on pipes with artificial defects could begin. A steel pipe with a diameter of 3.4 cm and wall thickness of 0.55 cm with three different defect sizes was examined. A defect with 8.3% Cross Section Area (CSA) was found by generating a torsional mode T(0,1) at 50 kHz on the pipe. Smaller defects were not found due to high reverberation levels in high frequency propagation. This was due to having only a limited number of transducers. Further work using more transducers and an experimental setup with a buried pipe (to include attenuation) is recommended.

Acknowledgments

I would like to express my deep and sincere gratitude to my supervisors, Professor Victor Humphrey and Doctor Mohamed Moshrefi-Torbati at the Institute of Sound and Vibration Research (ISVR) at the University of Southampton. Professor Victor Humphrey, with his wide knowledge and logical way of thinking have been of great value to me. I also thank Doctor Mohammad Torbati for his constructive comments, and for his important support throughout this work. I also wish to thank Scotia Gas Networks (SGN) for their support.

I owe my loving thanks to my family who, many times forgot themselves in order to support me throughout my life. I wish to thank my Dad especially for his deep understanding and warm hugs.

My most special thanks go to my best friend, Mark Vousden, who gave me his unconditional support and love through all this long process.

Lastly, I would like to thank the staff at the University of Southampton and my classmates who always were beside me in hard situations.

Contents

Section		Page
1	**Introduction**	**15**
1.1	Motivation and methodology	15
1.2	Project aims	16
1.3	Brief outline of content order of thesis.....	17
2	**Technologies investigated**	**18**
2.1	Traditional Methods: Eddy-Current, Electromagnetic, Saturated low frequency eddy current, Radiography, Ultrasonic.....	18
2.2	Current Methods: Electrochemical, Ultrasonic guided waves, Specialised tools and devices.....	20
2.2.1	Electrochemical.....	20
2.2.2	Ultrasonic Guided Waves.....	23
2.2.3	Specialised tools and devices.....	24
2.3	Conclusion.....	25
3	**Guided waves pipeline inspection**	**28**
3.1	Background	28
3.2	Equation of motion in isotropic media	29
3.3	Guided waves in plates.....	30
3.4	Guided waves in hollow cylinder	34
3.4.1	Background	34
3.4.2	Wave propagation in hollow cylinder	35
3.4.3	Axially symmetric and non-axially symmetric.....	39
3.4.4	Labelling	39
3.4.5	Dispersion.....	40
3.4.6	Group and Phase velocity.....	41
3.4.7	Phase and group velocity dispersion curve implementation in MATLAB.....	42

3.4.7.1 Torsional mode dispersion curves..... 42
3.4.7.2 Longitudinal phase and group velocity dispersion curves..... 46
3.4.7.3 Flexural phase and group velocity dispersion curves..... 47
3.4.7.4 Root finding methods..... 48
3.4.8 Cut-off frequency relation with wall thick and pipe size..... 50
3.4.9 Number of transducers..... 52
4 Torsional mode properties 56
4.1 Background..... 56
4.2 Torsional modes advantages..... 57
4.3 Mode conversion and reflection..... 57
5 Experimental 59
5.1 Guided wave instruments..... 59
5.2 Experimental setup..... 60
5.3 Coupling error for dry pressure coupling..... 63
5.4 Frequency tuning on plate..... 65
5.5 Frequency tuning on pipe..... 67
5.6 Wave velocity measurement..... 73
5.6.1 Shear Horizontal (SH) and longitudinal wave velocity measurements on plates..... 73
5.6.2 Torsional wave velocity measurements on pipes..... 77
5.7 Transmitter and receiver position..... 78
5.8 Defect finding..... 81
5.8.1 Average response measurement by rotating the receiver..... 83
5.9 Reverberation analysis..... 85
5.10 Defect reflection characteristics..... 87
5.11 Experimental conclusion..... 89
6 Conclusion 91
6.1 Main finding of this dissertation..... 91

6.2 Future work………………………………………………………………..…………..……........... 91

7 References 93

8 Appendices 99

Appendix A: Matrix elements 99

Appendix B: MATLAB Scripts 102

Appendix C: MATLAB Scripts 104

Appendix D: MATLAB Scripts 113

Appendix E: Equipment specifications 120

Appendix F: MATLAB Scripts 121

List of Symbols

Symbols	Meaning
a	Pipe internal radius
B	Stern-Geary constant and Tafel coefficient
c	Wave velocity
d	Height of plate
h	Pipe thickness
H	Equivoluminal vector potential
I_{corr}	Corrosion current density
I_n	Complex Bessel function
J_n	Real Bessel function
k	Wave vectors, wavenumber
K_n	Complex Bessel function
m	Counter variable
n	Circumferential order
r	Pipe radial direction
R_n	Noise resistance
t	Time
u	Three-dimensional displacement vector
U	Three-dimensional displacement basis vectors
x	Three-dimensional co-ordinate basis vectors
Y_n	Real Bessel function
z	Propagation direction vector
θ	*Angle position*
λ	Lame's constant
μ	Lame's constant
ρ	Material density
σ_{i_n}	Standard deviation of electrochemical current noise
σ_{v_n}	Standard deviation of potential noise
Φ	Compressional scalar potential
ω	Circular frequency
Subscripts	**Meaning**
0	Initial conditions
ext	External
g	Group
in	Internal
l	Longitudinal
s	Shear
p	Phase
Superscripts	**Meaning**
s	Denotes a symmetric mode
a	Denotes asymmetric mode

List of abbreviation

CSA	Cross Section Area
GPIB	General Purpose Interface Bus
EFM	Electrochemical Frequency Modulation
EFM_s	Electrical Field Mapping
EIS	Electrochemical Impedance Spectroscopy
ENM	Electrochemical Noise Measurement
EMAT	Electromagnetic Acoustic Transducers
FSM	Electrical Field Signature
LPR	Linear Polarisation Resistance
MFL	Magnetic Flux Leakage
MsS	Magnetostrictive Sensor
NDT	Nondestructive Test
OCP	Open-Circuit Potential
PIG	Pipeline Inspection Gauge
SH	Shear Horizontal
SLFEC	Saturated Low Frequency Eddy Current

List of Figures

2.1 Radial and axial coordinate of pipe domain (Lynch, 2009)..... 18

2.2 Hall effect sensor measuring magnetic flux leakage from pipe defect (Lynch, 2009)..... 19

2.3 Signal response to defects, (SLOFEC™) (Advanced inspection solution, 1999)..... 19

3.1 Shear Horizontal wave mode propagation. Particle displacement occurs along the X3 direction and the wave propagation is along the X1 direction..... 31

3.2 Phase velocity of Shear Horizontal (SH) mode in a 2mm thick mild steel plate. The solid curves (even n) represent symmetric modes and the dashed curves (odd n) represent asymmetric modes. This graph is compared with the similar configuration phase velocity curves were written by Rose (pp 245, 1999)..... 33

3.3 Group velocity of Shear Horizontal (SH) mode in a 2mm thick mild steel plate. The solid curves (even n) represent symmetric modes and the dashed curves (odd n) represent asymmetric modes. This graph is compared with the similar configuration phase velocity curves were written by Rose (pp 245, 1999)..... 34

3.4 Schematic of pipe geometry, z is along the pipe, r is radial direction, θ is angle position, a is the internal radius and h is the wall thick..... 36

3.5 Mode shapes of torsional T(0,1) and flexural F(1,2)..... 40

3.6 Phase velocity plot for torsional modes, T(0,m), of a stainless steel tube (Outer diameter 1.905 cm, wall thick 0.165 cm; $c_l = 5800\mathrm{ms}^{-1}, c_s = 3100\mathrm{ms}^{-1}$). This graph is compared with the same torsional modes dispersion curve written by Rose (pp 162, 1999)..... 44

3.7 Group velocity plot for torsional modes, T(0,m), of a steel pipe (Outer diameter 6 cm, wall thick 0.35 cm; $c_l = 6290 ms^{-1}, c_s = 3260 ms^{-1}$. This graph is compared with the same torsional modes dispersion curve written by Zenghua Liu et al. (2006)…… 45

3.8 Phase velocity dispersion for longitudinal modes L(0,m), of a schedule 40 (Outer diameter 7 cm, wall thick 0.55 cm. This graph is compared with the same torsional modes dispersion curve written by Demma (2003)…… 47

3.9 Phase velocity of 5mm wall thick, with 3.4 cm external diameter steel pipe in vacuum ($c_l = 6290 ms^{-1}, c_s = 3309 ms^{-1}$)…… 48

3.10 Cut-off frequency of T(0,m)modes results are shown for a steel pipe for m=2 to m=4, against pipe wall thick for the pipe with an inner radius of 50 mm(Outer diameter 6 cm, wall thick 0.35 cm; $c_l = 6290 ms^{-1}, c_s = 3260 ms^{-1}$)..... 50

3.11 Cut-off frequency of T(0,m)modes results are shown for a steel pipe for m=2 to m=4, against pipe thickness for constant mean radius, (Outer diameter 6 cm, wall thick 0.35 cm; $c_l = 6290 ms^{-1}, c_s = 3260 ms^{-1}$..... 51

3.12 Cut-off frequency of T(0,m) modes results are shown for a steel pipe for m=2 to m=4, against scale factor (Outer Radii/Inner Radii= 1.1), (Outer diameter 6 cm, wall thick 0.35 cm; $c_l = 6290 ms^{-1}, c_s = 3260 ms^{-1}$..... 52
.

3.13 Strain gauge incorporated into dry-coupled transducer (Alleyne, 1996)..... 53

3.14 The transducer produced by Guided Ultrasonics Ltd (Guided ultrasonic ltd., 2012)..... 53

3.15 The predicted group velocity dispersion curves for 7.5 cm steel pipes over the frequency range 0 -100 kHz (Alleyne, 1996)..... 54

5.1 Piezoelectric transducers with 1.4 cm long, 1.2 cm width and 1 cm height. Piezoelectric motion is along the length direction and active surface is a white part with 1.3 cm long, 0.3 cm width and 0.1 cm thickness..... 60

5.2 Two modules with 6 places for transducers when two transducers are already placed. When modules are placed on a pipe, transducers motion is in shear format..... 61

5.3 Experimental setup of two modules on plate..... 62

5.4 Experimental setup of two modules on pipe. The distances shows the transmitter and receiver transducers are 100 mm a part and each transducer is 170 mm and 2640 mm far from the end of the pipe..... 62

5.5 Amplitude receiver output vs. clamping load in dry-coupled case. The transmitting transducer was driven with a tune burst of two cycles of a 200 kHz a voltage of 18 Vp–p applied across the transducer. The receiver is placed 200 mm away from the transmitter..... 63

5.6 This test was undertaken with a load of 13.5N for eleven repetitions. The amplitude output of first arrival shown in each tests. The transmitting transducer was driven with a tune burst of two cycles of a 200 kHz a voltage of 18 Vp–p applied across the transducer. The receiver is placed 200 mm away from the transmitter..... 64

5.7 The left picture shows modules on plate (200 mm far apart) with weights on it for coupling and the right picture shows modules (100 mm far apart) on pipe which coupled with cable tie..... 65

5.8 5 cm Mini-Test collar assembly for Plant Integrity Ltd (Plant integrity ltd.,2012)..... 65

5.9 Experimental setup of two transducers and two modules on plate. 45N load was applied on each module due to the clamping force..... 66

5.10 Variation of direct arrival amplitude with frequency with two different clamping load 45N and 13.5N..... 66

5.11 Dispersion curves for SH (Shear-horizontal) mode for n=0 to n=7 in Frequency× $\mathrm{Thickness}$ (Shear velocity: 3250 ms^{-1})..... 67

5.12 Schematic diagram shows five wave propagation path in the pipe for direct and pipe-end echoes. First transmission is from direct arrival between receiver and transmitter and the second one is the pipe-end echo from the left side. The third and fourth echoes come from the right pipe-end and the fifth echo is from the left pipe-end..... 68

5.13 Echoes amplitude for different frequencies. The tests were done on a 3.4 cm diameter steel pipe with 5mm wall thick, with one transmitter and one receiver, 100 mm apart, with the transmitter placed 170mm away from one end of the pipe, and both were placed on the left side of the pipe. Direct arrival is the first wave and then the pipe end echoes are appeared and between the first end echo and second end echo in frequency higher than 50 kHz the reverberation appeared. The tests were done on a clean pipe without any defects..... 69

5.14 Group velocity dispersion curves for steel pipe (Outer diameter: 34 mm and 5mm wall thickness)(Source: PCDISP MATLAB scripts written by Seco and Jimenez (2012))..... 70

5.15 Received signal for the zero-degree configuration at 50 kHz..... 72

5.16 Average received signal around the circumference of the pipe, obtaining by averaging signals when receiver attached at 16 different positions (each 22.5° apart) at 50 kHz..... 73

5.17 Shear horizontal propagation and the piezoelectric receiver and transmitter setup. The image on the right shows the position of two modules with the weights above..... 74

5.18 Shear horizontal wave velocity (Distance of transmission / Travel time) results for stainless steel and galvanized mild steel plate. Least squares regression was used to estimate the slope and standard error in the slope..... 75

5.19 Transducer setup for the longitudinal propagation test. The image on the right shows the position of two modules with the weights above..... 76

5.20 Longitudinal wave velocity (Distance of transmission / Travel time) results for stainless steel and galvanized mild steel plate. Least squares regression was used to estimate the slope and standard error in the slope..... 76

5.21 Transducer configuration for the pipe case..... 77

5.22 Experimental setup and piezoelectric position (Modules are hidden bellow weights)..... 78

5.23 Amplitude (dB re 1V) of receiver signal vs. transducer angle. The 'line' represents what was measured and the 'line with points' expresses the theory due to the constrains of plotting points on polar graph in Excel…….. 78

5.24 Two transmitters and two receivers..... 80

5.25 One transmitter and one receiver..... 80

5.26 Transmitters and receivers in the 135° position..... 80

5.27 Transmitter distance within modules is 54 mm..... 80

5.28 Different defects tested on the pipe..... 82

5.29 The average response used to find defect #3 obtained by averaging over 8 circumferential position of the receiver for pipe with defect#3. The defect echo is identified at 1355µs..... 83

5.30 Echo Schematic. One transmitter and receiver are placed on the pipe and the echoes from pipe end and defect as well as the direct arrival between transmitter and receiver is shown. The transmitter and receiver are 70 mm away from each other and the transmitter is 200 mm from the left end of the pipe..... 84

5.31 Average response measured using a single transmitter and rotating the receiver at 50 kHz and 100 kHz for defect #1 and defect #3. Left top: Average response measured using single transmitter and rotating a receiver each 22.5° at 50 kHz for defect#1. Right top: Average response measured using single transmitter and rotating a receiver each 22.5° at 100 kHz for defect#1. Left bottom: Average response measured using single transmitter and rotating a receiver each 45° at 50 kHz for defect#3. Right bottom: Average response measured using single transmitter and rotating a receiver each 45° at 100 kHz for defect#3.(Predicted defect echoes location is shown in a dotted line box)…… 86

5.32 Defect reflections in different angels from defect which received by number of receivers..... 87

5.33 Defect reflection in different angle when focus method is applied..... 88

5.34 Amplitude (V) of defect echo against time for each receiver angle. The central polar graph shows the maximum amplitude (dB re 1V) as a function of the receiver angle..... 89

List of tables

2.1 Comparison of different monitoring devices (Morison and Cherpillod , 2005; Corbin and Willson, 2007). Linear Polarisation Resistance (LPR), Electrochemical Noise Measurement (EN), Ultrasonic, Electrochemical Frequency Modulation (EFM) and Electrical Field Signature (FSM), Magnetic Flux Leakage (MFL), Saturated low frequency eddy current (SLOFEC), Ultrasonic Guided Waves and SMART Layer Technology are compared..... 26

3.1 Bessel function used for different values of the frequency range corresponding values of λ_1, λ_2, α and β in terms of wavenumbers (λ_1 and λ_2 are just weighting coefficient and I_n and K_n are complex J_n and Y_n are real Bessel functions)..... 38

3.2 Material properties used for the steel pipe..... 40

3.3 Number of transducers predicted for 3.4 cm diameter pipe at different frequencies (The shear wave velocity on pipe is assumed $c_s = 3309 \mathrm{ms}^{-1}$ which will show in Section 5)..... 55

5.1 Group wave velocity and time travel of different modes in different frequencies..... 71

5.2 Description of all defects used in the study (All defects circumferential position are equal to 0°)..... 81

5.3 Compare the results from theory and experiments..... 84

5.4 Signal per noise ratio and reverberation level in different frequencies……. 85

Section 1

1 Introduction

1.1 Motivation and methodology

Corrosion is one of the major issues regarding the integrity of assets for a wide range of industries; hence inspections are currently conducted at regular intervals to ensure a sufficient quality of these assets. Obtaining the cost reduction while maintaining a high level of reliability and safety of installations is a major challenge. The concept of predictive maintenance using permanent sensors that monitor the integrity of an installation matches very well with the objective to reduce cost while maintaining a high safety level. In recent years, research has focused on finding effective, rapid, long-range and low cost methods of pipeline inspection. However, there is still a clear need for a sensitive and accurate method which is capable of detecting the location and the size of a small defect. Compared with existing methods such as visual, eddy-current, radiography, ultrasonic, electromagnetic, electrochemical, weight-loss coupons and electrical resistance, the use of ultrasonic guided waves is an attractive method for the inspection of pipelines. Compared to excavation costs for a limited distance (cases such as road crossings where the pipe is underground) associated with conventional ultrasonic inspection (upwards of $50,000), guided wave methods are particularly beneficial since excavation is only required during initial installation and replacement (Lowe and Cawley, 2006). Ultrasonic guided waves are faster than other methods when it comes to scanning a pipe. It is therefore useful to introduce a screening procedure which is fast and accurate to find the areas where there is significant corrosion. One fast screening technique for pipe testing uses classical ultrasonic bulk wave propagation; this is known as the pig method (Demma, 2003). In this method an ultrasonic probe is sent inside the pipe; this collects ultrasonic signals along the pipe length. This method is suitable for pipes with a large length or diameter. Another screening method uses an array of transducers to generate guided waves along the pipe. This method was

developed in the NDT Lab at Imperial College (Demma, 2003) again using pipes with a large length or diameter. Propagating non-dispersive torsional wave modes such as T(0,1) have been found to be- the most suitable to find a variety of defects in large pipes (Liu et al, 2006). However in general, this research has not been applied to smaller pipes; it is important to do this to ensure that an entire pipe network can be protected. In this project, the torsional mode T(0,1) was propagated along a small pipe (with a diameters less than 5 cm) to find axial and circumferential defects.

1.2 Project aims

Currently, guided wave technology seems to be the most successful method; however its main applications have been to relatively long and large diameter pipes (greater than 7.5 cm). The aim of this project is to investigate the suitability of torsional guided waves for inspecting small diameter buried pipes. In this project, number of items would be considered:

- Design a MATLAB simulation for finding group and phase velocity dispersion curves for plates and pipes.
- Investigate the feasibility of using limited number of shear piezoelectric transducers (reduce the costs).
- Clarify the problems of implementation shear piezoelectric transducers to have a sufficient coupling.
- Introduce the barriers to find defects on small diameter pipes.
- Recommend a method of placing transducers on pipe in order to find small defects.

1.3 Brief outline of content order of thesis

This project was started with finding the appropriate method for finding corrosion on small diameter buried steel pipes. Different technologies, traditional and current methods will be described as well as ultrasonic guided waves and special tools and devices in Section 2. This section will conclude with a table that shows the capability of different methods'. It will show that the ultrasonic guided wave method is suitable for this project.

In Section 3, guided waves on plates and pipes will be described theoretically. Different guided wave modes for the pipe case will be introduced. The main findings of this section are the dispersion curves produced by the MATLAB script; the difficulties of this implementation will also be discussed.

In Section 4, the torsional mode T(0,1) will be focused on. It was chosen specifically for this project so it will be compared to the other modes in order to clarify its advantages for this project over its counterparts.

Section 5 will illustrate the experimental work. Different tests will be performed to accurately determine wither or not defects on the pipe will be found. Difficulties and solutions in experimental tests will be discussed in this section.

In Section 6, this thesis will be concluded by summarizing the main findings as well as potential future work.

2 Technologies Investigated

2.1 Traditional Methods: Eddy-Current, Electromagnetic, Saturated low frequency eddy current, Radiography, Ultrasonic

Perhaps the oldest non-destructive testing method is the use of Eddy-Current, which is based on electromagnetic induction (Hamasaki and Ide, 1995). Limitations of this method include the low speed of inspection and the fact that it can only be applied to pipes close to the surface (Lord and Oswald, 1972). The Magnetic Flux Leakage (MFL) approach consists of two methods; the induction coil method, Hall effect method. With low sensor costs and small space requirements, MFL inspection has become a leading inspection technique for the energy pipeline industry, generally used for inspection of pipes of small diameter. Internal and external inspection techniques with MFL are different. The internal MFL is a robot equipped with fixed permanent magnet and Hall effect sensors which moves inside the pipe and collect off-line data. Pipeline Inspection Gauge (PIG) performs measurement operations without impeding the flow of the pipeline fluid hence there is no need to shut down the pipe for test. Magnetic flux density is measured by the Hall effect sensors which show the flux changes in axial and radial direction, Figure 2.1 (Lynch, 2009).

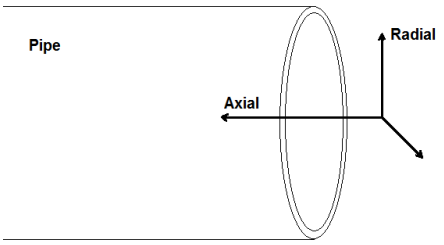

Figure 2.1. *Radial and axial coordinate of pipe domain (Lynch, 2009).*

For external inspection magnetic flux measurements are taken outside of the pipe. The magnetic field is generated through the pipe with an electromagnetic solenoid coil. When defects are present the magnetic flux density signal changes as shown in Figure 2.2. (Lynch 2009).

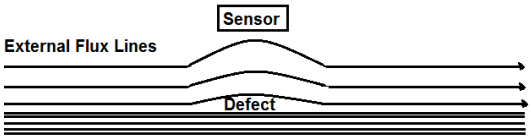

Figure 2.2. *Hall effect sensor measuring magnetic flux leakage from pipe defect (Lynch, 2009).*

MFL has some limitations since it requires magnetic saturation of the pipe wall, hence it is difficult to inspect small diameter and thick wall pipelines. Although as Hall effect sensors are widely used for flux measurement, because of their inherent quality, they are sensitive to temperature, which leads to measurement errors (Zhongli and Hongda, 2011).

Saturated low frequency eddy current (SLOFEC) is an advanced Eddy-Current technique. SLOFEC uses the eddy current principle in combination with a magnetic field using the changes in magnetic field density to show the defects. SLOFEC inspection can find localised gradual defects by the use of Eddy-Current Differential Channel, Figure 2.3.

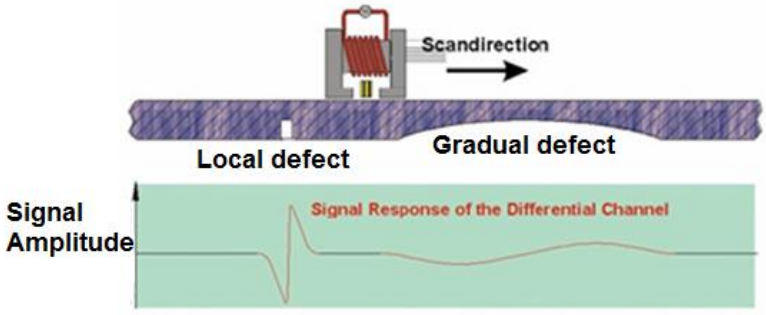

Figure 2.3. *Signal response to defects, (SLOFEC™) (Advanced inspection solution, 1999).*

The SLOFEC technique can differentiate between the defects on the top-side, under-side and through holes and is sensitive to smaller volumetric defects. It typically operates on pipes with diameter ranging from 2.5 cm to 140 cm and has also a capability to generate real-time scan result with coloured defect mapping. Due to its electromagnetic technical background, SLOFEC is often compared to the MFL. An Implementation of this method for underground pipes is hard however, so it is mostly used for pipes with a large diameter.

Radiography is another old NDT technique which permits an “inside view” of the material under test. Corrosion can be detected using either tangential or straight-through methods, both of which can often be used on the same radiograph of a small diameter component such as a small bore connector (Burch and Collett, 2005). Limitations of this method include its high costs, the necessity to cordon areas due to radiation hazards, and large time requirements partly due to its inability to examine large sections of a pipe at a time.

The early methods of non-destructive inspection involved high frequency ultrasonic signals to detect external cracks and defects caused by corrosion. Due to a high level of model complexity, this method is less desirable. Furthermore, ultrasonic inspection only detects surface defects and failures on the outside, and requires removing and replacing a plug of insulation as well as cleaning the surface (Lynch 2009), which is slow and expensive.

2.2 Current Methods: Electrochemical, Ultrasonic Guided Waves, Specialised Tools and Devices

2.2.1 Electrochemical

In the past two decades, monitoring methods using electrochemical potential for detecting the corrosion activity have been widely used in a metal pipeline inspection. Different electrochemical techniques such as Open-Circuit Potential (OCP), Linear

Polarisation Resistance (LPR), Electrochemical Impedance Spectroscopy (EIS) and Electrochemical Noise Measurement (ENM), Electrochemical Frequency Modulation (EFM), Electrical Field Signature (FSM) and Electrical Field Mapping (EFM_s) are used in corrosion detection (Zhang, *et al*., 2010). Of all electrochemical techniques, ENM has the most potential for being used successfully to measure general and localised corrosion rates of gas pipelines. ENM is increasingly being applied to field and industrial installations for *in situ* (without extracting the pipe from underground) corrosion monitoring (Bullard, *et al*., 2003). ENM techniques can differentiate between the general and localised corrosions and provide estimates of corrosion rates without external perturbation of the corroding system (Bullard, *et al*., 2003). It has been used to determine its suitability for monitoring internal and external corrosion damage on gas transmission pipelines. Electrochemical events on the surface of a corroding metal will generate noise (fluctuations) in the potential and current signals. Each type of corrosion is represented by a characteristic signature in the signal noise, which can be used to predict the type and severity of corrosion that is occurring. Noise signature refers to the characteristic patterns in corrosion potential which is able to find localised corrosion. The Noise Resistance

$$R_n = \frac{\sigma_{v_n}}{\sigma_{i_n}}, \tag{2.1}$$

is defined where σ_{v_n} is the standard deviation of potential noise and σ_{i_n} is the standard deviation of electrochemical current noise. σ_{v_n} is used to find general corrosion by means of Faraday's law. From the Stern-Geary approximation the corrosion current density i_{corr} is obtained as

$$i_{corr} = \frac{B}{R_n}, \tag{2.2}$$

where B = Stern-Geary constant and Tafel coefficient which comes from Harmonic Distortion Analysis (Bullard, *et al*., 2003).

More modern developments realise the potential of real-time systems using techniques such as ENM and electrical resistance. This has revolutionised the way the corrosion detection problem is approached, but it has some disadvantages as well:

- The pipe must be shut down to install and retrieve data.
- Outside sources of signal noise may distort data more than in other methods.
- Data is difficult to interpret.
- Methods are expensive to install and operate.
- ENM corrosion rate is sensitive to temperature change, as well as soil constituents.

In EFM, two sinusoidal potential signals are summed and applied to a corrosion sample. The resulting current is measured and the time-domain data is converted to the frequency domain to measure the signal at the applied frequency. The advantages of this method compared to other electrochemical methods are:

- Small potential signal (20mv), meaning that less power is required.
- Ability to measure corrosion without knowing the Tafel coefficient (required for other methods).
- Causality factor used as an internal check to validate the experimental data (Bosch, et al., 2001) (Khaled, 2008).

Electrochemical methods such as Linear Polarisation Resistance monitoring (LPR) and Electrochemical Impedance Spectroscopy (EIS) provide instantaneous measure of general and uniform corrosion rates but can only measure localised corrosion (Tan, 2009). LPR is limited to aqueous solutions, with optimum results being acquired in highly conductive media. A study on the corrosion of the top flow in wet gas environment proves that EIS cannot be used as a reliable corrosion monitoring technique in such an environment because a liquid phase or film may not be present at all times (George, *et al*., 2000). Finally, as corrosion is a nonlinear phenomenon linear

methods like Linear Polarization (LP) and linear EIS are not useful. In FSM, the induced current fed to the section of interest in pipe and the resulting voltage distribution is measured to detect corrosion damage. Both FSM and electrical field mapping can find just internal corrosion and they can inspect large sections of a pipe compared to other electrochemical methods (Napiah and Mukminin, 2009).

2.2.2 Ultrasonic Guided Waves

The use of ultrasonic waves as an attractive method of pipeline inspection is receiving growing interest. By understanding how waves propagate along a pipe (hollow cylinder) two important parameters, velocity and attenuation can be found. In pipes there are three main ultrasonic guided waves in the axial direction: Longitudinal, Torsional and Flexural.

These waves propagate along the pipe axially from the excitation area (transmitter transducer). Reflection of waves occurs from cracks or a weld cap, due to different acoustic impedance and is processed to find crack size and location. If the reflection is received by the same transducer, the system is pulse-echo; otherwise the system is through transmission. Pulse-echo is the preferred method as just one location of it needs to be accessible. In ultrasonic guided wave methods, different transducers have been used such as contact (e.g. piezoelectric), non-contact (e.g. Electromagnetic Acoustic Transducers (EMAT) and Magnetostrictive Sensor (MsS)) (Varma, 2011). These transducers are clamped on the circumference of the pipe with a collar which needs to locate them with an appropriate contact force and direction on the pipe. The inspection range and defect sensitivity depend on operating frequency, attenuation and the choice of guided wave probes. It is not easy to specify guided wave inspection range as it depends on the defect size, attenuation and capability of the guided wave system. Attenuation is related to a number of factors, including geometric features of the pipe, corrosion condition, pipe coating, insulation, and the nature and degree of compaction of surrounding soil. The attenuation also increases with wave frequency and soil depth.

In pipes with fewer functional layers (to provide coating and insulation for instance) the attenuation is lower than in pipes with those features.

The use of ultrasonic guided waves with time reversal techniques has recently been proposed with the intention of developing an active sensing and continuous monitoring system (Yujie Ying, *et al*., 2010). The suitability of this technique has been demonstrated through laboratory experiments with some promising results. However, ultrasonic guided waves are typically used on pipes of relatively large diameters (Volker and Bloom, 2010; Breon, *et al*., 2007; Liu, *et al*., 2011; Cawley, 2001) and the method may require modification in order to make it suitable for small pipe applications.

2.2.3 Specialised tools and devices

BG Transco plc. (Part of the BG Group plc.) have developed a specialised tool to detect and size corrosion in 10 cm cast iron distribution pipes (Burd and Smith, 2000). Utilizing the SMART Layer technology as a basis, a real-time active pipeline integrity detection system (RAPID) is developed for built-in *in situ* assessment of the health of new and existing pipelines. The RAPID system consists of a sensor network permanently mounted on the host pipeline, portable electronic hardware, and diagnostic software (Qing, *et al*., 2009).

The main advantages of the RAPID system include:

- Ease of use.
- Ability to provide a sufficient resolution.
- Reliability (due to self-diagnostic and environmental compensation).
- Quantified corrosion sizing.

To verify the detection capability of the RAPID system, a series of tests have been conducted on a 6.7 metre steel pipe with a diameter of 60 cm and a wall thickness of

6.25 cm with ten different types of corrosion flaws. The SMART Layers™ vary in complexity going from a simple 2-sensor flat strip to a complex 30-sensor 3-D shell (Lin, *et al*, 2005) .

2.3 Conclusion

This brief review confirms the main outcome of similar reviews (Costello, *et al.*, 2007) that there is no single technology which can accurately detect the corroded sites on all buried pipelines. Therefore, the development of multi-sensor tools (hybrid systems) may be required for detecting corrosion. To summarise this section, a comparison of the different monitoring devices that have been discussed is given in Table 2.1. on the following page . Currently, guided wave technology seems to be the most successful method; however its main applications have been to relatively long and large diameter pipes (greater than 7 cm). The suitability of torsional guided waves for small diameter buried pipes and preferably inspecting large size of pipes should be assessed.

Feature	LPR	EN	Ultrasonic	EFM and FSM	MFL	SLOFEC	Ultrasonic Guided Waves	SMART
Detects corrosion	Yes	Yes	No	No	Yes	Yes	Yes	Yes
Intrusive	Yes	Yes	No	No	No	No	No	No
Presence of electrolyte	Yes	Yes	No	No	No	No	No	No
Interference from conductive solids	High	High	No	No	No	No	No	No
Device surface condition dependency	Yes	Yes	No	No	Yes	Yes	No	Yes
Area of coverage	Point	Point	Point /Section	Section	Section	Section	Section	Section
Shut down for insulation	Yes	Yes	No /Yes	No	No	No	No	No
Consumable	Yes	Yes	No	No	No	No	No	No
Metal loss indication	No	No	Direct	Direct	Direct	Direct	Direct	Direct
Trending Capability	Yes	Yes	Yes	Yes	-	-	-	-
Repeatability	-	-	No	Yes	Yes	Yes	Yes	Yes
Resolution	Low	Low	Low	Low	-	-	High	High
Pitting indication	Not easy	Yes	Yes	Yes	Yes	-	Yes	-
Temperature Limitation	Threading +Sealant +Condensation point	Threading +Sealant +Condensation point	Piezoelectric drifts	400C	No	No	Piezoelectric drifts	No
Indication of remaining wall thickness	No	No	Yes	Yes	No	No	Yes	No

Feature	LPR	EN	Ultrasonic	EFM and FSM	MFL	SLOFEC	Ultrasonic Guided Waves	SMART
Indication of surface temperature	No	No	No	No	No	No	No	No
Indication of internal pressure	No	No	No	No	No	No	No	No
Continuous data reporting	Yes	Yes	No	No	Yes	Yes	Yes	Yes
Geometry limitation	Some	Some	None	None	None	None	None	None
Retrieval limitation	Shut down	Shut down	None	None	None	None	None	None
Multi-Phase Corrosion Monitoring	Yes	No	No	No	No	No	Yes	No
Inhibitor Monitoring	No	No	No	Yes	-	-	Yes	-
Can be used in high pressure Environment	Limited	Limited	Limited	Limited	Limited	Limited	Yes	Limited
Cost of equipment	Medium	high	high	high	High	Medium	high	Medium
Labour cost to install	Medium	Medium	high	high	high	Medium	Low	Medium

Table 2.1. *Comparison of different monitoring devices (Morison and* Cherpillod *, 2005; Corbin and Willson, 2007). Linear Polarisation Resistance (LPR), Electrochemical Noise Measurement (EN), Ultrasonic, Electrochemical Frequency Modulation (EFM) and Electrical Field Signature (FSM), Magnetic Flux Leakage (MFL), Saturated low frequency eddy current (SLOFEC), Ultrasonic Guided Waves and SMART Layer Technology are compared.*

Section3

3 Guided wave pipeline inspection

3.1 Background

This chapter introduces the basic concepts of ultrasonic guided wave propagation in hollow cylindrical tubes pipes. The use of ultrasonic waves is an attractive method and has gained interest in the field of pipeline inspection. By understanding how waves propagate along the hollow cylindrical structure two important wave parameters, velocity and attenuation, can be found. Guided waves are propagated from the excitation area along the length of the pipe. The waves are reflected by cracks or weld caps (change in acoustic impedance) and these reflections are sensed, since the crack size and location can be determined by the reflected amplitude. As mentioned in introduction two methods of doing this are pulse-echo (if the reflection is received by the same transducer) and through transmission (if a different transducer receives the reflected signal).

The use of ultrasonic waves is well established in NDT industry, although most of them use bulk waves in the material due to its simplicity. Furthermore, the fact that wave velocity remains constant with frequency during propagation, simple velocity and attenuation measurement are the advantages of using bulk waves. Also, monitoring of the structure is achieved by the use of two transducers as transmitters, or receivers, or one of each.

The propagation of guided waves such as surface waves, lamb waves and interface waves are dependent on the material boundary and material properties. Therefore, the solution for any guided wave must satisfy the equations of motion and physical boundary conditions, such as traction free surfaces of the bounded medium. At a given finite material structure there are an infinite number of solutions to the boundary condition. The standard method of solving this problem for the hollow cylinder, proposed by Gazis (1958), will be considered in this report.

Guided waves are preferred to bulk waves as they are reliable in areas of structures that are hard to access. With regard to wave characteristics, guided waves propagate either at the boundaries of the pipe (like surface waves) or between the boundaries (like lamb waves), though bulk waves travel in the bulk of the material away from boundaries (Demma, 2006). Hence in the bulk wave situation, there is no need to consider boundary conditions. The difficulty of using guided waves lies in the complexity of the solution since they are characterized by infinite number of modes (Demma, 2006). Guided wave modes in pipes, unlike bulk wave modes, have a wave velocity that depends on frequency; this is known as dispersion. In a dispersion curve each mode has a different shape and exists in a different frequency domain. The wave propagation in the pipe is also affected by the characteristics of the fluid inside the pipe, though in this project the pipe was considered to be in a vacuum since the main purpose was to extract a guided wave and find the feasibility of finding different defects regardless of the pipe's contents.

2.2 Equation of motion in isotropic media

Wave propagation in unbounded, isotropic media is well documented in many text book (Rose, 1999) and it is introduced briefly in this chapter. The equation of motion for an isotropic elastic medium without considering body forces

$$(\lambda + \mu)\nabla\nabla \cdot \mathrm{u} + \mu\,\nabla^2\mathrm{u} = \rho\left(\frac{\partial^2 \mathrm{u}}{\partial \mathrm{t}^2}\right), \tag{3.1}$$

is Navier's equation, where u is the three dimensional displacement vector, ρ is the material density, λ and μ are Lame's constants and ∇^2 is the three dimensional Laplace operator. The vector u is expressed by Helmholtz decomposition as the sum of a compressional scalar potential ∅, and equivoluminal vector potential, H according to:

$$\mathrm{u} = \nabla\emptyset + \nabla \times \mathrm{H} \tag{3.2}$$

$$\text{with } \nabla.\,\mathrm{H} = 0. \tag{3.3}$$

Substitution of Equation 3.2 into Navier's equation indicates

$$c_l{}^2\nabla^2\emptyset = \frac{\partial^2\emptyset}{\partial t^2} \text{ and} \tag{3.4}$$

$$c_s{}^2\nabla^2 H = \frac{\partial^2 H}{\partial t^2}; \tag{3.5}$$

the displacement equations of motion are satisfied if the potentials $\emptyset$ and H satisfy the wave equations. Equation 3.4 describes longitudinal waves and equation 3.5 describes shear waves. c_l and c_s are the longitudinal and shear wave velocities in the infinite isotropic medium which presented as

$$c_l = \sqrt{\frac{\lambda + 2\mu}{\rho}} \text{ and} \tag{3.6}$$

$$c_s = \sqrt{\frac{\mu}{\rho}}. \tag{3.7}$$

Longitudinal and shear waves are the only two types of waves that can propagate in an unbounded isotropic medium. Longitudinal and shear waves can propagate without interaction in unbounded media (this can be proved from Equation 3.4 and 3.5.)

For harmonic waves the scalar potential $\emptyset$ and directional component of vector potential H are defined by

$$\emptyset = \emptyset_0 e^{i(k_l \cdot z - \omega t)} \text{ and} \tag{3.8}$$

$$H = H_0 e^{i(k_s \cdot z - \omega t)}, \tag{3.9}$$

where k_l and k_s are the longitudinal and shear wave vectors and $\emptyset_0$ and H_0 are initial constants.

3.3 Guided waves in plates

Longitudinal and transverse modes of wave propagation in a plate were the most commonly used as they were simple to generate and easy to understand (Rose, Page 241). Shear horizontal waves are easily generated with a variety of different transducers and described in this section. In shear horizontal waves particle motion and velocities are parallel to the surface of layer with displacement as shown in Figure 3.1.

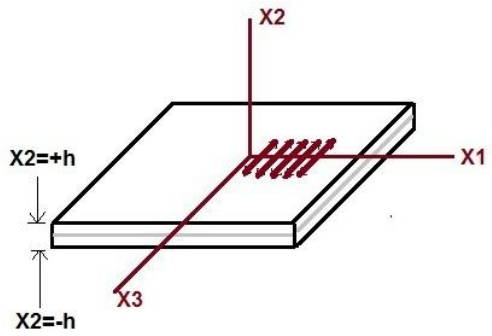

Figure 3.1. *Shear Horizontal wave mode propagation. Particle displacement occurs along the X3 direction and the wave propagation is along the X1 direction.*

From the Navier's displacement equation (Equation 3.1), the shear wave being constructed the three displacement components of $(x_1, x_2, x_{3)}$are

$$U_1(x,t) = 0, \tag{3.9}$$

$$U_2(x,t) = 0 \text{ and} \tag{3.10}$$

$$U_3(x_1, x_2, t) = f(x_2)e^{i(kx_1 - \omega t)} \tag{3.11}$$

where k is the wave number of mode $(\mathrm{k} = \frac{2\pi}{\lambda})$. When the U_3 component of the particle displacement field is nonzero and if $\mathrm{U}_3$is independent of x_3 , the Navier's equation can be written as

$$\frac{\partial^2 U_3}{\partial {x_1}^2} + \frac{\partial^2 U_3}{\partial {x_2}^2} = \frac{\partial^2 U_3}{\partial t^2}\frac{1}{{\mathrm{c_s}}^2} \tag{3.12}$$

where $\mathrm{c_s} = \sqrt{\frac{\mu}{\rho}}$ and from substituting Equation 3.11 into Equation 3.12 gives

$$\frac{\partial^2 f(x_2)}{\partial {x_1}^2} + \left(-\mathrm{k}^2 + \frac{\omega^2}{{\mathrm{c_s}}^2}\right) f(x_2) = 0 \tag{3.13}$$

And the general solution found as $f(x_2) = Asin(qx_2) + Bcos(qx_2)$ (Equation 3.14), where $q = \sqrt{\frac{\omega^2}{{\mathrm{c_s}}^2} - \mathrm{k}^2}$ and ω represents the circular frequency. Finally the displacement field is

$$U_3(x_1, x_2, t) = Asin(qx_2) + Bcos(qx_2)e^{i(kx_1 - \omega t)}\,, \tag{3.15}$$

where sin and cos in Equation 3.15 represent asymmetric and symmetric motions which can be shown as

$$U_3{}^{s}(x_1, x_2, t) = Bcos(qx_2)e^{i(kx_1-\omega t)} \text{and} \tag{3.16}$$

$$U_3{}^{a}(x_1, x_2, t) = Bsin(qx_2)e^{i(kx_1-\omega t)}\,. \tag{3.17}$$

The superscript **s** denotes a symmetric mode and denotes asymmetric mode. The boundary condition is zero shear stress at the plate surface

$$\sigma_{23}(x_1, x_2, t)|_{x_2=\pm h} = 0. \tag{3.18}$$

Applying this boundary condition to the displacement field gives sin(qh) = 0 and cos(qh)=0.

Now sin(x)=0 where x=n$\pi(n \in \{0,1,2, \dots\})$ and cos(x)=0 where x= $\frac{n\pi}{2}(n \in \{0,1,2, \dots\})$; so when $qh = \frac{n\pi}{2}$ where $n \in \{0,2,4, \dots\}$ for symmetric shear horizontal (SH) modes and $n \in \{1,3,5, \dots\}$ for non axially symmetric modes the boundary condition is applied. From $qh = \frac{n\pi}{2}$ and $q = \sqrt{\frac{\omega^2}{\mathrm{C_s}^2} - \mathrm{k}^2}$ the dispersion equation can be written as $\sqrt{\frac{\omega}{\mathrm{C_s}^2} - \mathrm{k}^2} = \frac{n\pi}{2h}$ where $(k = \frac{\omega}{\mathrm{C_p}})$ and finally it represented as

$$\frac{\omega^2}{\mathrm{C_s}^2} - \frac{\omega^2}{\mathrm{c_p}^2} = (\frac{n\pi}{2h})^2, \tag{3.19}$$

The phase velocity $\mathrm{C_p}$in terms of frequency thickness fd is written as

$$\mathrm{c_p(fd)} = \pm 2\mathrm{c_s}\left\{\frac{fd}{\sqrt{4(fd)^2 - n^2\mathrm{c_s}^2}}\right\}, \tag{3.20}$$

where (d=2h) and (ω=2πf) and Group velocity $\mathrm{c_g}$is given

$$\mathrm{c_g(fd)} = \mathrm{c_s}\sqrt{1 - \frac{(\frac{n}{2})^2}{(\frac{fd}{\mathrm{c_s}})^2}}, \tag{3.21}$$

when the phase velocity is infinite the cut-off frequency for each mode, can be calculated from Equation 3.20 as

$$(fd)_n = \frac{nc_s}{2}, \tag{3.22}$$

where even n represents symmetric modes and odd integer n represents asymmetric mode. Figure 3.2 plots the SH mode phase velocity curves for the first eight SH modes in mild steel plate with 2mm thickness and with shear wave velocity $c_s = 3235\text{ms}^{-1}$ and frequency 10 Hz-10 MHz simulated in MATLAB R2011a is given in Appendix B. Figure 3.3 shows SH group velocity for a same plate and in both plots the solid curves (even n) represent symmetric modes and the dashed curves (odd n) represent asymmetric modes. This graph is compared with the similar configuration phase velocity curves were written by Rose (pp 245, 1999).

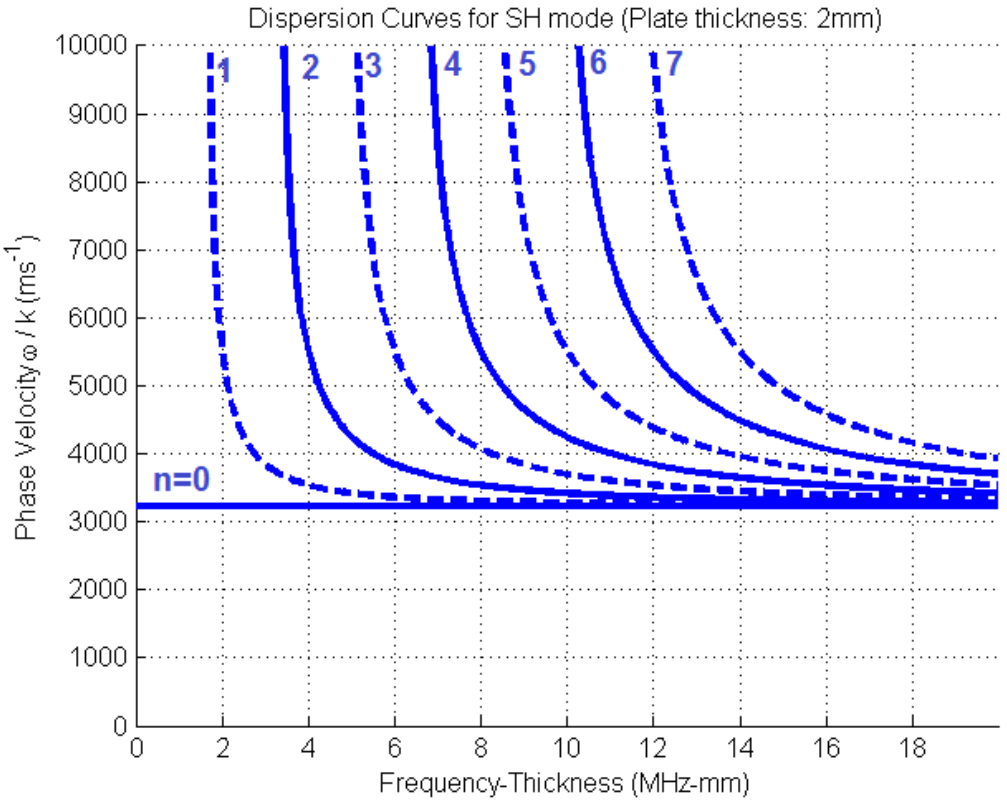

Figure 3.2. *Phase velocity of Shear Horizontal (SH) mode in a 2mm thick mild steel plate. The solid curves (even n) represent symmetric modes and the dashed curves (odd n) represent asymmetric modes. This graph is compared with the similar configuration phase velocity curves were written by Rose (pp 245, 1999).*

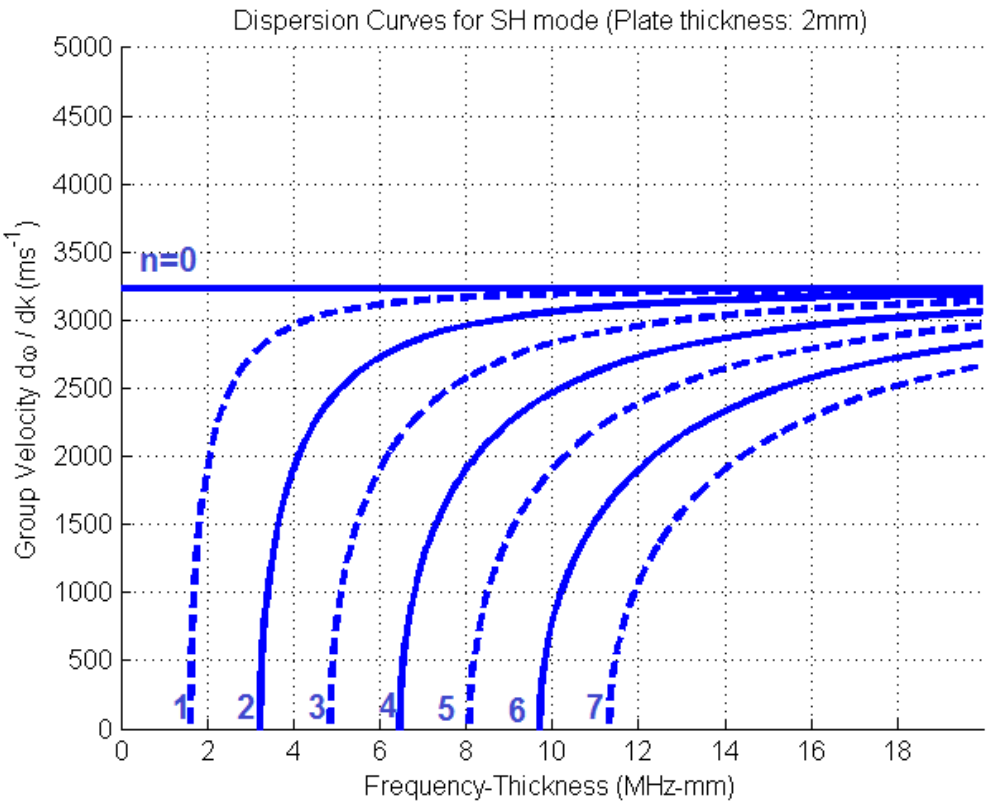

Figure 3.3. *Group velocity of Shear Horizontal (SH) mode in a 2mm thick mild steel plate. The solid curves (even n) represent symmetric modes and the dashed curves (odd n) represent asymmetric modes. This graph is comparable to the similar configuration phase velocity curves were written by Rose (pp 245, 1999).*

3.4 Guided waves in a hollow cylinder

3.4.1 Background

The theoretical treatment of wave propagation in hollow cylinders was started in late nineteenth century. Rayleigh and Lamb studied the elastic wave propagation in traction-free, isotropic plates (Rayleigh, 1945). The first investigation was in a free bar but in the late twentieth century, their work was furthered by Pochamer and Chree

(Demma, 2006). Also, the theoretical treatment of axially symmetric wave propagation in infinitely long hollow circular cylinders has been made by McFadden, Ghosh, and Herrmann and Mirsky (Fitch, 1963). Later work by many researchers such as Pao and Mindlin (1960), Onoe et al and Meeker (1962) and Meitzler (1972) was a way to develop the three-dimensional problems of a solid circular cylinder in a vacuum (Demma, 2006). Gazis (1959) developed an exact elastic solution for harmonic waves in a hollow cylinder of infinite extent. After that Fitch confirmatted the analytical prediction given by Gazis (Fitch, 1963). Many general references for wave propagation theory such as Graff (1991) and Rose (1999) are very useful for understanding wave characteristics.

3.4.2 Wave propagation in a hollow cylinder

The geometry of a cylindrical pipe is shown in Figure 3.4. showing the cylindrical co-ordinate system. For the propagation of waves in a hollow cylinder, the potential Ø and components of vector potential H can be described as

$$\begin{aligned} \emptyset &= f(r)\,\cos n\theta\,\cos(\omega t + kz), \\ H_r &= g_r(r)\,\sin n\theta\,\sin(\omega t + kz), \\ H_\theta &= g_\theta(r)\,\cos n\theta\,\sin(\omega t + kz) \text{ and} \\ H_z &= g_z(r)\,\sin n\theta\,\cos(\omega t + kz). \end{aligned} \tag{3.23}$$

Here k is the component of the wave vector in the axial direction and n is the circumferential order. Substitution of (3.23) into equations (3.8) and (3.9) gives the solution for the $f(r), g_r(r), g_\theta(r)$ and $g_z(r)$ in terms of Bessel functions J and Y and the modified Bessel functions, I and K with arguments of either β or α. β and α can be real or complex given by

$$\beta = \sqrt{\frac{\omega^2}{{c_s}^2} - k^2} \text{and} \tag{3.24}$$

$$\alpha = \sqrt{\frac{\omega^2}{{c_l}^2} - k^2}. \tag{3.25}$$

Also, $\beta_1 r = |\beta r|$, and $\alpha_1 r = |\alpha r|$ (Rose, 1999).

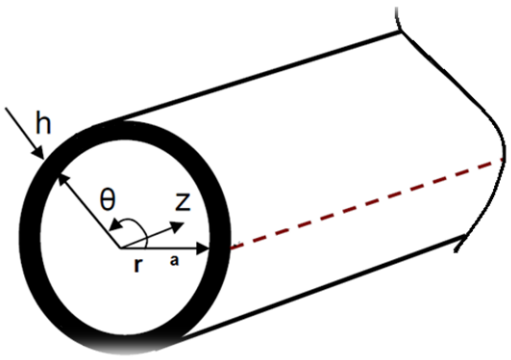

Figure 3.4: *Schematic of pipe geometry, z is along the pipe, r is radial direction, θ is angle position, a is the internal radius and h is the wall thick.*

The assumed particle displacement components in the radial (u_r), circumferential (u_θ), and axial (u_z) directions are (Gazis, 1985)

$$u_r = U_r(r)\cos n\theta \cos(\omega t + kz), \tag{3.26}$$

$$u_\theta = U_\theta(r)\sin n\theta \cos(\omega t + kz) \text{ and} \tag{3.27}$$

$$u_z = U_z(r)\cos n\theta \sin(\omega t + kz), \tag{3.28}$$

where $U_r(r), U_\theta(r)$ and $U_z(r)$ are the corresponding displacement amplitudes composed of Bessel functions or modified Bessel function depending on the wavenumber characteristic. Differentiation with respect to r yields the strain-displacement in cylindrical coordinates:

$$\varepsilon_{rr} = \frac{\partial u_r}{\partial r}, \tag{3.29}$$

$$\varepsilon_{r\theta} = \left(\frac{1}{2}\right)\left[r\frac{\partial}{\partial r}\left(\frac{u_\theta}{r}\right) + \frac{1}{r}\frac{\partial u_r}{\partial \theta}\right] \text{ and} \tag{3.30}$$

$$\varepsilon_{rz} = \left(\frac{1}{2}\right)\left[r\frac{\partial u_r}{\partial z} + \frac{1}{r}\frac{\partial u_z}{\partial \theta}\right]. \tag{3.31}$$

Hooke's Law can be used to define relationships between stresses and strains

$$\sigma_{rr} = \Delta\lambda + 2\mu\varepsilon_{rr}, \tag{3.32}$$

$$\sigma_{r\theta} = 2\mu\varepsilon_{r\theta} \text{and} \tag{3.33}$$

$$\sigma_{rz} = 2\mu\varepsilon_{rz}, \tag{3.34}$$

where $\Delta = \nabla^2\emptyset = -(\alpha^2 + k^2)f\cos n\theta\cos(\omega t + kz)$ is dilation. The boundary conditions for the pipe geometry for free motion are given by:

$$\sigma_{rr} = \sigma_{rz} = \sigma_{r\theta} = 0 \text{ at } r = a \text{ and at } r = a+h = b \tag{3.35}$$

where a is internal radius, b is the external radius and h is the pipe thickness.

Having related strains to the small displacements along the pipe, stresses are related to strains to yield the general form of Hooke's Law, so

$$\begin{bmatrix} \sigma_{rr} \\ \sigma_{\theta\theta} \\ \sigma_{zz} \\ \sigma_{\theta z} \\ \sigma_{rz} \\ \sigma_{r\theta} \end{bmatrix} = \begin{bmatrix} C_{11} & C_{12} & C_{13} & C_{14} & C_{15} & C_{16} \\ C_{21} & C_{22} & C_{23} & C_{24} & C_{25} & C_{26} \\ C_{31} & C_{32} & C_{33} & C_{34} & C_{35} & C_{36} \\ C_{41} & C_{42} & C_{43} & C_{44} & C_{45} & C_{46} \\ C_{51} & C_{52} & C_{53} & C_{54} & C_{55} & C_{56} \\ C_{61} & C_{62} & C_{63} & C_{64} & C_{65} & C_{66} \end{bmatrix} \times \begin{bmatrix} L^+ \\ L^- \\ SV^+ \\ SV^- \\ SH^+ \\ SH^- \end{bmatrix} \tag{3.36}$$

where SV is the vertical component of shear deformation, SH is the shear horizontal deformation component and L is longitudinal deformation component. The positive and negative signs refer to the direction of propagation. The characteristic equation formed by determinant of the Bessel functions is

$$\left|C_{ij}\right| = 0, (i, j = 1 \text{ to } 6), \tag{3.37}$$

where i denotes the row and j the column of the determinant. Hence the dispersion characteristic equation for a hollow cylinder is given by (Gazis, 1985)

$$\begin{bmatrix} C_{11} & C_{12} & C_{13} & C_{14} & C_{15} & C_{16} \\ C_{21} & C_{22} & C_{23} & C_{24} & C_{25} & C_{26} \\ C_{31} & C_{32} & C_{33} & C_{34} & C_{35} & C_{36} \\ C_{41} & C_{42} & C_{43} & C_{44} & C_{45} & C_{46} \\ C_{51} & C_{52} & C_{53} & C_{54} & C_{55} & C_{56} \\ C_{61} & C_{62} & C_{63} & C_{64} & C_{65} & C_{66} \end{bmatrix} = 0. \tag{3.37 }$$

The matrix elements (Equation 3.37) are given in the appendix A.

The terms W_n and Z_n in matrix elements (Appendix A) represent the Bessel functions with type depending on the value of the n. Table 3.1 shows the appropriate selection of

the Bessel functions for certain wave characteristics. As mentioned before n is circumferential order of guided waves in hollow cylinder. When n=0 then the modes are axially symmetric. It can change as θ change but it is still axially symmetric.

Wavenumber	Frequency range	Coefficient	Bessel Functions
Real	$\frac{w}{k} < C_l, C_s$	$\beta^2, \alpha^2 < 0$ $\lambda_1 = \lambda_2 = -1$	$Z_n(\alpha r) = I_n(\alpha r)$ $W_n(\alpha r) = K_n(\alpha r)$ $Z_n(\beta r) = I_n(\beta r)$ $Z_n(\beta r) = K_n(\beta r)$
Real	$C_s < \frac{w}{k} < C_l$	$\alpha^2 < 0$ $\beta^2 > 0$ $\lambda_1 = -1$ $\lambda_2 = 1$	$Z_n(\alpha r) = I_n(\alpha r)$ $W_n(\alpha r) = K_n(\alpha r)$ $Z_n(\beta r) = J_n(\beta r)$ $Z_n(\beta r) = Y_n(\beta r)$
Real	$\frac{w}{k} > C_l, C_s$	$\beta^2, \alpha^2 > 0$ $\lambda_1 = \lambda_2 = 1$	$Z_n(\alpha r) = J_n(\alpha r)$ $W_n(\alpha r) = Y_n(\alpha r)$ $Z_n(\beta r) = J_n(\beta r)$ $Z_n(\beta r) = Y_n(\beta r)$
Imaginary	any		
Complex	any	β^2, α^2Complex $\lambda_1, \lambda_2 = 1$	

Table 3.1. *Bessel function used for different values of the frequency range corresponding values of λ_1, λ_2, α and β in terms of wavenumbers (λ_1 and $\lambda_2$are just weighting coefficient and $I_n and\ K_n are\ complex\ \ J_n and\ Y_n\ are\ real\ Bessel\ functions$).*

For axially symmetric modes the frequency equation can be decomposed into the product of two sub determinants with

$$D_1 \cdot D_2 = 0 \tag{3.38}$$

where

$$D_1 = \begin{bmatrix} C_{11} & C_{12} & C_{14} & C_{15} \\ C_{31} & C_{32} & C_{34} & C_{35} \\ C_{41} & C_{42} & C_{44} & C_{45} \\ C_{61} & C_{62} & C_{64} & C_{65} \end{bmatrix} \text{ and } D_2 = \begin{bmatrix} C_{23} & C_{26} \\ C_{53} & C_{56} \end{bmatrix} \tag{3.39}$$

3.4.3 Axially symmetric and non-axially symmetric

Axially symmetric waves are symmetric around the tube axis; or in the other words wave is axially symmetric if its appearance is unchanged if the pipe rotated whole its axis. Flexural modes are non-axially symmetric but torsional and longitudinal modes are axially symmetric. For axially symmetric motion the transverse component u_θ of the displacement field $u = (u_r, u_z, u_\theta)$ is identically zero while its radial and axial component u_r and u_z are independentθ. Flexural modes displacement are dependent of θ. Also, the longitudinal and torsional modes are axially symmetric, meaning that the u_θ and u_z components do not change with θ (motion is independent of circumferential position).

3.4.4 Labelling

Longitudinal, torsional and flexural are three different mode types of wave that can propagate in a hollow cylinder. All modes propagate along the z axis. The wave mode notations are as follows (Rose, 1999):

- Longitudinal modes are labelled as L(0,m). $u_r, u_z \neq 0, u_\theta = 0$
- Torsional modes are labelled as T(0,m). $u_r, u_z = 0, u_\theta \neq 0$
- Flexural modes are labelled as F(n,m). $u_r, u_z, u_\theta \neq 0$

The first index in labelling is harmonic order or circumferential variation (n=1,2,3,…) and the second index is a counter variable (mode m=1,2,3,…). When m=1, is a fundamental mode and the higher modes are numbered continuously. There are an infinite number of torsional and longitudinal modes for n=0 and for n=1,2,3,… there are an infinite number of modes for each n (Rose, 1999).

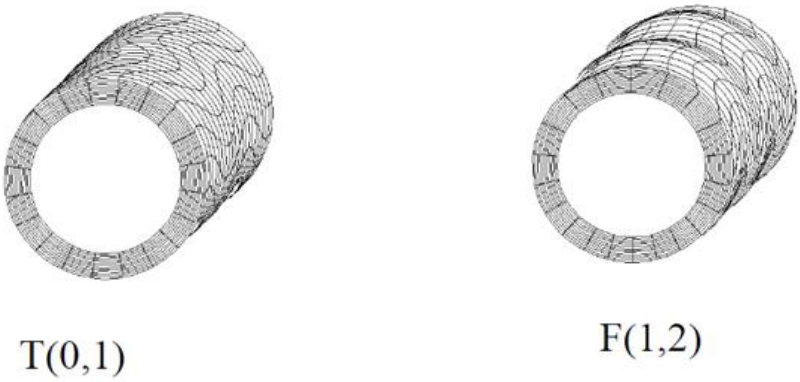

Figure 3.5. *Mode shapes of torsional T(0,1) and flexural F(1,2).*

Longitudinal modes can have displacements u_r and u_z which are independent of θ. The characteristic equation for the longitudinal modes is defined by the four-by-four determinant (3.39). Torsional pipe modes have displacement u_θ only. Also the only torsional non-dispersive mode is its first mode, where the solution is defined by the two-by-two determinant in equation (3.39). Flexural modes are non-axially symmetric and they have displacements u_r and u_z which depend on θ. The solution to flexural modes involves the full six dimensional determinant (3.37) as it has all three displacement components (Rose, 1999).

Material	**Longitudinal velocity (ms^{-1})**	**Shear velocity (ms^{-1})**	**Density (kg/m^3)**
Steel	5959	3260	7392

Table 3.2 *Material properties used for the steel pipe*

3.4.5 Dispersion

The dispersion curves describe the solutions to the modal wave propagation equations which give the properties of guided wave such as phase velocity, group velocity, energy velocity, attenuation and mode shape. This information enables the prediction of test results and decision making with regards to selecting the most appropriate guided wave for propagation. Dispersion curves can be generated for all

types of structures including plates, rods, tubes, multilayer structures, and rails, isotropic or anisotropic structures (Rose, 1999). From the relationships between stress, strain and displacement the characteristic matrix can be obtained by satisfying the boundary conditions. The coefficient matrix is set equal to zero in order to satisfy nontrivial solution (Eq 3.37). The characteristic matrix gives the characteristic function

$$\mathcal{F}(\text{Frequency}, \text{Wavenumber}) = 0. \tag{3.40}$$

This function is calculated for a given set of properties; specifically the characteristic matrix is a function of the thickness, material properties, frequency and wavenumber, introduced as a function of frequency and wavenumber. The roots of this characteristic function, which give the dispersion curves, are found using a numerical root-finding algorithm and the mode shapes are obtained by substituting these roots back into the governing equations. In this project the roots were extracted by finding the sign changes in the output function, and use of Muller's method. The solution gives the variation in velocity for a mode versus frequency or versus frequency thickness product; this product is effectively a normalised frequency. Hence the dispersion curve named from the changing of velocity versus frequency which shows waves are dispersed as they propagate. Dispersion curves were calculated in MATLAB by using the approach given in Section 3.4.7.

3.4.6 Group and phase velocity

Dispersion curves for a group of waves can be different from individual frequency waves, so it is necessary to clarify the concepts of and group velocities. The group velocity c_g , is the velocity at which group of waves will travel at a given frequency while the phase velocity is the wave velocity of each individual peaks of a single frequency wave. Phase velocity c_p and group velocity c_g are given as

$$c_p = \frac{\omega}{k} \; and \tag{3.42}$$

$$c_g = \frac{\partial \omega}{\partial k}, \tag{3.43}$$

where k is the wavenumber. Phase and group velocity are related to each other through

$$c_g = \frac{\partial (c_p k)}{\partial k} = c_p + k\frac{\partial (c_p)}{\partial k}. \tag{3.44}$$

Here $C_p = C_p(k)$ expresses the fact that $C_p$is a function of wavenumber. The group velocity concepts and equations are well covered by (Rose, 1999).

3.4.7 Phase and group velocity dispersion curve implementation in MATLAB

3.4.7.1 Torsional mode dispersion curves

The aim of this MATLAB interpretation is to plot the phase and group velocities for a domain of frequencies. To do this, it is necessary to find the wave number in the characteristic equation for torsional modes. As mentioned from equation 3.39, the determinant of this 'two by two' matrix can be considered as:

$$\mathrm{W_n}(\beta r_{in})Z_\mathrm{n}(\beta r_{ext}) - \mathrm{Z_n}(\beta r_{in})\mathrm{W_n}(\beta r_{ext}) = 0. \tag{3.45}$$

From the roots β ($\beta = \sqrt{\frac{\omega^2}{\mathrm{C_s}^2} - \mathrm{k}^2}$ (Equation 3.24)) the wavenumber k for real and complex β were found. When β was real, real Bessel functions used

$$\mathrm{Y_n}(\beta r_{in})J_\mathrm{n}(\beta r_{ext}) - \mathrm{J_n}(\beta r_{in})\mathrm{Y_n}(\beta r_{ext}) = 0\text{and} \tag{3.46}$$

for complex β

$$\mathrm{K_n}(\beta r_{in})I_\mathrm{n}(\beta r_{ext}) - \mathrm{I_n}(\beta r_{in})\mathrm{K_n}(\beta r_{ext}) = 0, \tag{3.47}$$

which is given from Table 3.1. Equation 3.46 and 3.47 were written as a function of β. (FuncToRoot.m) in MATLAB for different value of β is shown in appendix C.2. However in order to find β, a root finding method needs to be considered (before this determinant calculation in the script). The Root Sign Change method is used in this project as a first step to find the roots of Equation 3.46 and 3.47 by finding sign change intervals in the determinant function by varying β. Muller's method (implemented in muller_old.m), described later in Section 3.4.7.1, uses these intervals as an initial guess to find a more precise value of β. This specific combination of methods was chosen because they are a compromise between simplicity (required because this is a rolling project) and accuracy (required because the determinant function is sensitive to wayward changes in β). Interval sizing for the Sign Change Root Finder method is of critical importance because a grid too coarse may lead to some roots not being identified (resulting in missing values of β) and because a grid too fine will result in a script that takes a great amount of time to execute. Through experimentation, the most suitable domain and step-size for β values was found to be 0:100:50000; this was implemented in Sign_Change_Root_Finder.m file in appendix C.3. The calculated values of wavenumber may be real and complex; real value of wavenumbers corresponds to propagating wave modes. Here, we are working with a lossless system, so only the real roots are considered, but for the further work Muller's method can be used to find the complex roots as well. In the Section 3.4.7.1 the Muller's method and other root finding methods will describe and the difficulty of these methods will discuss.

Since β values for each torsional mode can be found at each frequency, a value known as the cut-off frequency needs to be found so that the dispersion curves can be plotted. The cut-off frequency is the frequency at which the phase velocity of a given dispersive mode approaches infinity from a higher frequency value. Mathematically speaking, it is also the value at which the wavenumber is zero. The cut-off frequency can also be defined as

$$f_{Cut-off} = \frac{C_s \times \beta}{2 \times \pi}. \tag{3.48}$$

The MATLAB script written for this project will only plot phase velocities after the cut-off frequency. Considering this, the phase velocity plot for torsional modes, T(0,m), of a stainless steel tube (Outer diameter 1.905 cm, wall thick 0.165 cm; $c_l = 5800ms^{-1}, c_s = 3100ms^{-1}$) is shown in Figure 3.6. This graph is comparable to the same torsional modes dispersion curve written by Rose (pp 162, 1999).

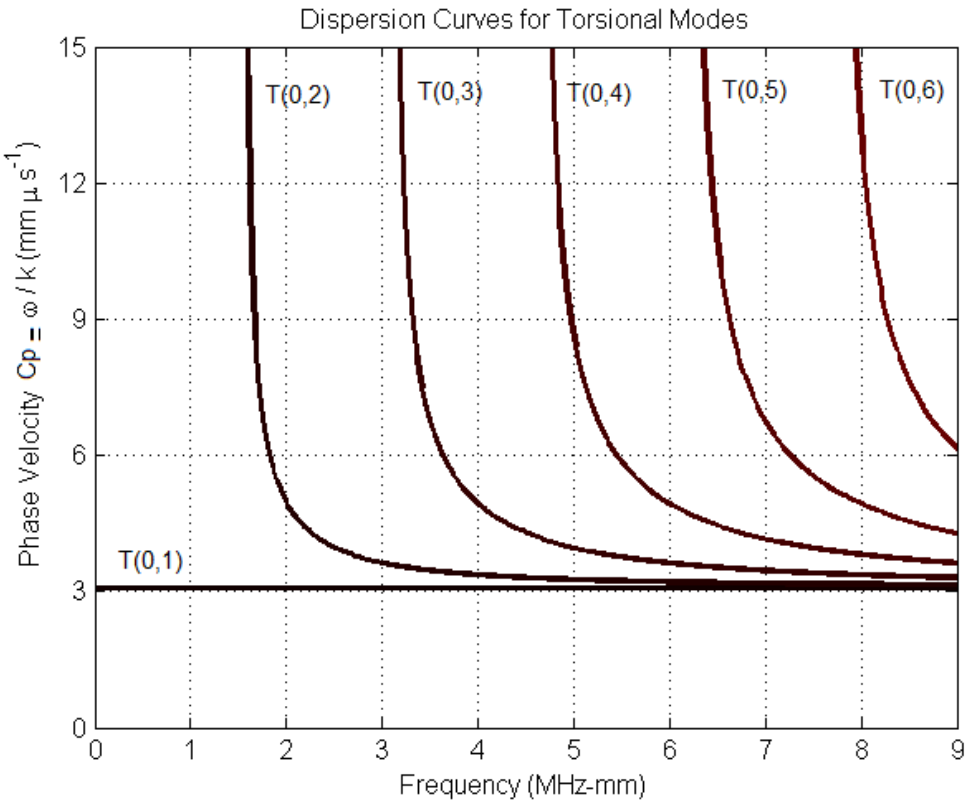

Figure 3.6. *Phase velocity plot for torsional modes, T(0,m), of a stainless steel tube (Outer diameter 1.905 cm, wall thick 0.165 cm;* $c_l = 5800ms^{-1}, c_s = 3100ms^{-1}$*). This graph is comparable to the same torsional modes dispersion curve written by Rose (pp 162, 1999).*

Now that the phase velocity dispersion curves for torsional modes can be found, it is possible to find the group velocity dispersion curves. The group velocity at a point is related to the phase velocity at a point by

$$c_g = \frac{\partial \omega}{\partial k} = \frac{k\, c_s}{\sqrt{k^2 + \beta^2}}. \tag{3.49}$$

Considering this, the group velocity plot for torsional modes, T(0,m), of a steel pipe (Outer diameter 6 cm, wall thick 0.35 cm; $c_l = 6290ms^{-1}, c_s = 3260ms^{-1}$) is shown in Figure 3.7. This graph is comparable to torsional modes dispersion curve written by Zenghua Liu et al. (2006).

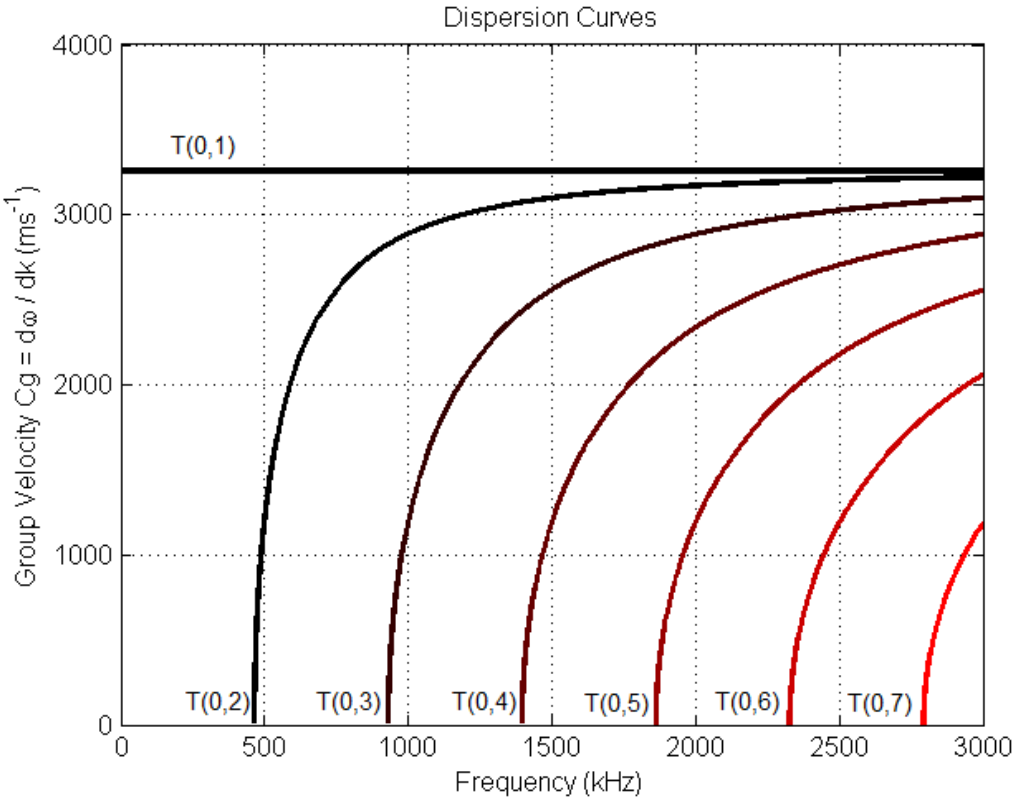

Figure 3.7. *Group velocity plot for torsional modes, T(0,m), of a steel pipe (Outer diameter 6 cm, wall thick 0.35 cm;* $c_l = 6290ms^{-1}, c_s = 3260ms^{-1}$. *This graph is comparable to the same torsional modes dispersion curve written by Zenghua Liu et al. (2006).*

3.4.7.2 Longitudinal phase and group velocity dispersion curves

In addition to the torsional mode dispersion curves discussed previously, it is also necessary to find the dispersion curves for the longitudinal mode. This is because of for finding the mode conversion which happens between torsional and longitudinal modes. The main difference is that the torsional and longitudinal modes have different characteristic functions. The functions differ also in the fact that the longitudinal one is itself a function of frequency, meaning that Muller's method needs to be applied for each frequency value separately. This is cumbersome, so a more time-efficient solution needs to be considered.

In this implementation, the determinant function' four by four matrix' (Equation 3.39) is calculated for each possible value of k for each frequency separately. The script finds the real sign changes in the function, thus finding the values of k that satisfy the characteristic equation. The domain and step-size for the k values to search through was found through experimentation, because they can cause the same problems as a poor domain choice for β as discussed in the previous section. The k values that correspond to roots are used to find the phase velocity by Equation (3.42).This yields the phase velocity dispersion for longitudinal modes L(0,m), of a schedule 40 (Outer diameter 7 cm, wall thick 0.55 cm; is shown in Figure 3.8. This graph is compared with the same torsional modes dispersion curve written by Demma (2003).

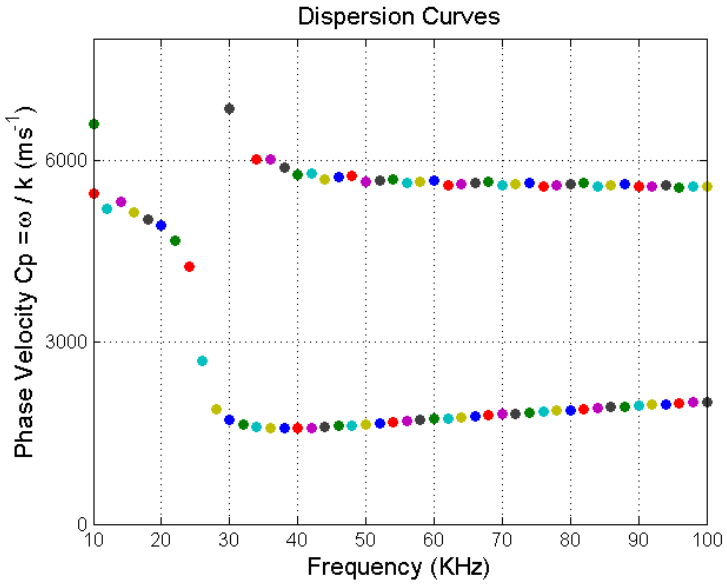

Figure 3.8 . *Phase velocity dispersion for longitudinal modes L(0,m), of a schedule 40 (Outer diameter 7 cm, wall thick 0.55 cm. This graph is comparable to the same torsional modes dispersion curve written by Demma (2003).*

Due to time constraints, and the fact that the MATLAB simulation is not the main focus of this project, the group velocity was found using a script written by Seco and Jimenez (2012).

3.4.7.3 Flexural phase and group velocity dispersion curves

Similar process chose for Flexural mode same as longitudinal mode. The Flexural mode is non axially symmetric mode and circumferential order is not zero (described in section 3.4.3) but longitudinal mode is axially symmetric and the circumferential order is always zero. This difference change the determinant function 'four by four matrix' (Equation 3.39). Also, The domain and step-size for the k values to search through was found through experimentation, and the step size compare to longitudinal modes are smaller because some roots were missing. Figure 3.9 shows the phase velocity dispersion curves for a 3.4 cm diameter steel pipe with 5 mm wall thick in vacuum. The frequency views from 1 kHz to 400 kHz. The graph was calculated using the technique outlined in section 3 and implemented in MATLAB (see Appendix C).

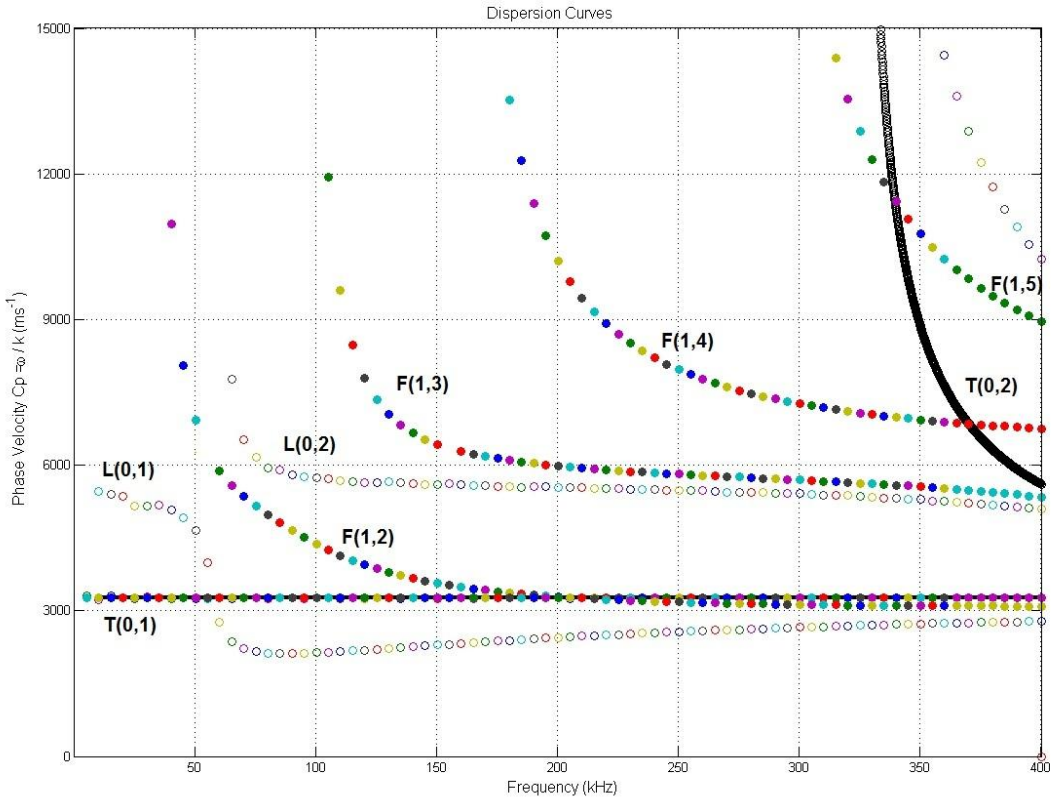

Figure 3.9. *Phase velocity of 5mm wall thick, with 3.4 cm external diameter steel pipe in vacuum* $(c_l = 6290ms^{-1}, c_s = 3309ms^{-1})$.

3.4.7.4 Root finding methods

Background

Research into ultrasonic NDE techniques for the inspection of hollow cylinder structures relies on the use of modelling tools which calculate dispersion curves and use them in experimental work. Calculating roots for dispersion curve generation is challenging, especially in some regions of wavenumber and frequency (Graff, 1991). The traditional numerical methods are based on determination of the zeros of the frequency equation by using an iterative root finding algorithm. Many researchers use iterative

techniques, such as linear or quadratic interpolation or extrapolation algorithms, which have very fast convergence on a single root. Newton-Raphson, bisection, and Mueller are used as safer iteration methods at the expense of speed. The bisection method takes an interval [i , i+1] such that f(i) and f(i+1) have opposite signs and then finds the midpoint of [i , i+1]. The root can lie on [i , (i +(i+1))/2] or [(i + (i+1))/2, i+1] which shows from the function sign change. Iteration will repeat the bisection until the interval is sufficiently small. Newton-Raphson is the other iterative method which finds the root by considering its derivative, and an initial value.

Muller's method is a useful root finding method for function, particularly those with both real and complex roots. It was presented by David E. Muller in 1956. Muller extends the idea of the secant method which works with a quadratic polynomial. If three initial guesses $k^{(i-2)}, k^{(i-1)}$ and $k^{(i)}$ are given for an unknown root. Muller's method asserts that the next logical value to consider

$$k^{(i+1)} = k^{(i)} + h_i q_i. \tag{3.50}$$

Here:

$$q_i = \frac{-2C_i}{B_i \pm \sqrt{B_i^2 - 4A_i C_i}}, \tag{3.51}$$

$$C_i = (1 + r_i) f\left(k^{(i)}\right), \tag{3.52}$$

$$B_i = (2r_i + 1) f\left(k^{(i)}\right) - (1 + r_i)^2 f\left(k^{(i-1)}\right) + r_i^2 f\left(k^{(i-2)}\right), \tag{3.53}$$

$$A_k = (r_i) f\left(k^{(i)}\right) - r_i (1 + r_i) f\left(k^{(i-1)}\right) + r_i^2 f\left(k^{(i-2)}\right), \tag{3.54}$$

$$h_k = k^{(i)} - k^{(i-1)} \text{and} \tag{3.55}$$

$$r_i = \frac{h_k}{h_{k-1}}. \tag{3.56}$$

The Muller's method plots the parabola that passes through the three points provided. It takes the intersection of the horizontal axis and the parabola as the next approximation. The order of convergence of Muller's method is approximately 1.84 (Mekwi, 2001). In this project, Muller's method will typically be used to solve the Characteristic equation function (FuncToRoot.m). The implementation of Muller's method written for this project is in Muller.m.

3.4.8 Cut-off frequency relation with wall thick and pipe size

When the torsional mode has chose as an excitation mode finding the first cut-off frequency in order to find the working boundary is important. I t is possible to propagate the non dispersive mode T(0,1) at frequencies bellow at which the first dispersive mode T(0,1). Hence, by comparing different cut-off frequencies by changing different pipe size and wall thick changing, the relation between them has found. Three different cases were evaluated, and graphs were plotted by the MATLAB program which was written for dispersion curve finding (Appendix D).

First, the thickness of the pipe wall was changed while the internal radius was laid constant; the cut-off frequency reduced as thickness increased. For example, as shown in Figure 3.10. when the thickness is 1.5 mm and the pipe internal radius is 5mm, the first dispersive mode appears at 1MHz, the second one at 2MHz and so on.

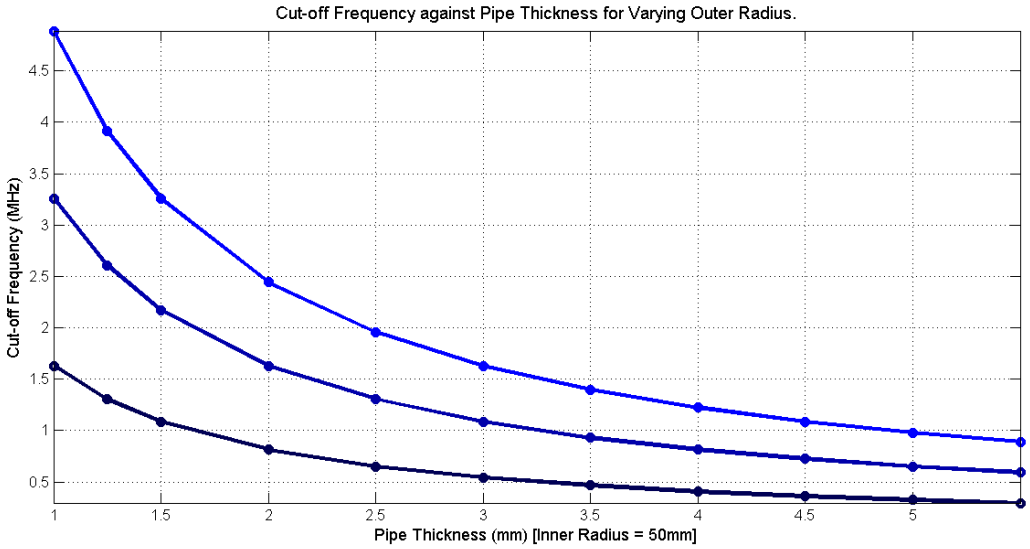

Figure 3.10. *Cut-off frequency of T(0,m)modes results are shown for a steel pipe for m=2 to m=4, against pipe wall thick for the pipe with an inner radius of 50 mm(Outer diameter 6 cm, wall thick 0.35 cm;* $c_l = 6290ms^{-1}, c_s = 3260ms^{-1}$*).*

Here results were calculated for a pipe with constant mean radius while wall thickness is constant. Figure 3.11 shows how the cut-off frequency reduced as pipe size increased. For example when the wall thickness is 2mm the first dispersive mode T(0,2)start from

800 kHz and the second one start from 1.7 MHz and so on. So when the pipe thickness increased the cut-off frequencies decreased.

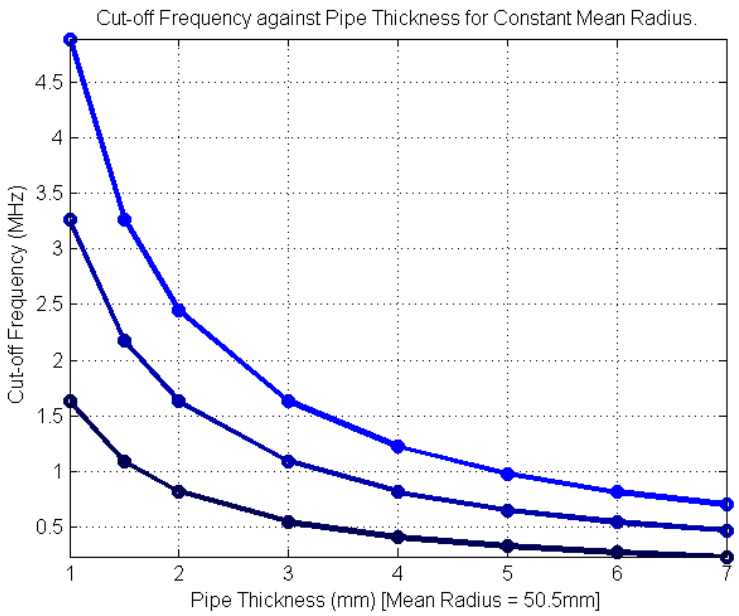

Figure 3.11. *Cut-off frequency of T(0,m)modes results are shown for a steel pipe for m=2 to m=4, against pipe thickness for constant mean radius, (Outer diameter 6 cm, wall thick 0.35 cm;* $c_l = 6290ms^{-1}, c_s = 3260ms^{-1}$.

When the pipe radius becomes for a constant wall thickness the cut-off frequency reduced (Figure 3.12). For example when the internal radius and external radius are 30mm and 33mm, the first dispersion mode comes at 500 kHz, the second dispersion mode 1 MHz and so on.

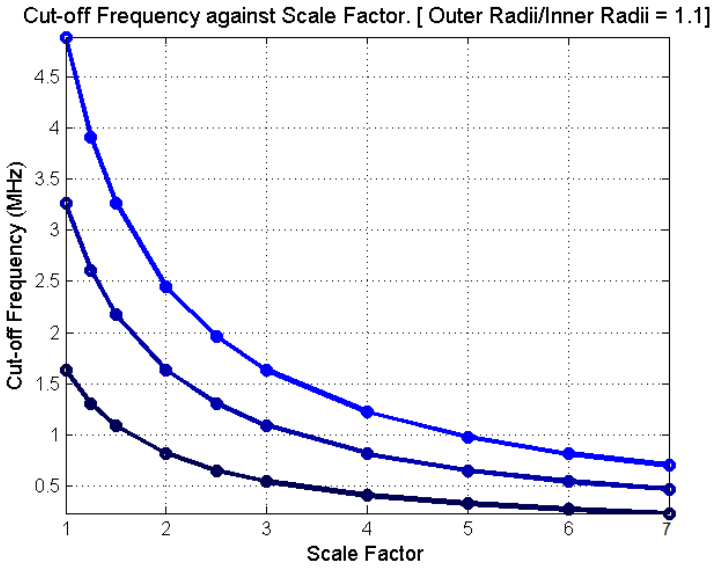

Figure 3.12. *Cut-off frequency of T(0,m) modes results are shown for a steel pipe for m=2 to m=4, against scale factor (Outer Radii/Inner Radii= 1.1), (Outer diameter 6 cm, wall thick 0.35 cm;* $c_l = 6290ms^{-1}, c_s = 3260ms^{-1}$.

In summation it found the cut-off frequency is related to the pipe thickness and pipe diameter, for small size pipes the first cut-off frequency is higher than the first cut-off frequency in larger size pipes.

3.4.9 Choose the number of transducers

Lowe and Cawley (2006) have affirmed that Plant Integrity Ltd. and Guided Ultrasonic Ltd. have used rings of new shear dry-coupled piezoelectric transducers (Imperial College university patent) which are shown in Figure 3.13. Each transducer module includes two (or more) transducers that are dry coupled and aligned along the longitudinal direction of the pipe diameter, Figure 3.14. Alleyne and Cawley (1996) suggested an array of dry-coupled piezoelectric transducers which excite cylindrical lamb waves for 7 cm _ 30 cm diameter pipes. Both Plant Integrity Ltd. and Guided Ultrasonic Ltd. produce the systems with piezoelectric transducers for 5 cm pipes. Eight modules are used in the Mini-Test tool to generate torsional wave modes for 5 cm pipes, and twelve modules for 7.5 cm and sixteen modules are used for 10 cm pipes.

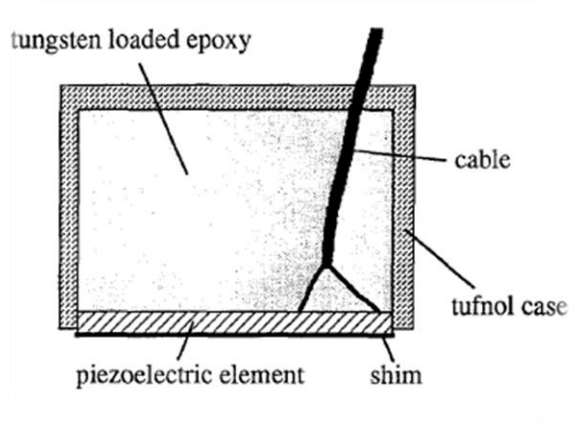

Figure 3.13. *Strain gauge incorporated into dry-coupled transducer (Alleyne, 1996).*

Figure 3.14. *The transducer produced by Guided Ultrasonic Ltd (Guided ultrasonic ltd., 2012).*

The number of piezoelectric transducers is related to order of modes of waves, pipe diameter and transducer spacing. The number of piezoelectric transducers must be greater than the highest order of modes of the wave; it can be present in the frequency range of the signal (Alleyne, 1998). For example, Alleyne explains how we can find out how many elements we can use for a 7.5 cm pipe to excite axially symmetric and asymmetric waves. Figure 3.15 shows the predicted group velocity dispersion curves for cylindrical lamb waves in (outer diameter 7.5 cm, wall thickness 0.55 cm) steel pipe over the frequency range 0-100 kHz (Alleyne, 1996). For instance, if flexural mode 13 is required at least 16 piezoelectric elements are needed in the range of frequency up to 100 kHz. It is also mentioned by Alleyne that the axially symmetric L(0,2) mode at a

frequency 70 kHz is an attractive mode to use for long distance propagation, which is fast and nondispersive at a frequency of 70 kHz. However, 12 piezoelectric transducer elements can be used for exciting an axially symmetric L(0,2) mode.

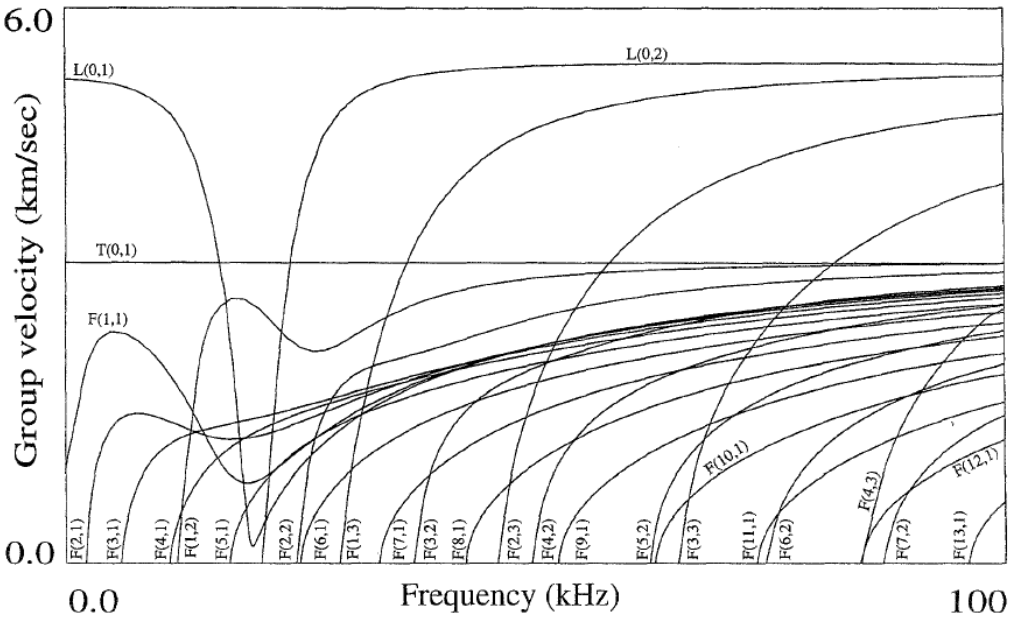

Figure 3.15. *The predicted group velocity dispersion curves for 7.5 cm steel pipes over the frequency range 0 -100 kHz (Alleyne, 1996).*

The number of piezoelectric transducers is roughly proportional to the pipe diameter. For example for a 15 cm diameter pipe, 32 piezoelectric elements around the pipe have been used, and 16 for a 7.5 cm pipe as mentioned previously (Alleyne, 1996). Another factor that should be taken into account is that if the system is to excite a pure axially symmetric mode then the transducer spacing Δ around the pipe should be less than half a wavelength λ of the inspection mode ($\Delta < \lambda/2$) according to Nyquist-shanon sampling criterion.

In this project 3.4 cm diameter steel pipe with 5 mm wall thick had chosen to inspect and at least eight transducers at frequency less than 100 kHz are needed according to Alleyne suggestions. Table 3.3 shows for a 3.4 cm diameter pipe how many transducers are needed at different frequencies (The shear wave velocity on pipe is assumed

$c_s = 3309 \mathrm{ms}^{-1}$ which will show in Section 5). After calculation it shows from table 3.3 at least seven transducers are needed at 100 kHz frequency.

Frequency (Hz)	Wave velocity ($\mathbf{ms^{-1}}$)	Wave length(m)	Pipe Circumference (m)	Delta	Number of transducers
10000	3309	0.33	0.107	0.17	1
20000	3309	0.17	0.107	0.08	2
30000	3309	0.11	0.107	0.06	2
40000	3309	0.08	0.107	0.04	3
50000	3309	0.07	0.107	0.03	4
60000	3309	0.06	0.107	0.03	4
70000	3309	0.05	0.107	0.02	5
80000	3309	0.04	0.107	0.02	6
90000	3309	0.04	0.107	0.02	6
100000	3309	0.03	0.107	0.02	7
150000	3309	0.02	0.107	0.01	10
200000	3309	0.02	0.107	0.01	14
300000	3309	0.01	0.107	0.01	20
400000	3309	0.01	0.107	0.00	27

Table 3.3 *Number of transducers predicted for 3.4 cm diameter pipe at different frequencies (The shear wave velocity on pipe is assumed $c_s = 3309 ms^{-1}$ which will show in Section 5).*

Section 4

4 Torsional modes properties

4.1 Background

In section 3 the guided wave characteristics of hollow cylinders were presented, in this section the torsional mode T(0,1), and other modes, are considered in order to compare the potential of different modes of propagation. Also, the difficulty in each mode will describe. Difficulty of using torsional guided waves has been about 'discontinuities in the geometry' of guided wave presented by Ditiri (1994), Alleyne and Crawley (1996), Alleyne and Pavlakovic (2001). Examples of the discontinuities of the geometry are; welds connecting two parts together, curved parts attached to the main structure, free ends and corrosion defects on discontinuities due to material property alteration. Ditiri (1994) worked on characterization of circumferential cracks in 1.88 cm diameter, 0.6 mm wall thickness hollow cylinder when the L(0,2) mode was incident. Alleyne and Cawley (1998) worked on declaration of a part-circumferential notch in a pipe with 7 cm diameter with 5.5 mm wall thickness when the axially symmetric L(0,2) mode was incident. In 2001 Alleyne and Pavlakovic reported their work on a 5 cm diameter pipe with 5.5mm wall thickness, to find different defects using axially symmetric L(0,2) and T(0,1) modes.

Furthermore the ability of guided waves to locate cracks and notches including effect of defect size on the reflected echo has been investigated by many researchers, Ditiri (1994), Alleyne (1998), Demma et al.(2003), Carandente (2011) and Hu (2011). The most recent works such as Demma et al.(2003), Carandente (2011) and Xiongwei Hu (2011) was with the axially symmetric T(0,1) mode and in a 7 cm diameter with 5.5 mm thickness steel pipes. Most of the previous investigators studied large pipes generally greater than 7 cm diameter, with axially symmetric L(0,2) and T(0,1) modes. In this project the challenges of using the axially symmetric and non-dispersive T(0,1) modes for small diameter pipes was investigated.

4.2 Choice of guided modes for testing

In a hollow cylinder, many different modes can potentially propagate at any frequency. It is important to choose a mode which is easily readable and reliably interpreted, which is also different for each specific defect. The basic factors that influence the choice of wave mode selection were defined by Wilcox et al. (Demma, 2003) as dispersion, attenuation, sensitivity, excitability, detect ability, mode selectivity, and in implementation speed of single test, testing tool design and the level of difficulty of analyzing the data should all be considered. In this project, attenuation factor of propagation modes was not considered because it is not applicable to lossless single layer steel pipe in vacuum conditions (as is these testing condition). For most applications, lower orders are used for selecting the propagating wave (Alleyne and Pavlakovic, 2001), and non-dispersive curves in torsional mode and non-dispersive area in longitudinal mode are used (Demma, 2003).

4.3 Torsional modes advantages

The T(0,2) mode is a dispersive axially symmetric mode, with mode shape and cut-off frequencies shown in Figure 3.6. At the axially symmetric modes torsional modes are used preferably over longitudinal modes as;

- The mode shape of the torsional T(0,1) mode is not frequency dependent. However, longitudinal modes in some frequency ranges are not frequency dependent.
- A large advantage of Torsional mode is that is unaffected by non-viscous fluid content (Alleyne and Pavlakovic, 2000). The rate of energy loss into the liquid is proportional to the radial displacement at the pipe surface, hence as a torsional wave has no radial displacement so it is unaffected by non-viscous liquid loading on the outside or inside of the pipe, The L(0,2) mode has non-zero radial displacement, hence it loses energy slowly into a fluid surrounding the pipe.
- A torsional mode can detect longitudinal cracks, whereas the longitudinal mode is essentially insensitive to narrow effects especially paralleled to the pipe axis as it

does not have radial displacement. Zenghua Liu et al. (2006) reveal that T(0,1) mode at 45kHz for 6 cm diameter with 3.5 mm wall steel pipe can find both circumferential and longitudinal defects compared to the longitudinal mode which proves that the torsional modes are dominant for all kinds of defect detection in pipes for their sensitivity.

However, the range of inspection in longitudinal mode L(0,2) is larger than the respective torsional mode. Also, as torsional modes are sensitive to circumferential changes, if there is a support bracket on the pipe, the reflected signal is strong and if there is corrosion on the bracket it is not easy to find it (Alleyne and Pavlakovic, 2000). In this project an incident T(0,1) mode is considered as a complete non-dispersive axially symmetric mode, but mode conversion to the non-symmetric modes could happen at non-axisymmetric defects.

Section 5

5 Experimental

In this Section, implementation of different tests on plates and pipes will describe. The first step of starting the experimental tests was choosing the appropriate transducer for generating waves on plate and pipe. When transducers were purchased from Plant Integrity Ltd. test were started by preparing the other equipment which was needed. Experiments started with finding a way to couple the shear piezoelectric transducers on plate and pipe, find the appropriate frequency to generate waves. Wave velocity measurement was important to find the other parameters such as end pipe and defect location. Hence, torsional wave velocity ($3309 \pm 11\ \mathrm{ms}^{-1}$) was found on pipe as well as shear and longitudinal wave velocity on plate. Although, the number of transducers were limited but the appropriate position of transducers (one receiver and one transmitter in each module) will recommend. Finally pipe with defects will examined and the advantages of using more transducers and placing the receiver in different position around the pipe will describe. The main problem which is the compromise between the limited number of transducers due to budget constraints and working in lower frequency (50 kHz) to have lower reverberation level with missing the defect echoes will discuss.

5.1 Guided wave instruments

Since ten years ago ultrasonic researchers and companies made different instruments to inspect large length of pipe. The UK company *Guided Ultrasonic Ltd.* introduced as a world leader in developing guided wave inspection equipment. The *wavemaker* (Instrument made by *Guided Ultrasonic Ltd.)* has an ability to apply rapid screening a long length of pipe to detect axial and circumferential cracking, external and internal corrosion. Guided wave methods were originally restricted to laboratory experiments and research, but over time industry adopted these methods over the

more traditional NDE inspection methods. As mentioned in Section 2.2.2 three different transducers are used in guided waves technology. Both Plant Integrity Ltd and Guided Ultrasonic Ltd clamp an array of piezoelectric elements individually to the pipe surface for their guided wave systems. Electromagnetic Acoustic Transducers (EMAT) are mostly used for higher frequency testing (20 kHz to 10 MHz), resolution and range are affected by wave propagation frequency. IZFP (Germany) and Sonic Sensor (United States of America) are the most famous companies which produce EMAT transducers. Magnetostrictive technology (MsS) is cheaper and easier to process than piezoelectric transducer systems, but it is more difficult to obtain satisfactory mode control; this means it has not become popular in industry (Lowe and Cawley, 2006). A magnetostrictive transduction technology has been developed, and sensors are produced at SWRI (United States of America) and M.K.C Korea.

In this experimental test four shear piezoelectric transducers and two modules were purchased to fix transducers on pipe from Plant Integrity Ltd. The piezoelectric transducers with 1.4 cm long, 1.2 cm width and 1 cm height have an active surface with 1.3 cm long, 0.3 cm width and 0.1 cm thickness. Piezoelectric motion direction and active surface (white part) are shown in Figure 5.1. Transducers are mounted in modules to have an easy access for placing on plate and pipe. In each module three transducers in shear position can be mounted. Figure 5.2 shows the two modules when one transducer is mounted in each.

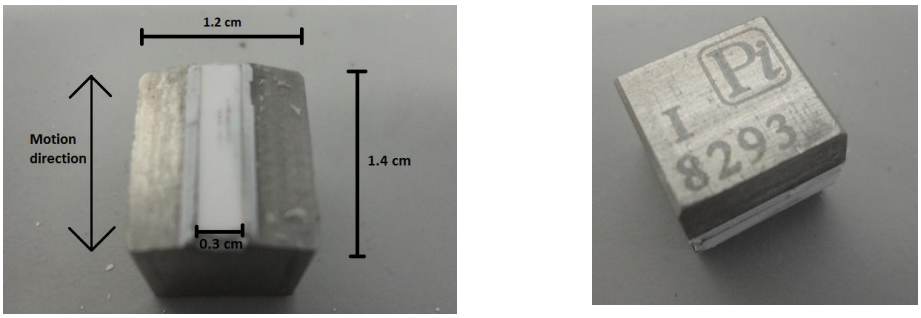

Figure 5.1. *Piezoelectric transducers with 1.4 cm long, 1.2 cm width and 1 cm height. Piezoelectric motion is along the length direction and active surface is a white part with 1.3 cm long, 0.3 cm width and 0.1 cm thickness.*

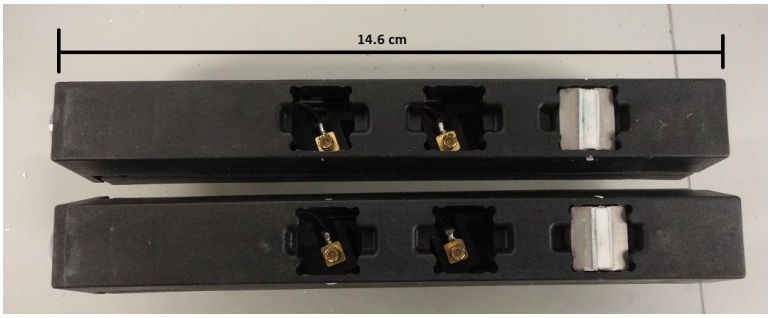

Figure 5.2. *Two modules with 6 places for transducers when two transducers are already placed. When modules are placed on a pipe, transducers motion is in shear format.*

5.2 Experimental setup

The plate case tests were performed on different sizes of plate depends on the tests and different instrument had used. A function generator (HP 33120A) triggered tone bursts of two cycles with a 10 Hz burst rate and an 18V peak-peak voltage and a signal amplifier (ORTEC Precision ac Amplifier 9452) was used to amplify the signals 70dB gain with a 1MHz and 100 kHz low pass and high pass filters. The system used the through–transmission method; two identical transducers (a receiver and a transmitter) were used (Figure 5.3). The input and output signals were digitized by the oscilloscope (LeCroy 9304C) and stored in computer. The oscilloscope was used to average the signal with 300 sweeps in its math function. Results from oscilloscope and controlling the oscilloscope were done with computer using GPIB by the MATLAB Scripts originally written by Yuan (2012) and it was modified for this project (MATLAB Scripts are given in Appendix F).

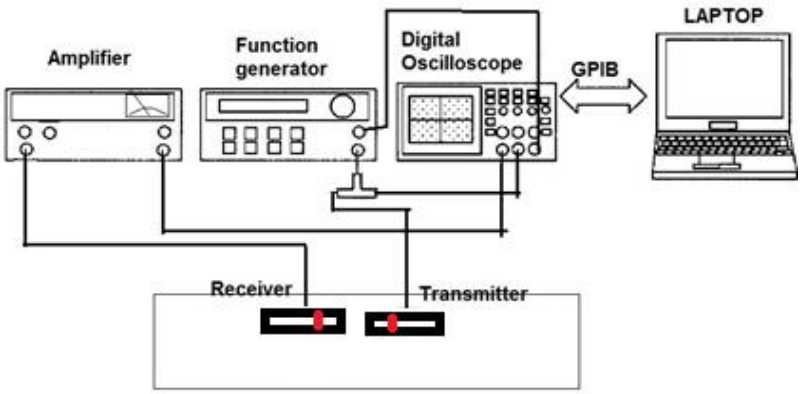

Figure 5.3. *Experimental setup of two modules on plate.*

The tests on pipe were done with a similar instrument as tests on plate and just a filter (KROHN-HITE, model: 3202 filter) was added. Figure 5.4 shows the experimental setup on pipe. Also, all the equipments specification used for tests on plate and pipes are given in Appendix E.

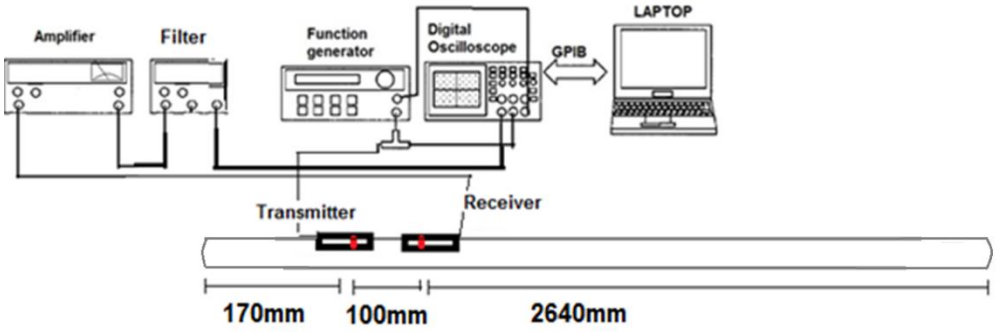

Figure 5.4. *Experimental setup of two modules on pipe. The distances shows the transmitter and receiver transducers are 100 mm a part and each transducer is 170 mm and 2640 mm far from the end of the pipe.*

Frequency bandpass filters including low-pass and high-pass, are very common in signal processing and are also used in several different applications using guided waves (Alleyene and Cawley, 1997). In the experimental tests bandpass filter was used, when the signals were rectified, some high frequencies were removed and it made the rectified signal smoother. Also, there are some projects that show the use of bandpass filters to reduce the amplitude of echoes (Gatts et al., Accessed: Aug 2011).

5.3 Coupling error for dry pressure coupling

Random coupling errors arise because shear transducers (receivers and transmitters) will not be perfectly coupled on to the pipe unless a non-Newtonian viscous fluid (like honey) is used. Variation of coupling pressures will reduce the amplitude of the T(0,1) mode to be excited into the pipe. High normal pressures on smooth hard surfaces can facilitate passage of sufficient energy when a coupling fluid is not used. It is possible to generate a shear wave on a thick pipe with sufficient and stable coupling. In order to investigate this, a variable force was applied by using weights on each module to vary the clamping load. The tests were carried out on a galvanized steel plate with 3mm thick. The transmitting transducer was driven with a tune burst of two cycles of a 200 kHz and a voltage of 18 Vp–p applied across the transducer. The incident signal's frequency 200 kHz and voltage 18 Vp-p (Open circuit output of voltage connected to the transducers) is also fixed during the tests. For the test setup, the receiver was placed 200 mm away from the transmitter. The results from Figure 5.5 indicate that the clamping load of under 40N is sufficient to achieve stable coupling on plate as there is not much variation in the transmitted amplitude when the force changes.

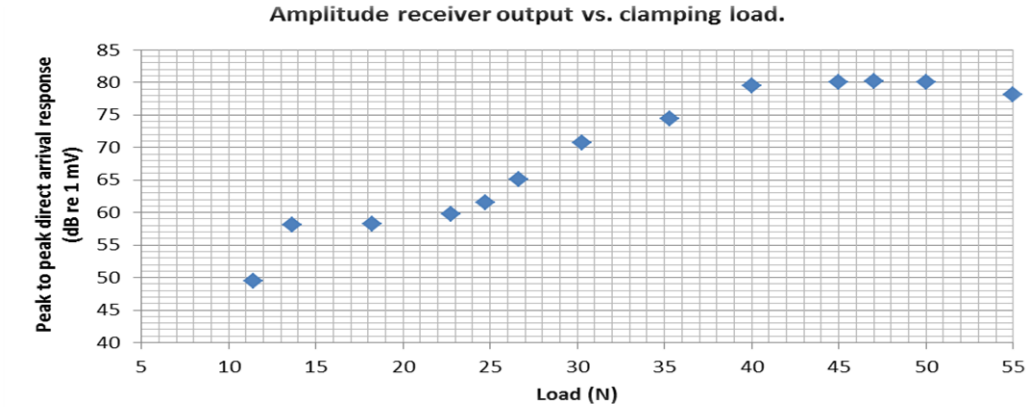

Figure 5.5. *Amplitude receiver output vs. clamping load in dry-coupled case. The transmitting transducer was driven with a tune burst of two cycles of a 200 kHz a voltage of 18 Vp–p applied across the transducer. The receiver is placed 200 mm away from the transmitter.*

To assess the repeatability of this experiment, the received level for a certain load was taken multiple times after removing and replacing the weights to measure how much the signal changed. This test was undertaken with a load of 13.5N for eleven repetitions. The result of this test is expressed in the graph below. Test 11 (in Figure 5.6) is the last test which is the value shown in Figure 5.5.

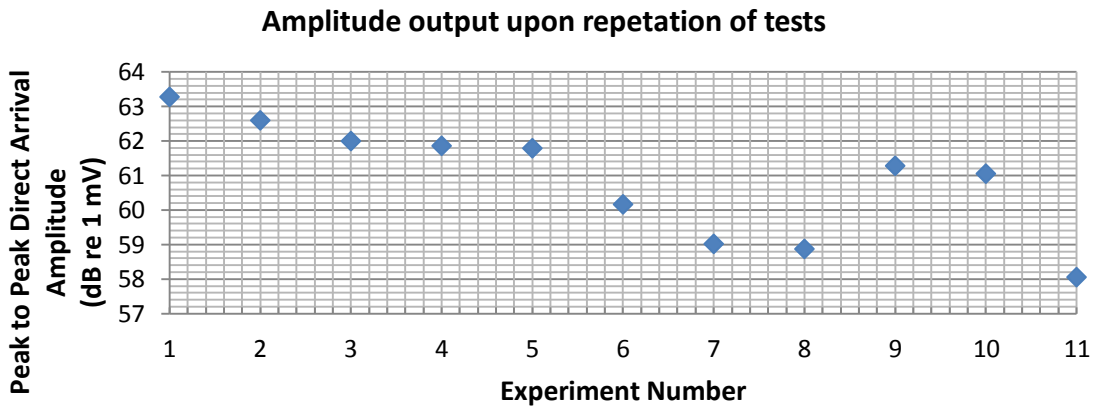

Figure 5.6. *This test was undertaken with a load of 13.5N for eleven repetitions. The amplitude output of first arrival shown in each tests. The transmitting transducer was driven with a tune burst of two cycles of a 200 kHz a voltage of 18 Vp–p applied across the transducer. The receiver is placed 200 mm away from the transmitter.*

The data in the above graph has a standard deviation of 1.7dB. These results suggest that using weights to apply a force on the pipe is inconsistent and not reliable (due to the low repeatability of the test). This occurred because it was impossible to place the weights in exactly the same location on the modules, so the force on each of the transducers varied. When the force changed to the 45 N the variation was not as much as 13.5 N, hence for the rest of experimental test 45 N used as clamping load.

Further tests on pipe were performed by using cable ties to apply a clamping force (Figure 5.7). This approach used because it was not easy to stabilize weights on a pipe when the transducers are rotating around the circumference of the pipe. Using cable

ties neatly solved this repeatability problem. For further work, a collar designed for clamping such as that shown, in Figure 5.8, is recommended. However, it would need to be redesigned because the collar designed by Plant Integrity Ltd. operates only on pipes larger than 3.75 cm.

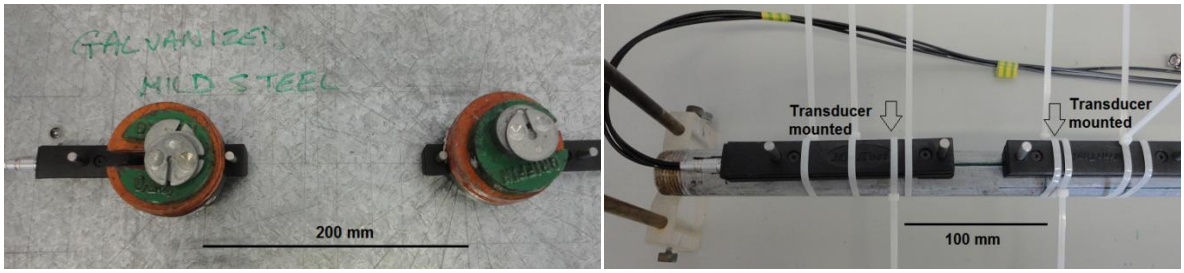

Figure 5.7. *The left picture shows modules on plate (200 mm far apart) with weights on it for coupling and the right picture shows modules (100 mm far apart) on pipe which coupled with cable tie.*

Figure 5.8. *5 cm Mini-Test collar assembly for Plant Integrity Ltd (Plant integrity ltd.,2012).*

5.4 Frequency tuning on plate

Guided wave focusing can be achieved when an array of transducers is used, specifically by timing the firing and excitation amplitude of the individual elements on the pipe. However, since only two modules were available due to budget constraints, that was not possible. In this case, the excitation frequencies were varied over a given range to maximise the amplitude of the response. In this Section tried to find a proper frequency for generating waves on different plates.

The plate case tests were done using a galvanized mild steel plate with a thickness of 3mm. The system uses the through–transmission method; two identical transducers (a receiver and a transmitter) were used (Figure 5.9).

Figure 5.9. *Experimental setup of two transducers and two modules on plate. 45N load was applied on each module due to the clamping force.*

Figure 5.10 shows the result obtaining by frequency tuning. These results were obtained with a constant transducer distance of 100 mm by applying forces of 45N and 13.5N in two different tests by changing frequency. These results show that, in the test using 45N force, the amplitude of direct transition is maximised in the 200 kHz-250 kHz frequency band. Due to this, 200 kHz was chosen as a test frequency to find the shear wave velocity in the plate case.

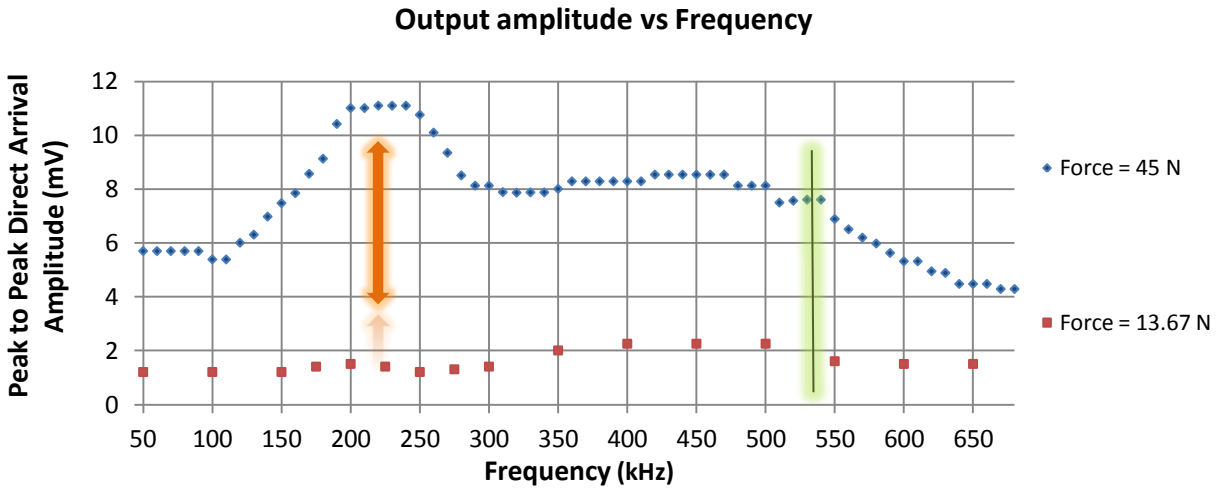

Figure 5.10. *Variation of direct arrival amplitude with frequency with two different clamping load 45N and 13.5N.*

Also, the frequency chosen should be less than the first nondispersive mode's cut-off frequency; hence group velocity dispersion curves were considered to find the cut-off frequencies (Figure 5.11). In Figure 5.11 the first non-dispersive mode cut-off frequency is approximately 540 kHz and the frequency was chose 200 kHz to be lower than the first cut-off frequency.

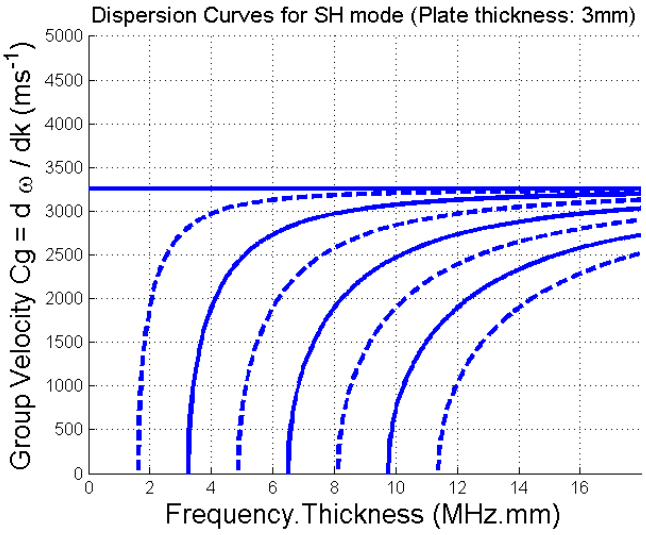

Figure 5.11. *Dispersion curves for SH (Shear-horizontal) mode for n=0 to n=7 in Frequency× Thickness (Shear velocity: 3250* ms^{-1}*).*

It is important to note that if the force on the transducers changes, this maximum frequency changes also as shown in Figure 5.10. This shows the importance of a good coupling between the transducers and the surface; a poor coupling used with the correct frequency will provide incorrect results.

5.5 Frequency tuning on pipe

Frequency tuning with the axis-symmetric mode T(0,1) was performed as an important and first step of each experiment (Liu et al., 2006). Here frequency tuning was used to find a proper frequency for detecting the pipe end and defect clearly. The tests were carried out on a 3.4 cm diameter steel pipe with 5mm wall thick. Tests were performed with one transmitter and one receiver, 100 mm apart, with the transmitter placed 170mm away from one end of the pipe, and both were placed on the left side of the

pipe as shown in Figure 5.4 in section 5.2. When transducers are placed on pipe and incident wave was generated as described in Section 5.2, the echoes from the end pipe and direct arrival expected to receive from the receiver. Figure 5.12 shows five main propagation paths that may occur during the test; the reflections generated by these paths are labeled on in Figures 5.12 and 5.13.

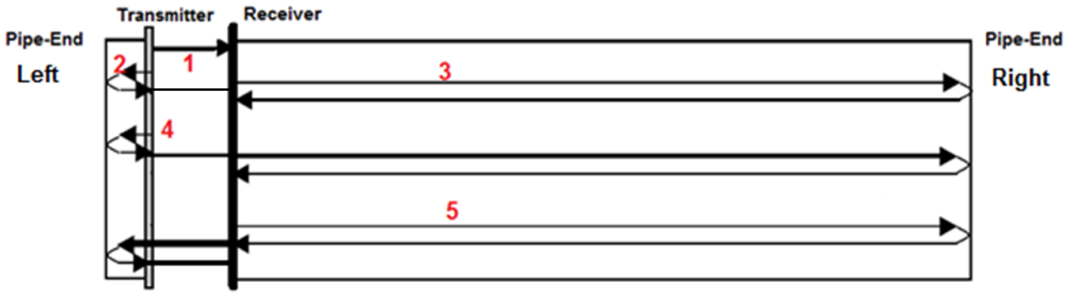

Figure 5.12. *Schematic diagram shows five wave propagation path in the pipe for direct and pipe-end echoes. First transmission is from direct arrival between receiver and transmitter and the second one is the pipe-end echo from the left side. The third and fourth echoes come from the right pipe-end and the fifth echo is from the left pipe-end.*

Defect responses are frequency-dependent so it is necessary to find the correct frequency in order to find the defect and have the maximum amplitude response. Also high frequency guided waves are utilized when sensitivity to small defects is important. In general, guided waves in the frequency range of 100 kHz - 800 kHz were used to identify defects as small as 0.1% of the pipe's total cross-sectional area (CSA). But Low frequency guided waves are used for inspecting larger distances where sensitivity to small defects is not a main concern. The frequency range of 20 kHz - 100 kHz can be used to inspect defects as small as 5% of the pipe's CSA (Demma, 2003). This report is concerned specifically with pipes with a 3.4 cm diameter with small size defects (0.1% CSA), so a higher frequency is preferable. However, after tests with different frequency which shows in Figure 5.13, understood higher frequencies (60 kHz – 200 kHz) produce stronger reverberations; this does not allow us to see the defect's reflection (This will

discuss in Section 5.9). The reason why this reverberation comes will discuss in this section.

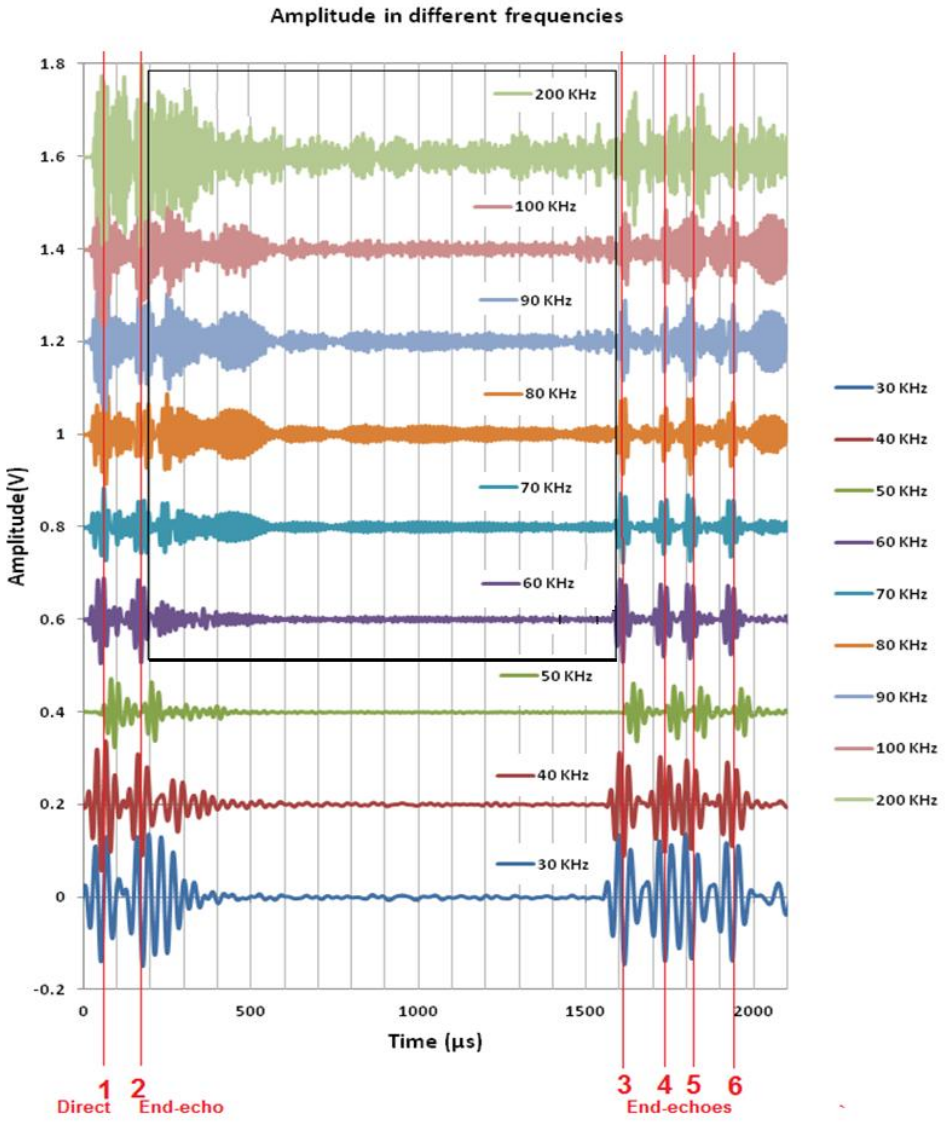

Figure 5.13. *Echoes amplitude for different frequencies. The tests were done on a 3.4 cm diameter steel pipe with 5mm wall thick, with one transmitter and one receiver, 100 mm apart, with the transmitter placed 170mm away from one end of the pipe, and both were placed on the left side of the pipe. Direct arrival is the first wave and then the pipe end echoes are appeared and between the first end echo and second end echo in frequency higher than 50 kHz the reverberation appeared. The tests were done on a clean pipe without any defects(In each tests signal amplitude was add up with a constant number).*

From research was done, found that when the single piezoelectric shear transducer attaches to the pipe it will excite longitudinal and flexural modes as well as torsional modes, however the array of elements were attached around the pipe (axially symmetric position recommended) to suppress the non axially symmetric F(m,n) modes (Alleyne and Cawley, 1996).

In the following test three different frequencies below first torsional non-dispersive mode (below 350 kHz) have chosen to clarify where this reverberation comes from. In Section 5.6.1 the reverberation and noise level are compared in different frequencies which show by increasing the frequency the reverberation and noise have increased. The dispersion graphs used to describe each mode's velocity variation with frequencies on 34 mm outer diameter with 5 mm thickness steel pipe ($c_s = 3309 \mathrm{ms}^{-1}$).Basically, the group velocity dispersion curves was used to find each mode wave velocity and consequently the effects of different modes on received signal reverberation.

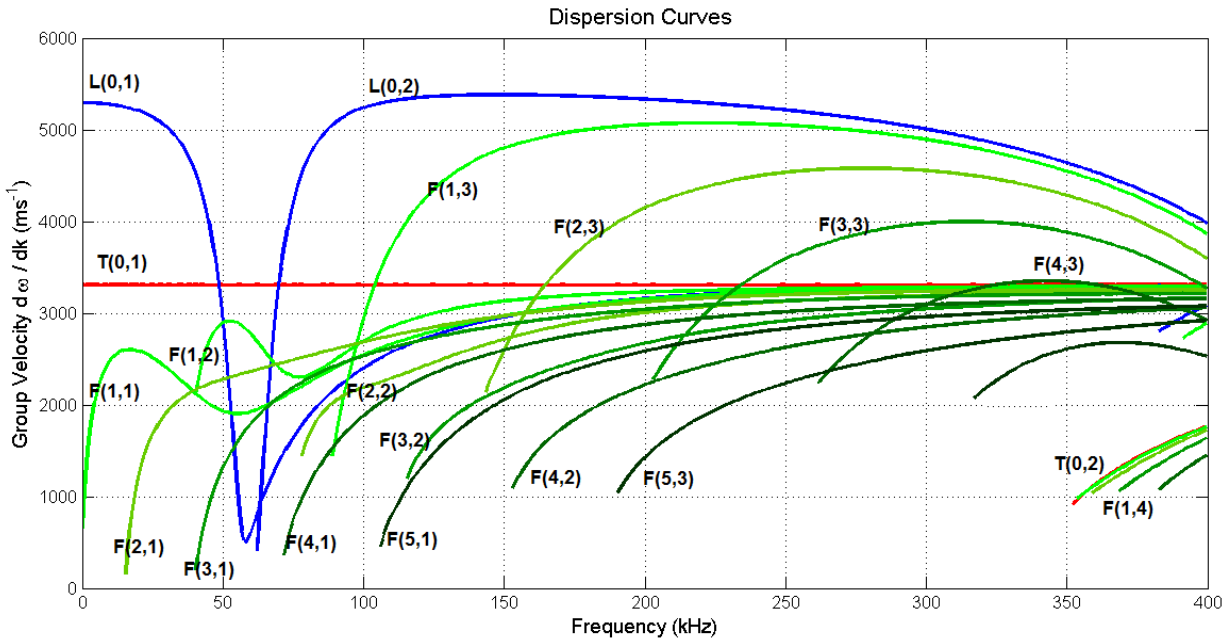

Figure 5.14. *Group velocity dispersion curves for steel pipe (Outer diameter: 34 mm and 5mm wall thickness)(Source: PCDISP MATLAB scripts written by Seco and Jimenez (2012)).*

The dispersion curves shown in Figure 5.14 shows modes propagate at 50 kHz, 100 kHz and 200 kHz. For each propagating mode time travel along the pipe was calculated as shown at Table 5.1. For example at 50 kHz, T(0,1), L(0,1), F(1,1), F(1,2), F(2,1) and F(3,1) propagated at different group velocities. The first echo from the pipe end should travel 440 mm , at a group velocity of 3309 ms^{-1} when T(0,1) is excited and the echo would have appeared at 133µs, but the other modes are slower and appear after that as described in Table 5.1.

	50 kHz			100 kHz			200 kHz		
Modes	**cg (ms^{-1})**	**Predicted travel time along 440mm (µs)**	**Predicted travel time along 5380mm (µs)**	**cg (ms^{-1})**	**Predicted travel time along 440mm (µs)**	**Predicted travel time along 5380mm (µs)**	**cg (ms^{-1})**	**Predicted travel time along 440mm (µs)**	**Predicted travel time along 5380mm (µs)**
T(0,1)	3309	133.0	1625.9	3309	133.0	1625.9	3309	133.0	1625.9
L(0,1)	2700	163.0	1992.6	2350	187.2	2289.4	3150	139.7	1707.9
L(0,2)	-	-	-	5300	83.0	1015.1	5250	83.8	1024.8
F(1,1)	1990	221.1	2703.5	2500	176.0	2152.0	3150	139.7	1707.9
F(1,2)	2700	163.0	1992.6	2700	163.0	1992.6	3200	137.5	1681.3
F(1,3)	-	-	-	2990	147.2	1799.3	5100	86.3	1054.9
F(2,1)	2250	195.6	2391.1	2700	163.0	1992.6	3050	144.3	1763.9
F(2,2)	-	-	-	2200	200.0	2445.5	3000	146.7	1793.3
F(2,3)	-	-	-	-	-	-	4300	102.3	1251.2
F(3,1)	1300	338.5	4138.5	2500	176.0	2152.0	3010	146.2	1787.4
F(3,2)	-	-	-	-	-	-	2550	172.5	2109.8
F(4,1)	-	-	-	1880	234.0	2861.7	2700	163.0	1992.6
F(5,1)	-	-	-	-	-	-	2500	176.0	2152.0
F(5,2)	-	-	-	-	-	-	1400	314.3	3842.9

Table 5.1. *Group wave velocity and time travel of different modes in different frequencies.*

After calculating all mode travel times they were compared with the received signal from the receiver (Figure 5.15) to find how reverberation match with the unwanted modes (here longitudinal and flexural). Figure 5.15 shows the received signal at 50 kHz when one transmitter and one receiver were used, they were placed in front of each other in 0°. In figure 5.15 the unwanted modes such as L(0,1) and F(1,2), F(2,1), F(1,1), L(0,1) and F(1,2), F(2,1) and F(1,1) are found match with the unwanted waves in results.

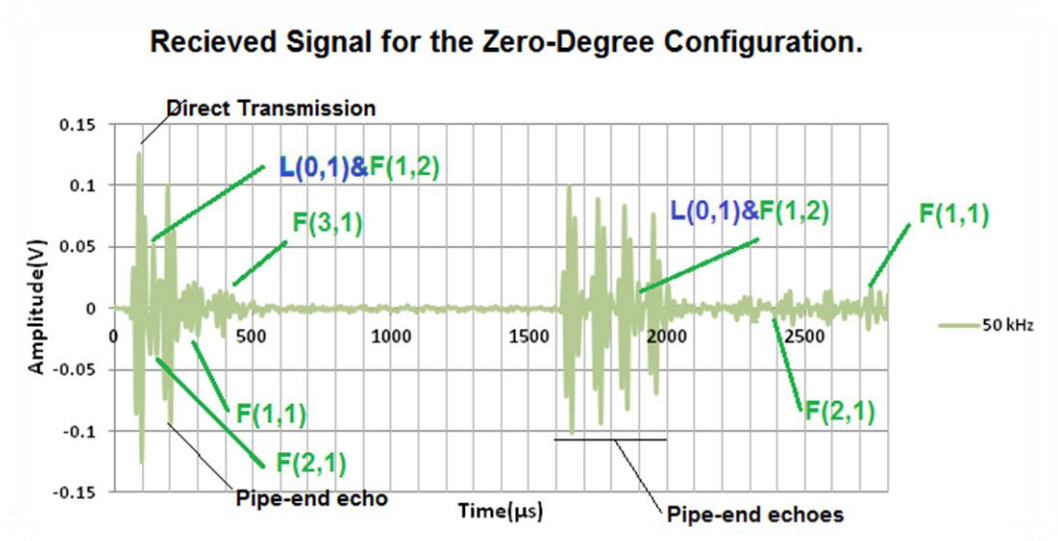

Figure 5.15. *Received signal for the zero-degree configuration at 50 kHz.*

Table 5.1 and Figure 5.15 are shown each longitudinal and flexural modes. As mentioned by Alleyne and Cawley (1996) increasing the number of element will suppress the flexural modes; tests were carried out by using 16 different receiver positions axially around the pipe (for one receiver used) and finally the average is presented. Figure 5.16 shows that the flexural and longitudinal modes amplitudes are decreased dramatically when 16 receivers arranged 22.5° around the pipe. The unwanted modes amplitude decreased dramatically which is seen in Figure 5.16.

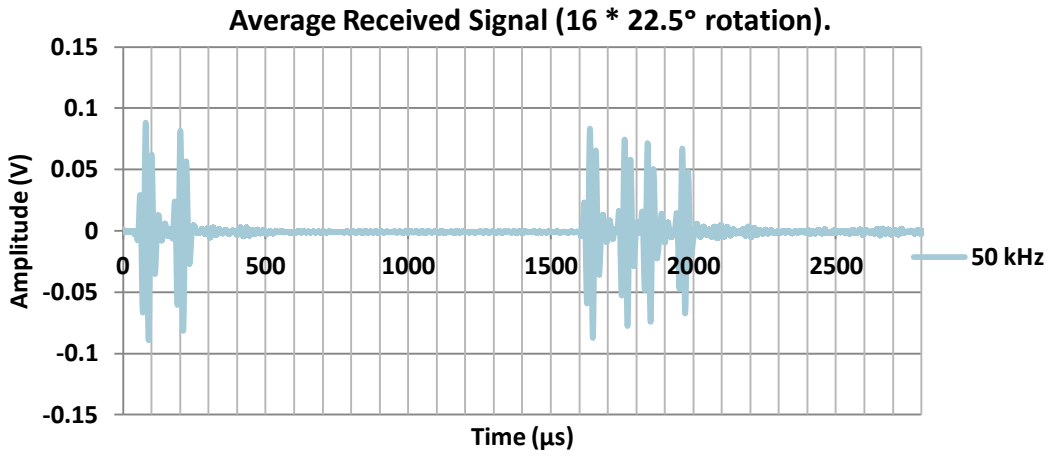

Figure 5.16. *Average received signal around the circumference of the pipe, obtaining by averaging signals when receiver attached at 16 different positions (each 22.5° apart) at 50 kHz.*

When the frequency increases to 100 kHz and 200 kHz, it is clear from Figure 5.13 and Table 5.1 that the number of non axially symmetric modes has increased and as a result the received signal displays signal from many different modes. In this case using an array of transducers and receivers around the pipe will suppress the unwanted modes.

To summarize, in order to use higher frequencies a number of elements are necessary to reduce the generation of unwanted modes. Here two modules were available to place transducers on the pipe, hence a lower frequency (50 kHz) was chosen to reduce the generation of unwanted modes. In Section 5.8 the impact of using low frequencies on finding small defects is described.

5.6 Wave velocity measurements

5.6.1 Shear Horizontal (SH) and longitudinal wave velocity measurements on plates

Piezoelectric transducers can generate both shear Horizontal (SH) and longitudinal waves on plates. The position of the transducer for each transmission case is different; to generate shear horizontal waves, the transducers should be placed so that the waves propagate in the same direction for both transducers, and particle motion is

perpendicular to the wave propagation. This case is shown in Figure 5.17. One transmitter and one receiver were used to measure the direct arrival travel time from the transmitter to the receiver. Tests were carried out in two different materials (galvanized mild steel and stainless steel plates) for a variety of transducer distances to find the shear velocity for each material.

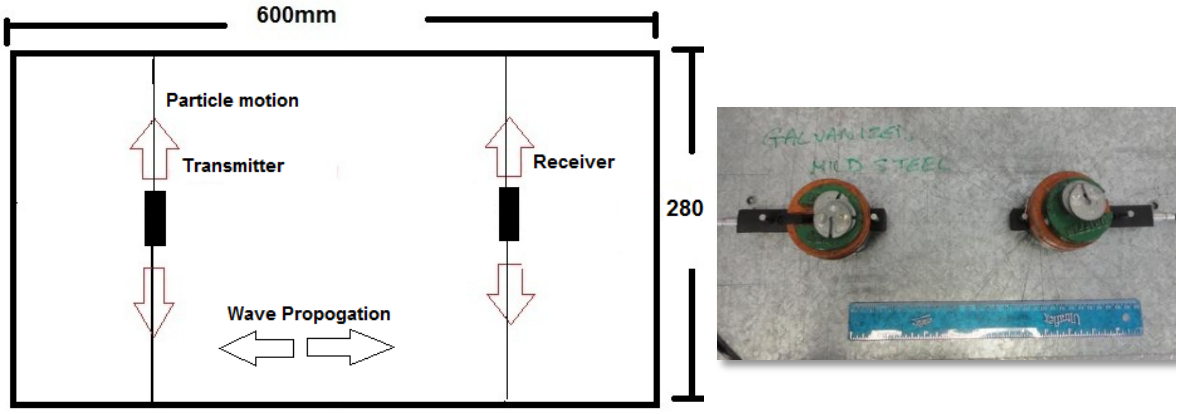

Figure 5.17. *Shear horizontal propagation and the piezoelectric receiver and transmitter setup. The image on the right shows the position of two modules with the weights above.*

To achieve the results shown in Figure 5.18, a function generator generated tone bursts of two cycles with a 10 Hz burst rate with 18 Vp-p voltages (Open circuit output of voltage connected to the transducers) and a frequency of 200 kHz. The power amplifier used a 70dB gain with 1MHz and 100 kHz upper and lower filters to amplify the signal at the receiver.

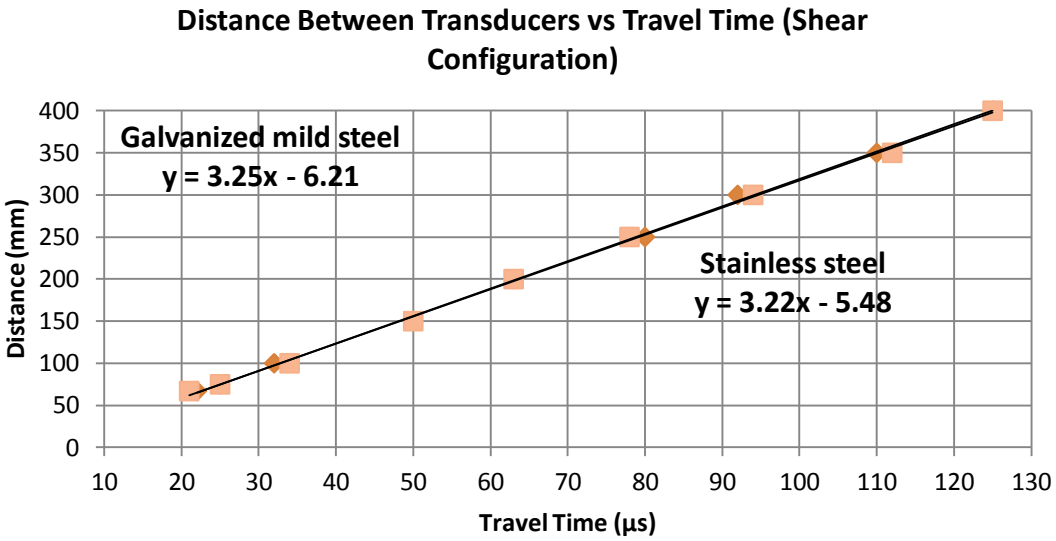

Figure 5.18. *Shear horizontal wave velocity (Distance of transmission / Travel time) results for stainless steel and galvanized mild steel plate. Least squares regression was used to estimate the slope and standard error in the slope.*

The results in Figure 5.18 show that the shear velocity in galvanized mild steel is $3255 \pm 38\ \mathrm{ms}^{-1}$ and is $3222 \pm 41\ \mathrm{ms}^{-1}$ in stainless steel.

To generate longitudinal waves, the transmitter's and receiver's wave propagation direction match; however in the case that particle motion is parallel with this direction as shown in Figure 5.19. Again, one transmitter and one receiver are used to measure the direct signal travel time for varying distances. Tests with the same parameters as the shear configuration tests were carried out in the longitudinal configuration to find the longitudinal velocities for each material.

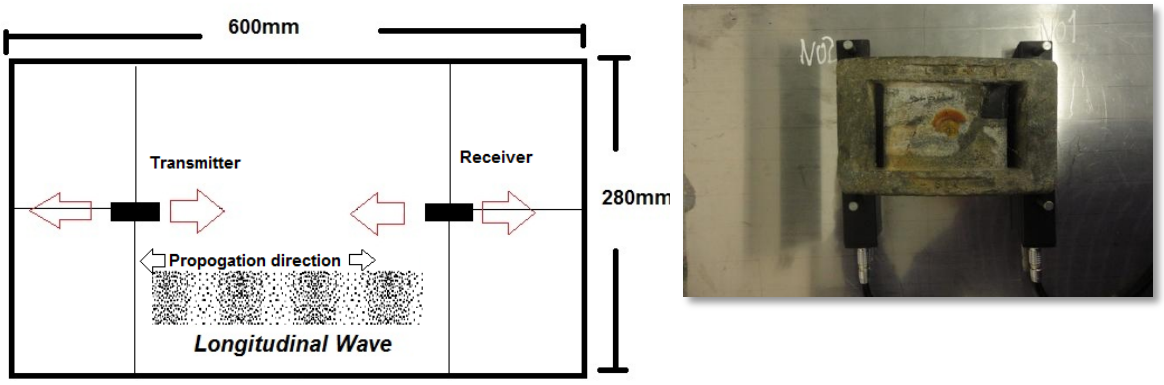

Figure 5.19.*Transducer setup for the longitudinal propagation test. The image on the right shows the position of two modules with the weights above.*

The same electrical setup and excitation signal used in the shear test was applied to the transducer. The results in Figure 5.20 show that the longitudinal velocity in galvanized mild steel is $5396 \pm 122\ \mathrm{ms}^{-1}$ and is $5262 \pm 87\ \mathrm{ms}^{-1}$ in stainless steel.

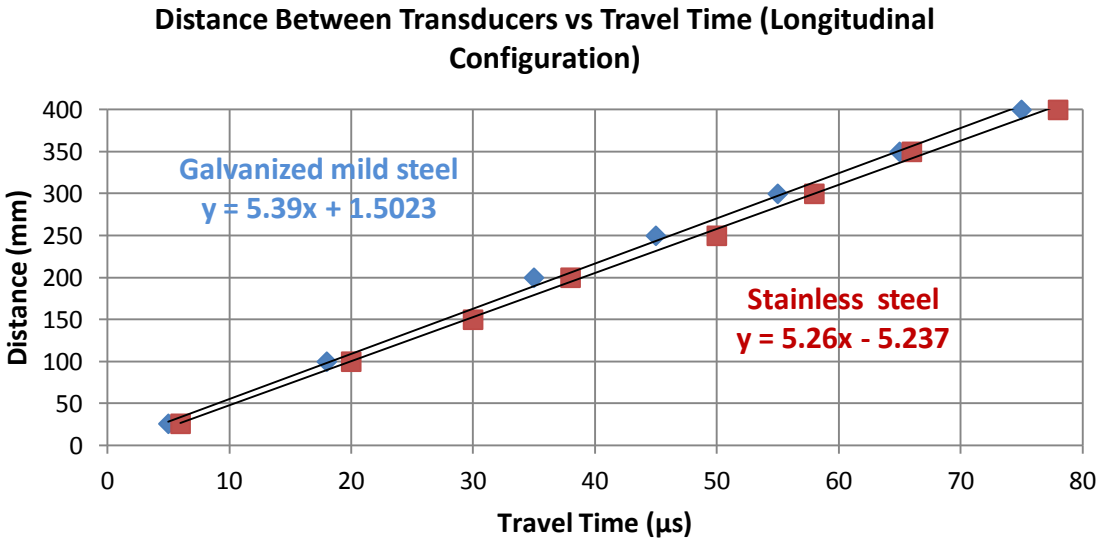

Figure 5.20. *Longitudinal wave velocity (Distance of transmission / Travel time) results for stainless steel and galvanized mild steel plate. Least squares regression was used to estimate the slope and standard error in the slope.*

5.6.2 Torsional wave velocity measurements on pipes

A similar process for finding the torsional wave velocity on the plate was used in the pipe case. The transducers were mounted in modules and were placed on the pipe to generate torsional waves. The first mode (known as T(0,1)) was generated. The group velocity was found by dividing the total distance travelled by the time taken, though it is important to note that for this non-dispersive mode the phase velocity and group velocity are equal. The same electrical setup and excitation signal were used as previously. The steel pipe under test had a thickness of 5 mm and an outer diameter of 34 mm. As shown in Figure 5.21, the transmitter was fixed close to the left end of the pipe and the receiver was moved along the length of the pipe; a measurement of the travel time of the wave is taken at various lengths. The tests were performed in a pipe without any defects so the pipe end reflection is also a pure T(0,1) which travels with an axial phase velocity equal.

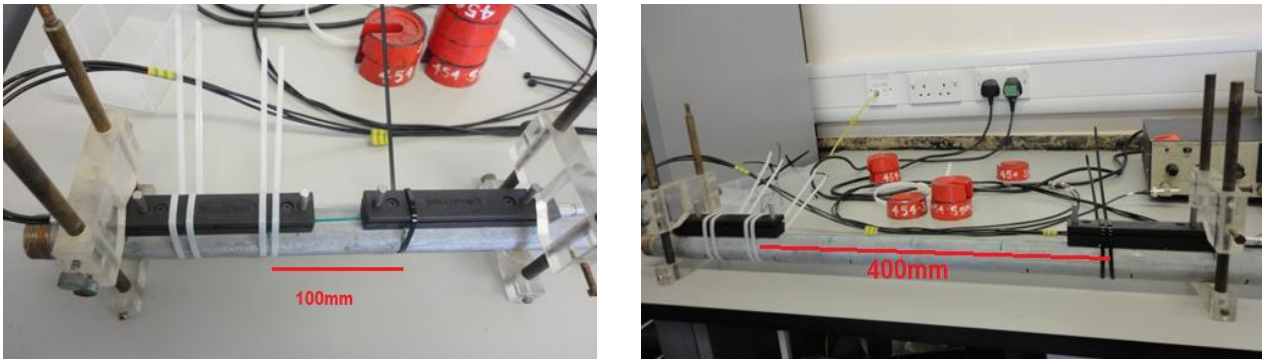

Figure 5.21. *Transducer configuration for the pipe case.*

In Figure 5.18, the travel time of echo reflected from the far end of the pipe as well as direct signal were used to find the shear velocity. The shear velocity calculated using just the direct response was $3309 \pm 11\ \mathrm{ms}^{-1}$.

5.7 Transmitter and receiver position

From previous research it is known that when piezoelectric transducers vibrate, they generate waves which can be sent in all directions, though the strength of the vibration tends to be strongest in one direction. This is shown by the zero-degree line of the left transducer (transmitter) in Figure 5.22. Likewise, the receivers will have directionality so that their response varies with the angle of the transmitting wave. Drawing from this, it is clear that the angle of the receiving transducer (with respect to the transmitter) will affect the amplitude of the output. Hence an experiment was devised to find this dependency.

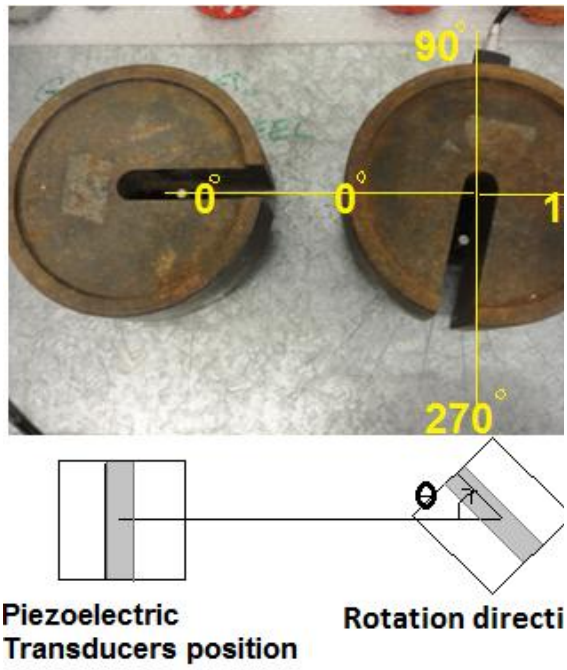

Figure 5.22. *Experimental setup and piezoelectric position (Modules are hidden bellow weights).*

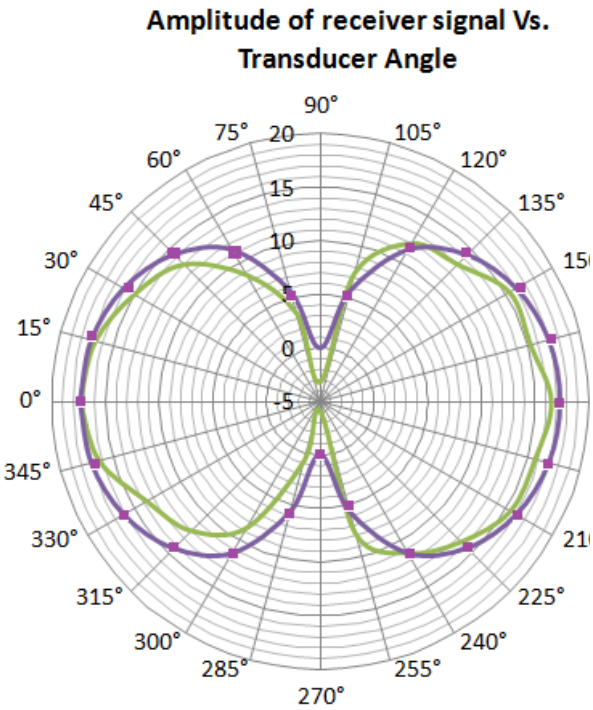

Figure 5.23. *Amplitude (dB re 1V) of receiver signal vs. transducer angle. The 'line' represents what was measured and the 'line with points' expresses the theory due to the constrains of plotting points on polar graph in Excel.*

In order to investigate the above, the transmitter was kept at a constant position and the receiver was rotated in angle by fifteen degrees (Figure 5.22.). A measurement of the received amplitude was taken, and the receiver was rotated further, until an entire rotation had been completed. This experiment was repeated five times and the results were averaged to produce the graph shown in Figure 5.23.

These results were obtained with the following sending parameters: frequency = 200 kHz, amplitude = 18V p-p (Open circuit output of voltage connected to the transducers), transmitter spacing = 200 mm. These results show that the amplitude is greatest at 0° and 180° of rotation, and least at 90° and 270°. This is because the receiver detects the vibration in a particular direction; when the receiver axis is perpendicular to the in crossing direction the signal, strength is greatly reduced. Another important point to note is that the output is approximately symmetrical. Furthermore, since this experiment is conducted at the centre of a plate, reflections from the plate edges will not interfere with the results. In Figure 5.23, the 'line' represents what was measured and the 'line with points' expresses the theory due to the constrains of plotting points on polar graph in Excel. The theory considers that the cosine of the angle of the receiver determines the strength of the received signal. However, the experimental results differ from this due to factors that have already been discussed (Section 5.5).

Once an understanding of how piezoelectric transducers generate shear waves had been obtained, experimental work was carried out on the pipe to find a suitable position for the transducers. The different transducer configurations that were examined are shown in Figures 5.24, 5.25 and 5.26. The traditional commercial approach uses an array of transducers around the pipe; this works via the pulse-echo system with the same transducer to transmit and receive. In order to enhance the echoes from the end of the pipe and from the defect, the idea of using two transducers in phase was considered (as shown in Figure 5.24 and Figure 5.27); the constructive interference would improve this reading. The original method required the use of only one transmitter and one receiver used at a frequency of 50 kHz. The advantages of this frequency have been discussed

previously in the section 5.5 of this report. Using two transducers (Figure 5.24) in phase was not practical since a frequency of 50 kHz in this case produces a wave with wavelength 66.2 mm; this cannot be achieved with the modules provided since the closest slot distance is 54 mm. Hence, one transmitter and one receiver were used in the layout shown in Figure 5.27. Placing the transducers at a 135° angle on the pipe as shown in Figure 5.26 was considered, but the difficulty of providing appropriate coupling without a collar provided unconvincing results.

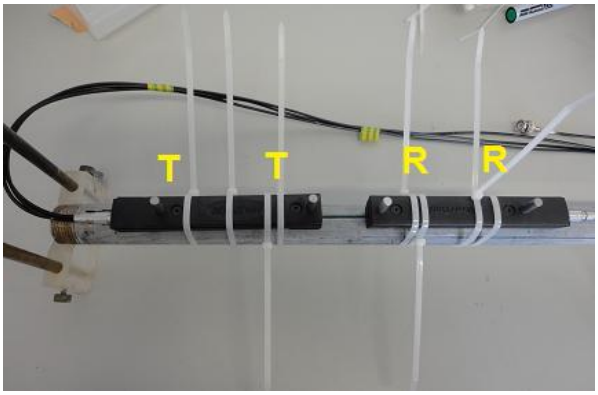

Figure 5.24. *Two transmitters and two receivers.*

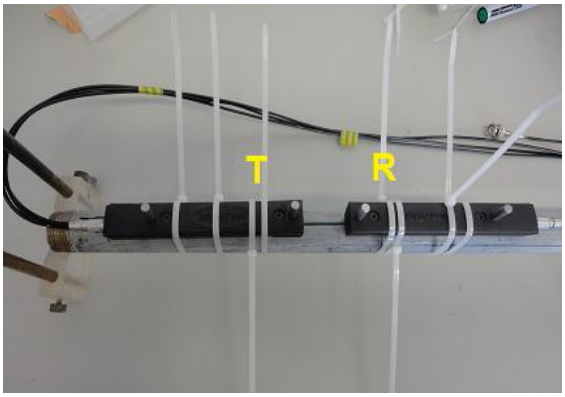

Figure 5.25. *One transmitter and one receiver.*

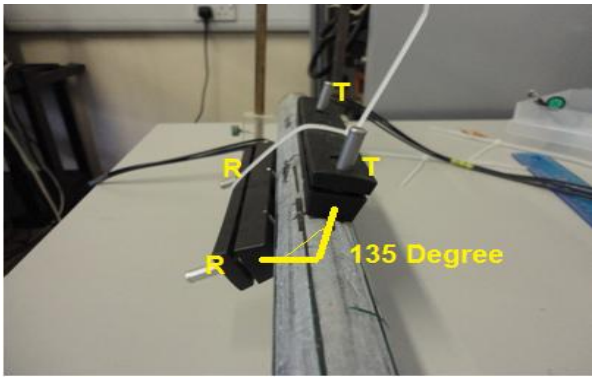

Figure 5.26. *Transmitters and receivers in the 135° position.*

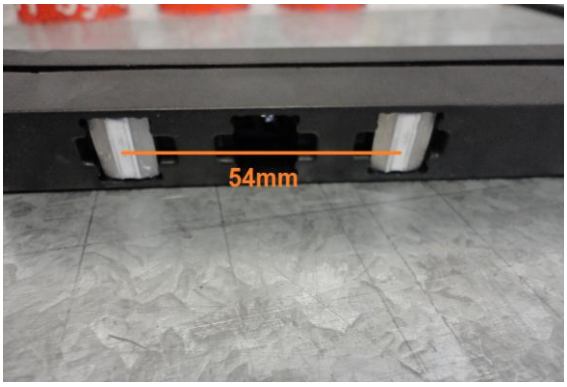

Figure 5.27. *Transmitter distance within modules is 54 mm.*

To summarise, finding defects with one transmitter and one receiver is used for this project. The receiver was moved around the pipe and the average received signal was

analysed. From the rotating-receiver experiment shown in section 5.8.1, the position of receiver should be always parallel to the receiver to get the maximum and most reliable amplitude.

5.8 Defect Finding

The lowest torsional mode T(0,1) at 50kHz was excited to detect defects in a 2912 mm long, 34 mm external diameter and 5 mm wall thick steel pipe using shear mode piezoelectric transducers. Three different artificial defects were generated in the pipe. The defects were added in steps, and are described in Table 5.2. The first two were simple radial drill holes, the third was a slot. These are shown in Figure 5.28. As mentioned in section 5.7 of this report, one transmitter and one receiver were used to generate and receive signals

Defect	Distance from transmitter (mm)	Distance from receiver (mm)	Depth	Circumferential length (mm)	Axial Length (mm)	Cross Section Area (CSA)
Defect#1	2270	2200	40%(2 mm)	4	4	1.7%
Defect#2	2270	2200	100%(5 mm)	4	4	4.39%
Defect#3	2270	2200	100%(5 mm)	20	4	8.3%

Table 5.2. *Description of all defects used in the study (All defects' circumferential position are equal to 0°).*

As shown in Figure 5.28, defects of different size were added to the pipe and tests were carried out to see if they could be detected. The first test was with defect #1 which was not found; even when averaging the results of rotating the receiver through 22.5° intervals. The reason for averaging the signals was discussed later in section 5.8.

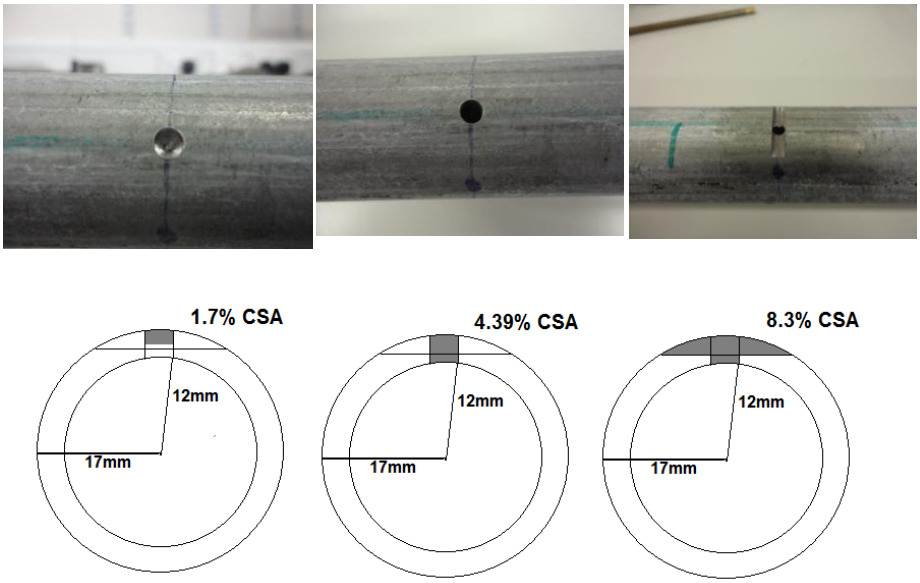

Figure 5.28. *Different defects tested on the pipe.*

At a frequency of 50 kHz, the wavelength is calculated as $\boldsymbol{\lambda}$ =66.2mm when C_s= 3309ms^{-1}. This signal wavelength is probably too large to find a small defect, hence for finding the defects as small as 4 mm length the frequency should increase. From section 5.5, the high reverberation is a problem for finding the small defects, so simply increasing the frequency doesn't solve this problem. Even for a through hole (defect #2), no detection was possible.

Defect #3 with a 20mm circumferential length and a 4mm axial length produced reasonable echoes (and hence successful detection) as shown in Figure 5.29. The reverberation level is 27.95 dB re 1mV (Calculated by finding standard deviation of reverberation level) and the normalized echo amplitude with respect to the echo from the end of the pipe is -19dB. In order to increase the sensitivity of the system, the signal of the receiver was averaged over the entire pipe circumference as it was rotated.

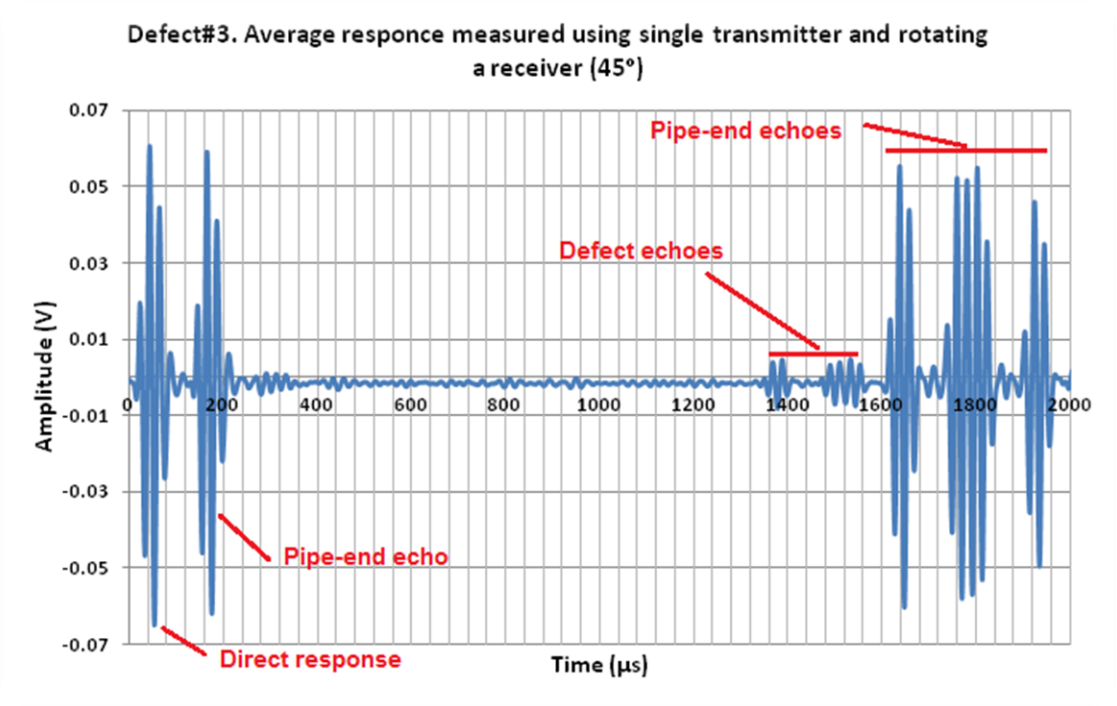

Figure 5.29. *The average response used to find defect #3 obtained by averaging over 8 circumferential position of the receiver for pipe with defect#3. The defect echo is identified at 1355µs.*

5.8.1 Average response measurement by rotating the receiver

Using the transmitter and receiver in different modules results in echoes off both directions of the pipe. Figure 5.30 shows the echoes received by the receiver when the transmitter vibrates, as well as their direction. In this Figure, middle numbers (1,2 and 3) show the echoes from the defect, the right and left numbers(1,2,3,4 and 5) are from the first direct transmission and the echoes due to the end of the pipe. The scale shows how far the defect is from the receiver and distance away from the ends of the pipe.

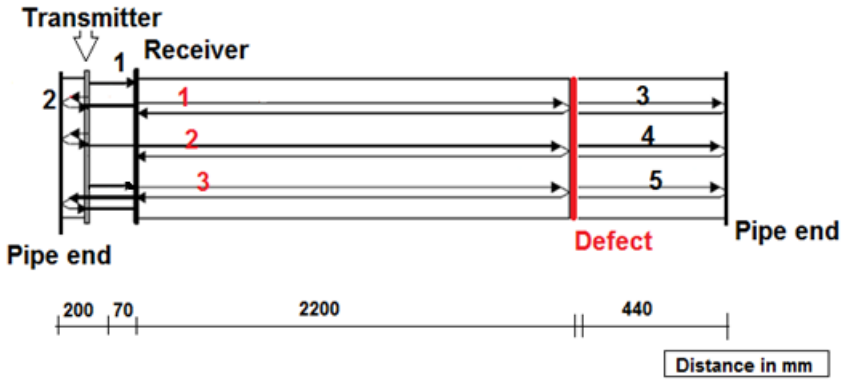

Figure 5.30. *Echo Schematic. One transmitter and receiver are placed on the pipe and the echoes from pipe end and defect as well as the direct arrival between transmitter and receiver is shown. The transmitter and receiver are 70 mm away from each other and the transmitter is 200 mm from the left end of the pipe.*

In this case the transmitter and receiver are 70 mm away from each other and the transmitter is 200 mm from the left end of the pipe. By using CS = 3309 ms^{-1}, the location of the defects can be predicted. Table 5.3 produced the travel time for the first direct transmission, defect and pipe ends. The deviation of the experimental results from the theory is 1 % error.

Type	Distance (mm)	Calculated travel Time (µs)	Average travel time from results (µs)
Direct transmission	70	2	18
Echo from left end	470	142	136
First echo from defect	4470	1351	1349
Second echo from defect	4870	1472	1470
Third echo from defect	5010	1514	1517
First echo from end	5354	1618	1618
Second echo from end	5754	1739	1738
Third echo from end	5894	1781	1781
Forth echo from end	6294	1902	1903

Table 5.3. *Compare the results from theory and experiments.*

5.9 Noise and reverberation analysis

Signals with frequencies of 50 kHz, 100 kHz and 200 kHz combined with a bandpass filter were applied to the transmitter in turn. The resulting signal to reverberation ratio (echo signal from defect#3) and reverberation were measured and tabulated in Table 5.4 below.

Frequency	Echo signal to reverberation ratio(dB)	Reverberation (dB re mV)
50 KHz	8.9	3.5
100 KHz	6.36	23.5
200 KHz	5.1	27.9

Table 5.4 *Signal per noise ratio and reverberation level in different frequencies.*

From the Table 5.4, it can be seen that as frequency increases the reverberation level increases. High reverberation level at high frequency was the problem that caused the defect to be lost in reverberation as shown in Figure 5.31. When the small defect (Defect #1) was studied, it was not clear where the echoes were.

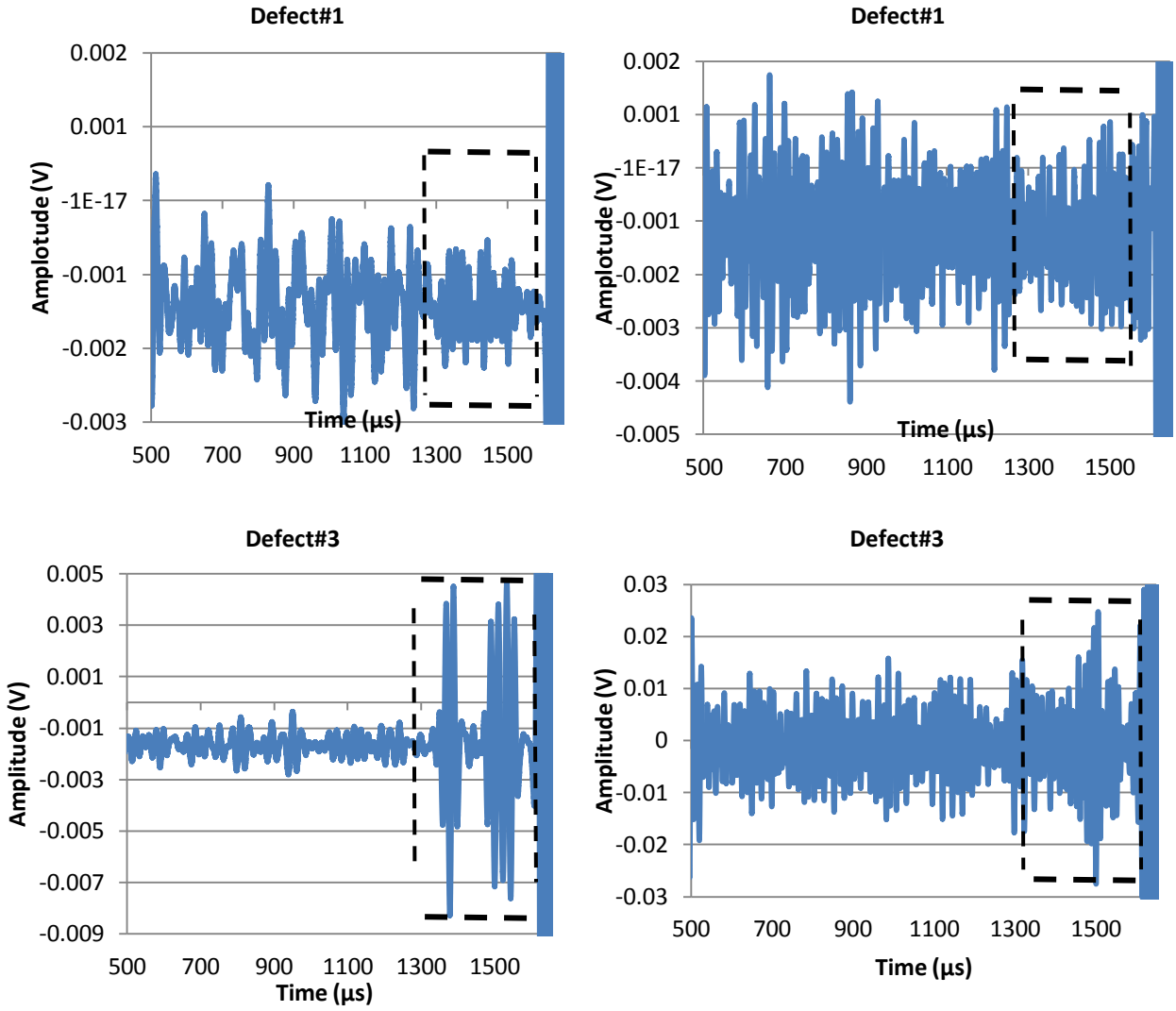

Figure 5.31. *Average response measured using a single transmitter and rotating the receiver at 50 kHz and 100 kHz for defect #1 and defect #3. Left top: Average response measured using single transmitter and rotating a receiver each 22.5° at 50 kHz for defect#1. Right top: Average response measured using single transmitter and rotating a receiver each 22.5° at 100 kHz for defect#1. Left bottom: Average response measured using single transmitter and rotating a receiver each 45° at 50 kHz for defect#3. Right bottom: Average response measured using single transmitter and rotating a receiver each 45° at 100 kHz for defect#3.(Predicted defect echoes location is shown in a dotted line box).*

Figure 5.31 shows the defect echo just before the echo due to the end of the pipe. The dashed boxes show where the echo should be. For the smaller defect (#1), it is not obvious where the defect is regardless of frequency; this is likely due to the reverberation problem. The difference is clear for the lower frequency and larger defects, however.

5.10 Defect reflection characteristics

The tests were run with one transducer and reflect from the defect is in different direction and modes. In general, when the defect is symmetric there is a mode conversion to other symmetric modes which have near wave velocity with T(0,1) will appear and when the reflection is non axially symmetric the non axially symmetric mode (Flexural) as well as other mode will be expected to appear. Figure 5.32 shows clearly when one transmitter with array of receivers used and the reflection signals from the defect.

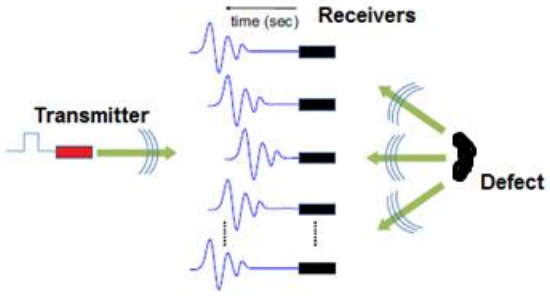

Figure 5.32. *Defect reflections in different angels from defect which received by number of receivers.*

The reflections delay time from one receiver can be calculate and it is useful for other methods like focusing method. In focusing method (Figure 5.33) the first array of receiver receive the signal and the defect position and characteristic will be understood then other methods like Angular profile tuning and signal based focusing can be applied (To Kang, Accessed: Aug 2011). The transmitting then is applied by considering the delay

time which calculated to have focus of energy of all transducers on defect position, this increase the amplitude of the echo from the defect.

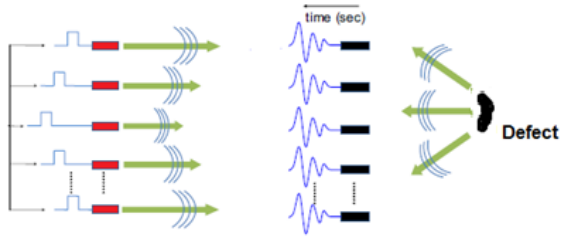

Figure 5.33. *Defect reflection in different angle when focus method is applied.*

Test were carried out by finding the amplitude change of the echo when the receivers are placed in different position around the pipe. As mentioned in Section 5.7 one transmitter placed fix on a pipe and the receivers are rotating for doing averaging of the signal from receivers.

It was predicted that maximum amplitude is achieved when the transmitter and receiver are in line with the defect (i.e. the zero degree case). However, Figure 5.34. above shows that this occurs in the 45° case, which the reason was not clear. Furthermore, the polar graph shows that the maximum amplitude is symmetric. This is due to the fact that defect #3 itself is symmetric. It is also worth noting that the peak amplitude is minimal in the 180 degree case because it is the farthest distance that the signal has to travel from the defect.

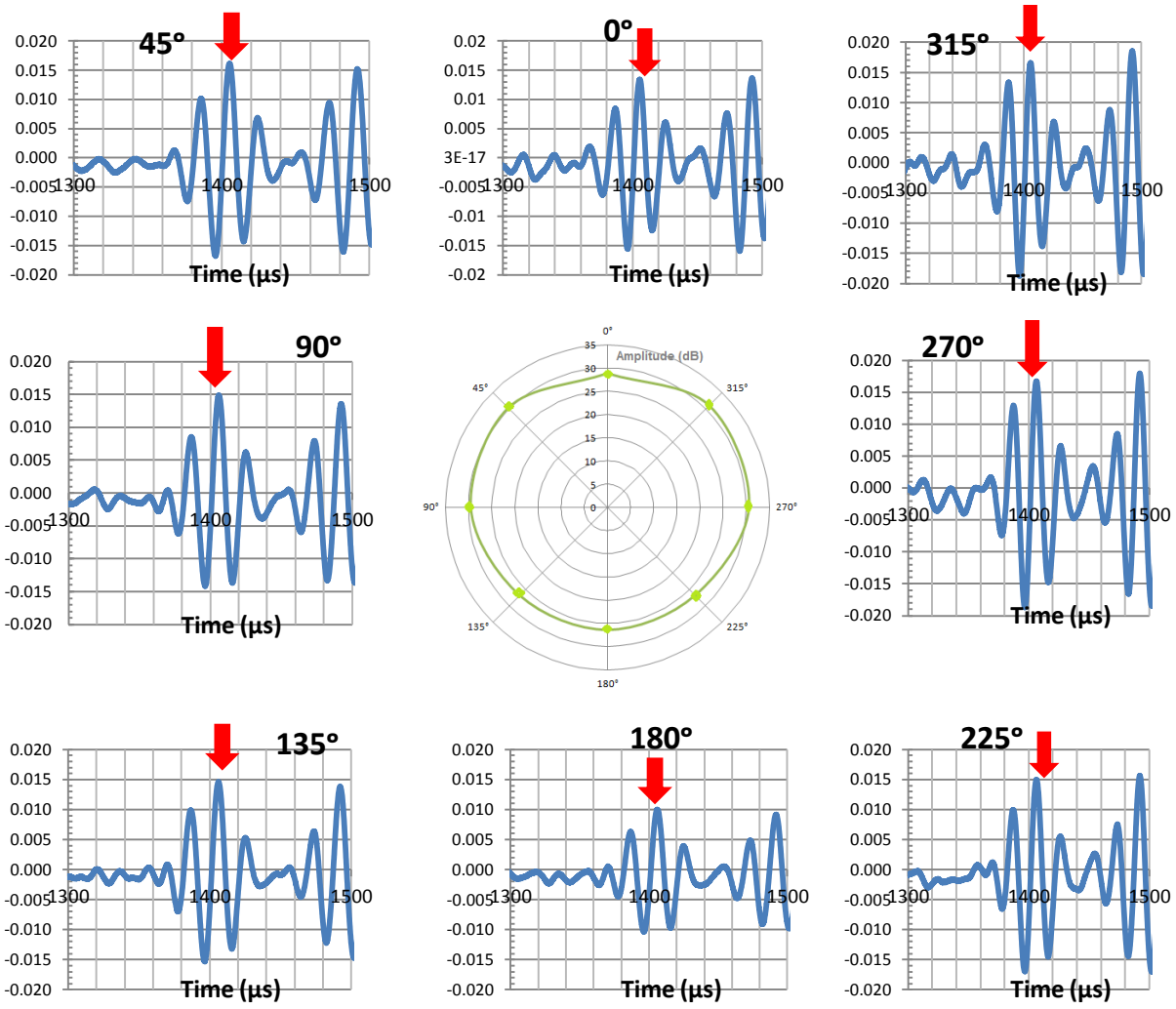

Figure 5.34. *Amplitude (V) of defect echo against time for each receiver angle. The central polar graph shows the maximum amplitude (dB re 1V) as a function of the receiver angle.*

5.11 Experimental conclusion

Tests were carried out on plate and pipe, in each case different results were compared. The challenge of high reverberation level at high frequency was presented from the dispersion curve as a result of unwanted modes (Longitudinal and Flexural). Using just one transmitter and receiver was not appropriate to suppress the unwanted modes. Rotating the receiver around the pipe and average the signals suppressed some of the unwanted modes. In this condition, defect size 8.3% CSA found by using one

transmitter and one receiver locate 0° in front of each other, when the torsional wave T(0,1) at 50 kHz generated.

Section 6

6 Conclusions

6.1 Main finding of this thesis

As previously discussed, ultrasonic guided waves were studied to help create MATLAB scripts. These scripts found the phase and group velocities of Shear Horizontal (SH) waves on plates with varying thickness. After this, the phase velocity of torsional, longitudinal and flexural modes at lower frequencies were implemented on pipes with varying diameters and wall thicknesses. Difficulties of this work were illustrated in Section 3.4.7.

The experimental tests were performed on a steel pipe with a diameter of 3.4 cm a wall thickness of 5 mm. From three different defect sizes, a defect of 8.3% CSA in size was found by using one transmitter and one receiver on the pipe, transmitting at a frequency of 50 kHz. Increasing the frequency caused an increase in the reverberation level when only two transducers were used. In order to decrease the reverberation level at higher frequencies, increasing the number of receivers and transmitters in order to suppress the unwanted modes were described. Two transducers were used in this project, and it was found that by rotating the receiver around the pipe allowed the defects to be found after processing the received signals (after taking measurements at discrete angles, and averaging the results). In averaging the signal, some modes cancelled each other out, leaving the resultant signal with a low reverberation level.

6.2 Future work

As is often case in projects such as this, time and money and the management of them is of great importance. If time and money were less limiting in this project, this section describes how this work can be taken further.

Firstly, the MATLAB scripts could be improved in a number of ways. The effect of losses (due to pipe contents and its underground surroundings) in the pipe system could be accounted for in the MATLAB scripts. The implementation of a two-layered pipe in the MATLAB script could help to expand the scope of research for this project. If more time was available for executing the script, the accuracy of the root finder could be improved by reducing the step size.

Secondly, a larger number of transducers would help to further this investigation. The reflection from the defect and pipe end has been shown to increase with frequency, though this has problems as described in Section 5.5. To solve these problems (including detection of smaller defects), a larger number of transducers is recommended. For a pipe with 3.4 cm diameter, it is estimated that eight transducers would be required if the frequency was chose 100 kHz. Hence, the possibility of finding smaller defects by increasing the frequency and the number of transducer can be examined.

Finally, in this project the circumferential defects were found. The feasibility of using torsional waves for finding longitudinal defects can be studied. Also, as described in Section 4.3 the reflections from asymmetric defects are a combination of asymmetric and axially symmetric modes. This further influences the reverberation of the system; another point for further investigation.

References

Advanced inspection solution, (1999). Innospection Ltd. [online] (Available at:< http://www.innospection.com/) ,(Accessed 10 May 2010).

Alleyne, D. N. and Cawley, P. (1996)' The excitation of Lamb waves in pipes using dry-coupled piezoelectric transducers'.,J NDE, 15:11–20.

Alleyne, D.N., Cawley, P. (1997) Long range propagation of lambwaves in chemical plant pipework, Materials Evaluation 504–508.).

Alleyne, D.N., Pavlakovic, B., (2000)' Rapid longe range inspection of chemical plant pipework using guided waves', Guided ultrasonic Ltd, Dept Mechanical Engineering, Imperial College.

Breon, L.J., Van Velsor, J.K. and Rose, J.L. (2007), 'Guided wave damage detection tomography for structural health monitoring in critical zones of pipelines', *Materials Evaluation* 65. pp. 1215-1219.

Bosch R.W, Hubrecht, J, Bogaerts, W.F, Syrett, B.C. (2001), 'Electrochemical Frequency Modulation: A new electrochemical technique for online corrosion monitoring', *Corrosion science section* , vol.57, No.1.

Bullard, S.J., Covino, B.S., Russell, J. H., Holcomb, G. R., Cramer, S. D., and Ziomek-Moroz, M. (2002) 'Electrochemical Noise Sensors for Detection of Localized and General Corrosion of Natural Gas Transmission Pipelines', Albany Research Center,U.S. Department of Energy, Albany, DOE/ARC-TR-03-0002.

Bullard, S.J., Covino, B.S. Russell J. H., Holcomb, G. R., Cramer, S. D., and Ziomek-Moroz, M., (2003)' Laboratory Evaluation of an Electrochemical Noise System for Detection of Localized and General Corrosion of Natural Gas Transmission Pipelines', NACE International Corrosion conference San Diego.

Burch, S.F. and Collett, N.J. (2005)'Recommended Practice for The Rapid Inspection of Small Bore Connectors Using Radiography', *Oxfordshire: AEA Technology plc*.

Burd, J.F. and Smith, S. (2000) Corrosion detection and assessment in gas distribution pipes, *Insight* 42 pp. 85-87.

Carandente, R.,Cawlet, P., Lowe, M. (2011)'Guided wave testing of pipe: the influence of the shape of corrosion defects on the reflected signals' 5th Pan American conference for NDT, Cncun, Mexico.

Cawley, P. (2001), in: *Proc. Instit. Mech. Eng. Part l-J. Mater-Design and Applications*, 215 pp. 213-223 (doi: 10.1243/1464420011545058).

Challis, E., Phang, A. P. Y., Lowe, M. J. S. and Mather, M. L., (2008) 'A System for Magnetostrictive Transduction of Guided Waves in Fluid-Filled Pipes of Small Diameter', *Ultrasonics,Feroelectrics and Frequency Control*, vol. 55, pp. 1-13.

Corbin D., Willson E. , (2007),'New Technology for Real-Time Corrosion Detection'. Enviroline Monitoring Systems LLC,. Langdon, Alberta T0J 1X1, Canada.

Costello, S.B., Chapman, D.N., Rogers, C.D.F. and Metje, N., (2007) 'Underground asset location and condition assessment technologies', *Tunnelling and Underground Space Technology* pp. 524-542.

Davies, J.O.,(2008) 'Inspection of Pipes Using Low Frequency Focused Guided Waves', 2008, *A thesis submitted to the university of London for the degree of Doctor of Philosophy*.

Davies, J. and Cawley, P.,(2008) Long Range Guided Wave Inspection Usage – Current Commercial Capabilities and Research Directions.

Demma, A. (2003) 'The interaction of guided waves with discontinuities in structures,' Published PhD thesis. University of London.

Ditiri, J.J. (1994) 'Utilization of guided elastic waves for the charachterization of circumferential cracks in hollow cylindes', Pennsylvania 19111, 43.20Mv, 43.35.Cg, 43.35. Zc.

Fitch, H., (1963) 'Obseravation of Elastic-Pulse Propogation in axially Symmetric and Nonaxially Symmetric Longitudinal Modes of Hollow Cylinders.

Gatts b, C.E.N. , da Silva a, Rebello J.M.A. 'The use of ultrasonic guided waves and wavelets analysis in pipe inspection' .

Gazis, D.C., (1985) 'Three dimensional investigation of propogation of waves in hollow circular cylinders. I. Analytical foundation. J.Acoust.Soc.am., 31:pp568-578.

Gloria, N.B.S., Areiza, M.C.L., Miranda, I.V.J. and Rebello, J.M.A., (2009) 'Development of a magnetic sensor for detection and sizing of internal pipeline corrosion defects', *NDT & E International* 42 (2009) pp. 669-677.

George, K., T. Hong and W. P. Jepson H. B. Wang, (2000) 'Corrosion Monitoring of yop Flow in Wet Gas Environment', in *Corrosion*, Ohio University, Athens, OH, p. 1_16.

Graff, K.F., (1991), Waves motion in elastic solids, Oxford University Press [On line] . Available at:http://books.google.co.uk/books?id=5cZFRwLuhdQC&printsec=frontcover&dq=Wave+motion+in+elastic+solids+Graff&hl=en&sa=X&ei=q972T6TlMYrY8APJ5OS5Bw&ved=0CDcQ6AEwAA#v=onepage&q=Wave%20motion%20in%20elastic%20solids%20Graff&f=false (Accessed: 12 July 2011) .

Guided Wave Analysis LLC., (2012). Guided wave systems. [Online](Available from: http://www.gwanalysis.com), (Accessed: 10 March 2011).

Guided ultrasonic ltd., (2012). Services.[Online] (Available from : http://www.guided-ultrasonics.com/public2012/?page_id=772), (Accessed: 1 April 2011).

Haig, A.G, Mudge, p., and Balachandran, W.,(2008)'Advanced Transducer Development for Long Range Ultrasonic Inspection Systems' Proceedings of the 2008 Conference for the Engineering Doctorate in Environmental Technology.

Hamasaki, Y. and T. Ide, (1995) 'A Multi-Layer Eddy Current Micro Sensor for Non-Destructive Inspection of Small Diameter Pipes,' in *The 8th International Conference on Solld-State Sensors and Actuators, and Eurosensors IX Stockholm, Sweden*, pp. 136-139.

Hu, X., Feng, X.,Zhou J., (2011)'Reflection charachteristics of guided waves in a pipe with a cirrcumferential crack', The 6th International workshop on advanced smart materials and smart thechnology.Dalian, C hina.

Khaled, K.F., (2008) 'Evaluation of electrochemical frequency modulation as a new technique for monitoring corrosion and corrosion inhibition of carbon steel in perchloric acid using hydrazine carbodithioic acid derivatives', Springer Science + Business Media B.V.

Lin M, Qing, Kumar, Shawn, Beard, J., (2005) Smart Layer And Smart Suitcase For Structural Health Monitoring Applications, Acellent Technologies, Inc, marklin@acellent.com;

(408) 745-1188; http://www.acellent.com; Acellent Technologies, Inc., 562 Weddell Drive Suite 4, Sunnyvale, CA 94089 .

Liu, J.M., Davis, C.E., Regin, T.M., Brophy, J., (2011)' Monitoring the growth of hidden corrosion discontinuities in a pipeline with complex geometry using torsional mode ultrasonic guided wave', *Materials Evaluation* 69pp. 393-400.

Liu, Z., He, C. Wu, B., Wang, X., Yang, Sh., (2006) 'Circumferential and longitudinal defect detection using T(0,1) mode excited by thickness shear mode piezoelectric element' ,Ultrasonic 44(2006) e1135-e1138.

Lord, W. and D. J. Oswald, (1972) 'Leakage Field Methods of Defect Detection,' in *International Journal of Nondestructive Testing.* pp. 249-274.

Lowe, M. J. S., Alleyne, D. N. and Cawley, P., (1998) 'Defect detection in pipes using guided waves'. Ultrasonics, 36:147–154.

Lowe M.J.S. and Cawley P., (2006)'Long Range Guided Wave Inspection Usage Current Commercial Capabilities and Research Directions'. Department of Mechanical Engineering, Imperial College London.

Lynch, A.J., (2009) 'Magnetic Flux Leakage Robotic Pipe Inspection: *Internal and External Methods*, Thesis Submitted'Master of Science.

Mekwi, W.R, (2001)'Iterative Methodes for Roots of Polynomials' A thesis submitted in Exeter college, University of Oxford.

Morison W.D., Cherpillod T., (2005) Solving common corrosion problems with Non-Intrusive Fiber Optic corrosion and process monitoring sensors. Middle East Nondestructive Testing Conference & Exhibition. Bahrain, Manama.

Napiah, M. N. B., Mukminin, M.A., (2009) Managing Integrity Of Feed Condensate Pipeline: On-Line Internal Corrosion Monitoring Via Electric Field Mapping (Efm) And Field Signature Methodtm (Fsmtm) Technique, Transmission Operations Division, Segamat, Johor, Malaysia.

Pavlakovic, B. and D.N. Alleyne, (2001) 'Rapid Long range Inspection of Chemical Plant Pipework Using Guided Waves,' in *Roma2000*, Guided Ultrasonics Ltd and Dept Mechanical Engineering, Imperial College, Exhibition Road, London, SW7 2BX, UK.

Plant integrity ltd., (2012). Teletest focus and mini tools. [Online](Available from: http://www.plantintegrity.com/teletest/index.jsp), (Accessed: 1 April 2011).

Plotnikov, A. And Clapham, L., (2002), Stress effects and magnetic nde methodes for pipeline inspection: a study of interacting defects,. Insight, 44:74-78.

Qing, X.L.P., Beard, S., Shen, S.B., Banerjee, S., Bradley, I., Salama, M.M. and Chang, F.K., (2009) 'Development of a real-time active pipeline integrity detection system, *Smart Materials & Structures'* ,Article number 115010 (doi: 10.1088/0964-1726/18/11/115010).

Rayleigh, J.W.S., (1945) The theory of sound. Dover publications, Inc. Newyork, N. Y. 10014. [Online](http://books.google.co.uk/books?id=Frvgu1wSFfUC&printsec=frontcover&source=gbs_ge_summary_r&cad=0#v=onepage&q&f=false)(Accessed :12 May 2012).

Rose, J.L., (1999). Ultrasonic waves in solid media. University Press, Cambridge.

Seco, F., Jimenez, A.R.,(2012)'Modelling the generation and propagation of ultrasonic signals in cylindrical waveguides. Center de Automatica y Robotica (CAR),Spain.

Tan, Y., (2009) 'Sensing localised corrosion by means of electrochemical noise detection and analysis, '*Sensors and Actuators B: Chemical*, pp. 688–698.

Thien, A.B., Chiamori, H.C., Ching, J.T., Wait, J.R. and Park, G., (2008), 'The use of macro-fibre composites for pipeline structural health assessment', *Structural Control & Health Monitoring* pp. 43-63 (doi: 10.1002/stc.203).

Varma, V.K., (2011) State-of-the-art Natural Gas Pipe Inspection, Oak Ridge National Laboratory,OakRidge,TN378316304,[Online]http://www.netl.doe.gov/technologies/oil/gas/publications/status_assessments/5_pager_1.pdf [Accessed in December 2011].

Volker, A. and Bloom, J., (2010) Experimental results of guided wave travel time tomography, Review of Progress in Quantitative Nondestructive Evaluation, in: AIP Conference Proceedings, 1335 pp. 215-22 (doi: 10.1063/1.3591859).

Yujie Ying, Harley, J., Garrett, J.H., Yuanwei Jin, Moura, J.M.F., O'Donoughue, N., Oppenheim, I.J. and Soibelman, (2010) L. in: *Proc. SPIE - The International Society for Optical Engineering* 7647 pp. 76473S (12 pp).

Zenghua Liu, He,C., Wu, B., Wang,X., Yang,SH., (2006)'Circumferential and longitudinal defect detection using T(0,1) mode excited by thickness shear mode piezoelectric elements', Ultrasonics 44. e 1135-e1138.

Zhang, J., C. Zou, Z. Shi, Y. Wang, Sh. Zhang and H. Kuang, (2010) 'Electrochemical Methods for Corrosion Monitoring': A Survey of Recent, *Recent Patents on Corrosion Science*, pp. 34-39.

Zhongli, Ma., Hongda liu., (2011)Tempreture error compensation New method on MFL sensor to oil-gas pipeline corrosion detection. Advanced Materials., pp.1026-1030.

Appendix A

Matrix elements

Matrix elements of equation 3.37 as below are presented here:

$$\begin{bmatrix} C_{11} & C_{12} & C_{13} & C_{14} & C_{15} & C_{16} \\ C_{21} & C_{22} & C_{23} & C_{24} & C_{25} & C_{26} \\ C_{31} & C_{32} & C_{33} & C_{34} & C_{35} & C_{36} \\ C_{41} & C_{42} & C_{43} & C_{44} & C_{45} & C_{46} \\ C_{51} & C_{52} & C_{53} & C_{54} & C_{55} & C_{56} \\ C_{61} & C_{62} & C_{63} & C_{64} & C_{65} & C_{66} \end{bmatrix} = 0. \qquad (3.37)$$

$$C_{11} = \left[2n(n-1) - \left(\beta^2 - k^2\right)a^2\right] Z_n(\alpha_1 a) + 2\lambda_1\alpha_1 a Z_{n+1}(\alpha_1 a),$$

$$C_{12} = 2k\beta_1 a^2 Z_n\left(\beta_1 a\right) - 2ka(n+1)Z_{n+1}\left(\beta_1 a\right),$$

$$C_{13} = -2n(n-1)Z_n\left(\beta_1 a\right) + 2\lambda_2 n\beta_1 a Z_{n+1}\left(\beta_1 a\right),$$

$$C_{14} = \left[2n(n-1) - \left(\beta^2 - k^2\right)a^2\right]W_n(\alpha_1 a) + 2\alpha_1 a W_{n+1}\left(\beta_1 a\right),$$

$$C_{15} = 2\lambda_2 k\beta_1 a^2 W_n\left(\beta_1 a\right) - 2(n+1)kaW_{n+1}\left(\beta_1 a\right),$$

$$C_{16} = -2n(n-1)W_n\left(\beta_1 a\right) + 2n\beta_1 a W_{n+1}\left(\beta_1 a\right),$$

$$C_{21} = 2n(n-1)Z_n(\alpha_1 a) - 2\lambda_1 n\alpha_1 a Z_{n+1}(\alpha_1 a),$$

$$C_{22} = -k\beta_1 a^2 Z_n\left(\beta_1 a\right) + 2ka(n+1)Z_{n+1}\left(\beta_1 a\right),$$

$$C_{23} = -\left[2n(n-1) - \beta^2 a^2\right] Z_n\left(\beta_1 a\right) - 2\lambda_2\beta_1 a Z_{n+1}\left(\beta_1 a\right),$$

$$C_{24} = [2n(n-1)]\, W_n(\alpha_1 a) - 2n\alpha_1 a W_{n+1}(\alpha_1 a),$$

$$C_{25} = -\lambda_2 k\beta_1\, a^2 W_n(\beta_1 a) + 2ka(n+1)W_{n+1}(\beta_1 a),$$

$$C_{26} = -[2n(n-1) - \beta^2 a^2]\, W_n(\beta_1 a) - 2\beta_1 a W_{n+1}(\beta_1 a),$$

$$C_{31} = 2nk\alpha_1 Z_n(\alpha_1 a) - 2\lambda_1\alpha_1 k a^2 Z_{n+1}(\alpha_1 a),$$

$$C_{32} = n\beta_1 a Z_n(\beta_1 a) - (\beta^2 - k^2)a^2 Z_{n+1}(\beta_1 a),$$

$$C_{33} = -nkaZ_n(\beta_1 a),$$

$$C_{34} = 2nkaW_n(\alpha_1 a) - 2k\alpha_1 a^2 W_{n+1}(\alpha_1 a),$$

$$C_{35} = n\lambda_2\beta_1 a W_n(\beta_1 a) - (\beta^2 - k^2)a^2 W_{n+1}(\beta_1 a),$$

$$C_{36} = -nkaW_n(\beta_1 a),$$

$$C_{41} = [2n(n-1) - (\beta^2 - k^2)b^2]\, Z_n(\alpha_1 b) + 2\lambda_1\alpha_1 a Z_{n+1}(\alpha_1 b),$$

$$C_{42} = 2k\beta_1 b^2 Z_n(\beta_1 b) - 2kb(n+1)Z_{n+1}(\beta_1 b),$$

$$C_{43} = -2n(n-1)Z_n(\beta_1 b) + 2\lambda_2 n\beta_1 b Z_{n+1}(\beta_1 b),$$

$$C_{44} = [2n(n-1) - (\beta^2 - k^2)b^2]W_n(\alpha_1 b) + 2\alpha_1 b W_{n+1}(\beta_1 b),$$

$$C_{45} = 2\lambda_2 k\beta_1 b^2 W_n(\beta_1 b) - 2(n+1)kbW_{n+1}(\beta_1 b),$$

$$C_{46} = -2n(n-1)W_n(\beta_1 b) + 2n\beta_1 b W_{n+1}(\beta_1 b),$$

$$C_{51} = 2n(n-1)Z_n(\alpha_1 b) - 2\lambda_1 n\alpha_1 b Z_{n+1}(\alpha_1 b),$$

$$C_{52} = -k\beta_1 b^2 Z_n(\beta_1 b) + 2kb(n+1)Z_{n+1}(\beta_1 b),$$

$$C_{53} = -[2n(n-1) - \beta^2 b^2]\, Z_n(\beta_1 b) - 2\lambda_2\beta_1 b Z_{n+1}(\beta_1 b),$$

$$C_{54} = [2n(n-1)]\, W_n(\alpha_1 b) - 2n\alpha_1 b W_{n+1}(\alpha_1 b),$$

$$C_{55} = -\lambda_2 k\beta_1\, b^2 W_n(\beta_1 b) + 2kb(n+1)W_{n+1}(\beta_1 b),$$

$$C_{56} = -[2n(n-1) - \beta^2 b^2]\, W_n(\beta_1 b) - 2\beta_1 b W_{n+1}(\beta_1 b),$$

$$C_{61} = 2nk\alpha_1 Z_n(\alpha_1 b) - 2\lambda_1\alpha_1 k b^2 Z_{n+1}(\alpha_1 b),$$

$$C_{62} = n\beta_1 b Z_n(\beta_1 b) - (\beta^2 - k^2)b^2 Z_{n+1}(\beta_1 b),$$

$$C_{63} = -nkbZ_n(\beta_1 b),$$

$$C_{64} = 2nkbW_n(\alpha_1 b) - 2k\alpha_1 b^2 W_{n+1}(\alpha_1 b),$$

$C_{65} = n\lambda_2\beta_1 bW_n(\beta_1 b) - (\beta^2 - k^2)b^2 W_{n+1}(\beta_1 b)$ and

$C_{66} = -nkbW_n(\beta_1 b).$

Appendix B

MATLAB Scripts

main.m

```
% This script plots the dispersion curves for Shear Horizontal guided
wave in plates.
%
%
% Written by Bahareh Zaghari, bz2e11@soton.ac.uk.
%
%
%In the graph solid curves denote symetric modes and dashed curves
denote antisymmetric modes.
% This file has checked with graph in page 245 Rose book and graph in
Jacob

%% Preamble
clear;clc;close all;
%%
%Shear Horizontal in plate

Cs = 3250;% Steel shear velocity.
d = 0.003;%Thickness of plate in mm.
f = 10:1e4:6e6; %Frequency (domain).
n = 0:7;%Number of modes.



for jt = 1:length(n)

    Fcutoff = n(jt) * Cs / 2 / d; %Finding the cut-off frequency.
  %% Calculate the phase and group velocity.
    new_freq = Fcutoff:1e4:f(end);
    cp = zeros( 1, length(new_freq) );% Phase velocity array
declaration.
    cg = zeros( 1, length(new_freq) );% Group velocity array
declaration.

    for it = 1:length(new_freq)
        cp(it)= 2*Cs*( (new_freq(it)*d) / sqrt( 4*(new_freq(it)*d)^2 -
n(jt)^2 * Cs^2) );% Finding the phase velocity.
        cg(it)= Cs*sqrt( 1- (  (n(jt)/2)^2/(new_freq(it)*d/Cs)^2  ));%
Finding the group velocity
    end
     %% Plot phase and group velocity.
    if( mod(n(jt),2) == 1 )
        figure(1);
        hold on;
        plot( new_freq*d/1000, cp, '--','linewidth',3 );
```

```
        figure(2);
        hold on;
        plot( new_freq*d/1000, cg, '--','linewidth',3 );

    else
        figure(1);
        hold on;
        plot( new_freq*d/1000, cp, '-','linewidth',3 );

        figure(2);
        hold on;
        plot( new_freq*d/1000, cg, '-','linewidth',3 );
    end

end
    figure(1);
    grid on;
    axis([0,f(end)*d/1000,0,1e4]);
    xlabel( 'Frequency-Thickness (MHz-mm)','fontsize',16 );
    ylabel( 'Phase Velocity Cp= \omega / k (ms^-^1)','fontsize',16 );
    title( 'Dispersion Curves for SH mode (Plate thickness:
3mm)','fontsize',16);


    figure(2);
    grid on;
    axis([0,f(end)*d/1000,0,5e3]);
    xlabel( 'Frequency.Thickness (MHz.mm)','fontsize',16 );
    ylabel( 'Group Velocity Cg = d \omega / dk (ms^-^1)'
,'fontsize',16);
    title( 'Dispersion Curves for SH mode (Plate thickness:
3mm)','fontsize',13 );
```

Appendix C

MATLAB Scripts

C.1 main.m

```
% This script plots the dispersion curves for torsional, longitudinal
and
% flexural modes for a given pipe configuration. The system is assumed
to
% be lossless, attenuation is not present, and the pipe is assumed to
be a
% single-layer steel pipe.
%
% Written by Bahareh Zaghari, bz2e11@soton.ac.uk.

clear;clc;close all;

%% Declaring common constants and arrays.

cl = 6290; % Longitudinal wave velocity (ms^(-1))
cs = 3260; % Shear wave velocity (ms^(-1))
n = 0; % Circumferential order (unitless)
m = 0:5;%Counter variable
f = 10:1e4:4e5; % Frequency domain (Hz).
a = 0.012; % Internal pipe radius (m).
b = 0.017; % External pipe radius (m).
f_khz_thickness = f*10^(-3); % Frequency for plotting (kHz).

%% Torsional mode: Finding beta bounds.

root_ests(1,:) = [1,1];
for it = 1:length(m) % For each counter variable,
    new_roots = Sign_Change_Root_Finder( m(it), a, b ); % Find the mth
root
    root_ests( it, : ) = new_roots( it, : );            % and store it.
end

%% Torsional mode: Other calculations

for jt = 1:length(m) % For each m,
    %% Use Muller's method to find precise values of beta.
    beta = muller_old( @FuncToRoot, [ root_ests(jt,1),
0.5*(root_ests(jt,1) + root_ests(jt,2) ), root_ests(jt,2) ], 10^(-5),
10000, n, a, b );

    %% Declare arrays
    k = zeros( 1, length(f) );
    omega = zeros( 1, length(f) );
    cp = zeros( 1, length(f) );
    cg = zeros( 1, length(f) );
```

```
    %% Calculate cut-off frequency and the frequency array index that
best corresponds to it.
    fcutoff(jt) = cs*(beta)/2/pi; % Cut-off frequency.

    start_it = 1; % Consider the first array index.
    while( fcutoff(jt) > f(start_it) && start_it < length(f) ) % If
this index is before the cut-off frequency,
        start_it = start_it + 1; % Increase it.
    end

    %% Calculate the phase and group velocity for this m.

    for it = start_it:length(f) %For each frequency value past the cut-
off frequency
        k(it) = sqrt( ( 4*pi^2*f(it).^2  / cs^2 ) - beta^2 ); %
Calculate wavenumber.
        omega(it) = 2*pi*f(it); % Calculate omega.
        cp(it) = omega(it)/k(it); % Calculate phase velocity.
        cg(it) = k(it).*cs./sqrt(k(it).^2 + beta^2); % Calculate group
velocity
    end

    %% Plot phase and group velocity for this m.

    figure(1); % Phase velocity
    plot(
f_khz_thickness(start_it:end),real(cp(start_it:end)),'o','Color',[m(jt)
/m(end),0,0],'linewidth',1);
    grid on;
    hold on;
    axis([f_khz_thickness(1) f_khz_thickness(end) 0 15000 ]);
    set(gca,'YTick',[0,3,6,9,12,15]*1000)
    xlabel( 'Frequency (kHz)' );
    ylabel( 'Phase Velocity Cp =\omega / k (ms^-^1)' );
    title( 'Dispersion Curves' );

    figure(2); % Group velocity
    plot( f_khz_thickness(start_it:end),real(cg(start_it:end)),'o',
'Color',[m(jt)/m(end),0,0],'linewidth',1);
    grid on;
    hold on;
    axis([f_khz_thickness(1) f_khz_thickness(end) 1000 6000]);
    set(gca,'YTick',[0,1,2,3,4,5,6]*1000)
    xlabel( 'Frequency (kHz)' );
    ylabel( 'Group Velocity Cg = d \omega / dk (ms^-^1)' );
    title( 'Dispersion Curves' );

end

% Plot the T(0,1) mode seperately.
figure(1);
plot( [f_khz_thickness(1),f_khz_thickness(end)],
[cs,cs],'k','linewidth',3);
```

```
figure(2);
plot( [f_khz_thickness(1),f_khz_thickness(end)],
[cs,cs],'k','linewidth',3);

%% Longitudinal mode: Preamble

figure(1); % Plot scatter points on the phase velocity graph.
hold on;
grid on;

plot_tol = 50;
k_re = 0:1:3000; % Real wavenumber domain (for root finder)
%Longitudinal works well with K_re:0.1 and 1000 frequency interval
det = zeros(length(k_re),length(f)); % Matrix to store determinany
values for varying wavenumber and frequency.
fprintf( 'Longitudinal calculation: %f percent complete.\n', 0 );

%% Longitudinal mode: Other calculations

for jt = 1:length(f) % For each frequency value,
    %% Finding determinant for each wavenumber.

    for it = 1:length(k_re) % For each wavenumber value,
        det(it) = determinant_function( k_re(it), 0, a, b, cs, cl,
f(jt) );
    end

    %% Plot point if root exists for each wavenumber.
    for it = 1:length(k_re-1) % For each wavenumber value,
        if( det(it) * det(it+1) < 0 ) % If there is a root,

            this_cp = 2*pi*f(jt)/(k_re(it) + k_re(it+1))*2; % Calculate
the corresponding phase velocity.

            if((this_cp >= cl-plot_tol && this_cp <= cl+plot_tol)&&(
this_cp >= cs-plot_tol && this_cp <= cs+plot_tol))

            else  % If value is accceptable,
                scatter( f(jt)/1000, 2*pi*f(jt)/(k_re(it) +
k_re(it+1))*2 ); % Plot it.

            end
        end
    end

    fprintf( 'Longitudinal calculation: %f percent complete.\n',
jt/length(f)*100 );

end

%% Flexural mode

figure(1);% Plot scatter points on the phase velocity graph.
hold on;
```

```
grid on;


k_re = 0:0.11:3000;% Real wavenumber domain (for root finder)
det = zeros(length(k_re),length(f));
fprintf( 'Flexural calculation: %f percent complete.\n', 0 );


for jt = 1:length(f)

      for it = 1:length(k_re)
        if (jt <= 30000)
        det(it) = determinant_function_Flexural( k_re(it), 1, a, b, cs,
cl, f(jt) );
        else
        det(it) = determinant_function( k_re(it), 1, a, b, cs, cl,
f(jt) );
        end
    end

    for it = 1:length(k_re-1)
        if( det(it) * det(it+1) < 0 )
            this_cp = 2*pi*f(jt)/(k_re(it) + k_re(it+1))*2;
            if ((this_cp >= cl-plot_tol && this_cp <= cl+plot_tol)&&(
this_cp >= cs-plot_tol && this_cp <= cs+plot_tol))

            else% If value is accceptable,
                scatter( f(jt)/1000, this_cp,'filled' );
                hold on;
                kt = kt + 1;
            end
        end
    end

   fprintf( 'Flexural calculation: %f percent complete.\n',
jt/length(f)*100 );
 end
```

Appendix C.2 FuncToRoot.m

```
function out = FuncToRoot( beta,n,a,b )
% This function represents the characteristic equation for torsional
modes;
% the equation is satisfied when out is equal to zero.
%
% Written by Bahareh Zaghari, bz2e11@soton.ac.uk.

if(imag(beta) ~= 0) % If beta is real,
    out = besseli( n, beta*a ) * besselk( n, beta*b ) -besseli( n,
beta*b ) * besselk( n, beta*a );
else  % If beta is imaginary,
```

```
    out = besselj( n, beta*a ) * bessely( n, beta*b ) -besselj( n,
beta*b ) * bessely( n, beta*a );
end

end
```

C.3 Sign_Change_Root_Finder.m

```
function roots = Sign_Change_Root_Finder( n, a, b )
% This function finds the sign changes of the function FuncToRoot
(already
% defined in the namespace) with arguments n, a and b. These sign
changes
% are expressed in the matrix roots with an upper bound and lower bound
for
% a root in each column.
%
% Written by Bahareh Zaghari, bz2e11@soton.ac.uk.
%% Define arrays.

beta = 0:100:50000; %Range of beta values to analyse (function domain)
l = length(beta);
y = zeros( 1, l ); %Solutions (function range)

for it = 1:l
    y(it) = real( FuncToRoot( beta(it), n, a, b ) ); %Calculating
result.
end

%% Finding sign changes.

roots = 0; %Initially allocating the root matrix. This value is
returned if no roots are found.
jt = 1; %Root iterator

for it = 1:l-1 %For each element except the final one,

    if( y(it) * y(it + 1) < 0 ) %If there is a sign change between this
and the next element,
        roots(jt,1) = beta(it);    %
        roots(jt,2) = beta(it+1); % Store the root
        jt = jt + 1;               %
    end
end

end
```

C.4 muller_old.m

```
function root = muller_old(f,z,tol,max_it,n,a,b)
% This function is an implementation of Muller's method. This will find
the
% root of a function f given three estimates in increasing order of
```

```
% magnitude z(1), z(2) and z(3). It will solve to a tolerance of tol or
% until max_it iterations are reached. It passes the arguments n, a and
b
% to the function f.
%
% Written by Bahareh Zaghari, bz2e11@soton.ac.uk.
%% Preamble
q=3; % Three initial guesses are considered.
it = 1; % Number of iterations.
fz = zeros(1,q); % Function evaluation of z.

while( abs(z(q) - z(q-1)) > tol && abs(z(q-2) - z(q-1)) > tol && it <
max_it )
% While tolerance or max iteration criteria are not satisfied,

    %% Calculating f(z) for each guess and checking for roots.
    fz(q) = real( f(z(q),n,a,b) );
    fz(q-1) = real( f(z(q-1),n,a,b) );
    fz(q-2) = real( f(z(q-2),n,a,b) );

    if( fz(q) * fz(q-1) < 0 && fz(q-1) * fz(q-2) < 0 ) % If roots exist
in both brackets,
        fprintf( 'Muller: Error 1.\n' ); % Print an error.
    end

    %% Calculating the next root.
    h = z(q) - z(q-1);
    h_prev = z(q-1) - z(q-2);
    r = h / h_prev;

    a_coeff = r * fz(q) - r * (1+r) * fz(q-1) + r^2 * fz(q-2);
    b_coeff = (2*r+1) * fz(q) - (1+r)^2 * fz(q-1) + r^2 * fz(q-2);
    c_coeff = (1+r) * fz(q);

    E = sqrt(b_coeff^2 - 4*a_coeff*c_coeff);
    root1 = -2*c_coeff /(b_coeff + E);
    root2 = -2*c_coeff /(b_coeff - E);

    zmax = max(z(q-2:q));
    zmin = min(z(q-2:q));

    %% Choosing which root (root1 or root2) to consider.
    if( z(q) + h*root1 > zmax || z(q) + h*root1 < zmin ) % If root1 is
outside the upper and lower bounds,
        z_new = z(q) + h*root2; % Use root2.
    else
        z_new = z(q) + h*root1; % Otherwise use root1.
    end

    %% Ordering the new three root guesses.
    if( fz(q) * fz(q-1) < 0 )
        if( z_new > z(q-1) )
            z(q-2) = z(q-1);
            z(q-1) = z_new;
        else
```

```
            z(q-2) = z_new;
        end
    else
        if( z_new > z(q-1) )
            z(q) = z_new;
        else
            z(q) = z(q-1);
            z(q-1) = z_new;
        end
    end

    it = it + 1; % Increment the iterator

end

%% Output result (and error if appropriate)
if( it == max_it ) % If maximum number of iterations was reached before
tolerance limit,
    fprintf( 'Muller: Error 2.\n' ); % Print an error.
end

root = z(q-1);

end
```

C.5 determinant_function.m

```
function out = determinant_function( k,n,a,b,cs,cl,f )
% This function represents the characteristic equation for longitudinal
% modes; the equation is satisfied when out is equal to zero.
%
% Written by Bahareh Zaghari, bz2e11@soton.ac.uk.

%% Calculating values of beta and alpha.
beta = sqrt ((2*pi*f)^2 / cs^2 - k^2);
alpha = sqrt ( ((2*pi*f)^2/cl^2) - ((2*pi*f)^2/cs^2) + beta^2 );
beta_1 = abs(beta);
alpha_1 = abs(alpha);

%% Determining which bessel functions and signs to use for the
characteristic equation.
if( alpha^2 > 0 && beta^2 > 0 )

    lambda1 = 1;
    lambda2 = 1;

    Zn_alpha_a = besselj( n,alpha*a   );
    Zm_alpha_a = besselj( n+1,alpha*a );%Zm = Zn+1
    Wn_alpha_a = bessely( n,alpha*a   );
    Wm_alpha_a = bessely( n+1,alpha*a );%Wm = Wn+1

    Zn_alpha_b = besselj( n,alpha*b   );
    Zm_alpha_b = besselj( n+1,alpha*b );%Zm = Zn+1
    Wn_alpha_b = bessely( n,alpha*b   );
```

```
    Wm_alpha_b = bessely( n+1,alpha*b );%Wm = Wn+1


    Zn_beta_a = besselj( n,beta*a   );
    Zm_beta_a = besselj( n+1,beta*a );%Zm = Zn+1
    Wn_beta_a = bessely( n,beta*a   );
    Wm_beta_a = bessely( n+1,beta*a );%Wm = Wn+1

    Zn_beta_b = besselj( n,beta*b   );
    Zm_beta_b = besselj( n+1,beta*b );%Zm = Zn+1
    Wn_beta_b = bessely( n,beta*b   );
    Wm_beta_b = bessely( n+1,beta*b );%Wm = Wn+1

elseif( alpha^2 < 0 && beta^2 > 0 )

    lambda1 = -1;
    lambda2 = 1;

    Zn_alpha_a = besseli( n,alpha_1*a   );
    Zm_alpha_a = besseli( n+1,alpha_1*a );%Zm = Zn+1
    Wn_alpha_a = besselk( n,alpha_1*a   );
    Wm_alpha_a = besselk( n+1,alpha_1*a );%Wm = Wn+1

    Zn_alpha_b = besseli( n  ,alpha_1*b );
    Zm_alpha_b = besseli( n+1,alpha_1*b );%Zm = Zn+1
    Wn_alpha_b = besselk( n  ,alpha_1*b );
    Wm_alpha_b = besselk( n+1,alpha_1*b );%Wm = Wn+1


    Zn_beta_a = besselj( n,beta*a   );
    Zm_beta_a = besselj( n+1,beta*a );%Zm = Zn+1
    Wn_beta_a = bessely( n,beta*a   );
    Wm_beta_a = bessely( n+1,beta*a );%Wm = Wn+1

    Zn_beta_b = besselj( n,beta*b   );
    Zm_beta_b = besselj( n+1,beta*b );%Zm = Zn+1
    Wn_beta_b = bessely( n,beta*b   );
    Wm_beta_b = bessely( n+1,beta*b );%Wm = Wn+1


elseif( alpha^2 < 0 && beta^2 < 0 )

    lambda1 = -1;
    lambda2 = -1;

    Zn_alpha_a = besseli( n,alpha_1*a   );
    Zm_alpha_a = besseli( n+1,alpha_1*a );%Zm = Zn+1
    Wn_alpha_a = besselk( n,alpha_1*a   );
    Wm_alpha_a = besselk( n+1,alpha_1*a );%Wm = Wn+1

    Zn_alpha_b = besseli( n  ,alpha_1*b );
    Zm_alpha_b = besseli( n+1,alpha_1*b );%Zm = Zn+1
    Wn_alpha_b = besselk( n  ,alpha_1*b );
    Wm_alpha_b = besselk( n+1,alpha_1*b );%Wm = Wn+1
```

```
    Zn_beta_a = besseli( n,beta_1*a   );
    Zm_beta_a = besseli( n+1,beta_1*a );%Zm = Zn+1
    Wn_beta_a = besselk( n,beta_1*a   );
    Wm_beta_a = besselk( n+1,beta_1*a );%Wm = Wn+1

    Zn_beta_b = besseli( n,beta_1*b   );
    Zm_beta_b = besseli( n+1,beta_1*b );%Zm = Zn+1
    Wn_beta_b = besselk( n,beta_1*b   );
    Wm_beta_b = besselk( n+1,beta_1*b );%Wm = Wn+1

end

%% Calculation of the numerical value of the characteristic equation.

C11 = (2*n*(n-1) - (beta^2 - k^2)*a^2) * Zn_alpha_a + 2*lambda1 *
alpha_1 * a * Zm_alpha_a;
C12 = 2*k*beta_1*a^2*Zn_beta_a - 2*k*a*(n+1)*Zm_beta_a;
C14 = (2*n*(n-1)-(beta^2-k^2)*a^2)*Wn_alpha_a + 2*alpha_1*a*Wm_alpha_a;
C15 = 2*lambda2*k*beta_1*a^2*Wn_beta_a - 2*(n+1)*k*a*Wm_beta_a;

C31 = 2*n*k*alpha_1*Zn_alpha_a + 2*lambda1*k*alpha_1*a^2*Zm_alpha_a;
C32 = -n*beta_1*a*Zn_beta_a + (beta^2-k^2)*a^2*Zm_beta_a;
C34 = -2*n*k*a*Wn_alpha_a + 2*k*alpha_1*a^2*Wm_alpha_a;
C35 = -lambda2*n*beta_1*a*Wn_beta_a + (beta^2-k^2)*a^2*Wm_beta_a;

C41 = (2*n*(n-1) - (beta^2 - k^2)*b^2) * Zn_alpha_b + 2*lambda1 *
alpha_1 * b * Zm_alpha_b;
C42 = 2*k*beta_1*b^2*Zn_beta_b - 2*k*b*(n+1)*Zm_beta_b;
C44 = (2*n*(n-1)-(beta^2-k^2)*b^2)*Wn_alpha_b + 2*alpha_1*b*Wm_alpha_b;
C45 = 2*lambda2*k*beta_1*b^2*Wn_beta_b - 2*(n+1)*k*b*Wm_beta_b;

C61 = 2*n*k*alpha_1*Zn_alpha_b + 2*lambda1*k*alpha_1*b^2*Zm_alpha_b;
C62 = -n*beta_1*b*Zn_beta_b + (beta^2-k^2)*b^2*Zm_beta_b;
C64 = -2*n*k*b*Wn_alpha_b + 2*k*alpha_1*b^2*Wm_alpha_b;
C65 = -lambda2*n*beta_1*b*Wn_beta_b + (beta^2-k^2)*b^2*Wm_beta_b;

out = det( [ C11 C12 C14 C15;
             C31 C32 C34 C35;
             C41 C42 C44 C45;
             C61 C62 C64 C65] );

end
```

Appendix D

MATLAB Scripts

D.1 torsional_1.m

```
% This script plots the dispersion curves for torsional modes for a
given pipe configuration.
%The system is assumed to be lossless, attenuation is not present, and
the pipe is assumed to be a
% single-layer steel pipe.
%
% Written by Bahareh Zaghari, bz2e11@soton.ac.uk.

clear;clc;close all;

%% Declaring common constants and arrays.

cl = 6290; % Longitudinal wave velocity (ms^(-1))
cs = 3260; % Shear wave velocity (ms^(-1))
cp1 = cs;
n = 0; % Circumferential order (unitless)
m = 0:2;%Counter variable
f = 10:1e4:4e5; % Frequency domain (Hz).
a = 0.05;%Internal pipe radius (m).
b =
[0.051,0.05125,0.0515,0.052,0.0525,0.053,0.0535,0.054,0.0545,0.055,0.05
55];%External pipe radius (m).
fcutoff = zeros( length(m), length(b) );

%%

for kt = 1:length(b)

    root_ests(1,:) = [1,1];
    for it = 1:length(m)
        new_roots = Sign_Change_Root_Finder( m(it), a, b(kt) );
        root_ests( it, : ) = new_roots( it, : );
    end

    for jt = 1:length(m)

        beta = muller_old( @FuncToRoot, [ root_ests(jt,1),
0.5*(root_ests(jt,1) + root_ests(jt,2) ), root_ests(jt,2) ], 10^(-5),
10000, n, a, b(kt) );
        k = zeros( 1, length(f) );
        k_f = k;
        omega = k;
        cp = k;

        %Cutoff Frequency
        fcutoff(jt,kt) = cs*(beta)/2/pi;
```

```
        start_it = 1;
        while( fcutoff(jt,kt) > f(start_it) && start_it < length(f) )
            start_it = start_it + 1;
        end

        for it = start_it:length(f)
            k(it) = sqrt( ( 4*pi^2*f(it).^2  / cs^2 ) - beta^2 );
            k_f(it) = 4*pi^2*f(it)/k(it)/cs^2;
            omega(it) = 2*pi*f(it);
            cp(it) = omega(it)/k(it);
        end

        if( kt == 1 )
            figure(1);
            plot(
f(start_it:end),real(cp(start_it:end)),'Color',[m(jt)/m(end),0,0],'line
width',3 );
            grid on; hold on;
            axis([f(1) f(end) 0 15000 ]);
            set(gca,'YTick',[0,3,6,9,12,15]*1000)
            xlabel( 'Frequency (MHz)','FontSize',13 );
            ylabel( 'Phase Velocity \omega / k (ms^-^1)','FontSize',13
);
            title( 'Dispersion Curves for Torsional
Modes','FontSize',13 );

            figure(2);
            plot( f(start_it:end),real(2.*pi./k_f(start_it:end)),
'Color',[m(jt)/m(end),0,0],'linewidth',3 );
            grid on; hold on;
            axis([f(1) f(end) 1000 6000]);
            set(gca,'YTick',[0,1,2,3,4,5,6]*1000)
            xlabel( 'Frequency (MHz)','FontSize',13 );
            ylabel( 'Group Velocity d \omega / dk (ms^-
^1)','FontSize',13 );
            title( 'Dispersion Curves for Torsional
Modes','FontSize',13 );
        end

    end

end

figure(1);
plot( [f(1),f(end)], [cp1,cp1],'k','linewidth',3);

figure(2);
plot( [f(1),f(end)], [cp1,cp1],'k','linewidth',3);

figure(3);
for it = 1:length(m)
    plot( (b-a)*10^3, fcutoff(it,:)*10^(-6), '-o', 'Color',
[0,0,it/length(m)], 'linewidth', 3 );
    hold on;
end
```

```
grid on;
axis tight;
xlabel( 'Pipe Thickness (mm) [Inner Radius = 50mm]','FontSize',11 );
ylabel( 'Cut-off Frequency (MHz)','FontSize',11 );
title( 'Cut-off Frequency against Pipe Thickness for Varying Outer
Radius.','FontSize',12 );
```

D.2 torsional_2.m

```
% This script plots the dispersion curves for torsional modes for a
given pipe configuration.
%The system is assumed to be lossless, attenuation is not present, and
the pipe is assumed to be a
% single-layer steel pipe.
%
% Written by Bahareh Zaghari, bz2e11@soton.ac.uk.

clear;clc;close all;

%% Declaring common constants and arrays.

cl = 6290; % Longitudinal wave velocity (ms^(-1))
cs = 3260; % Shear wave velocity (ms^(-1))
cp1 = cs;
n = 0; % Circumferential order (unitless)
m = 0:2;%Counter variable
f = 10:1e4:4e5; % Frequency domain (Hz).
a = [0.0500,0.04975,0.0495,0.0490,0.0485,0.0480,0.0475,0.0470];
%Internal pipe radius (m).
b = [0.0510,0.05125,0.0515,0.0520,0.0525,0.0530,0.0535,0.0540];
%External pipe radius (m).
fcutoff = zeros( length(m), length(b) );

% NB: length(a) must equal length(b).

%%

for kt = 1:length(b)

    root_ests(1,:) = [1,1];
    for it = 1:length(m)
        new_roots = Sign_Change_Root_Finder( m(it), a(kt), b(kt) );
        root_ests( it, : ) = new_roots( it, : );
    end

    for jt = 1:length(m)

        beta = muller_old( @FuncToRoot, [ root_ests(jt,1),
0.5*(root_ests(jt,1) + root_ests(jt,2) ), root_ests(jt,2) ], 10^(-5),
10000, n, a(kt), b(kt) );
        k = zeros( 1, length(f) );
        k_f = k;
```

```
        omega = k;
        cp = k;

        %Cutoff Frequency
        fcutoff(jt,kt) = cs*(beta)/2/pi;

        start_it = 1;
        while( fcutoff(jt,kt) > f(start_it) && start_it < length(f) )
            start_it = start_it + 1;
        end

        for it = start_it:length(f)
            k(it) = sqrt( ( 4*pi^2*f(it).^2  / cs^2 ) - beta^2 );
            k_f(it) = 4*pi^2*f(it)/k(it)/cs^2;
            omega(it) = 2*pi*f(it);
            cp(it) = omega(it)/k(it);
        end

        if( kt == 1 )
            figure(1);
            plot(
f(start_it:end),real(cp(start_it:end)),'Color',[m(jt)/m(end),0,0] );
            grid on; hold on;
            axis([f(1) f(end) 0 15000 ]);
            set(gca,'YTick',[0,3,6,9,12,15]*1000)
            xlabel( 'Frequency (MHz)' );
            ylabel( 'Phase Velocity \omega / k (ms^-^1)' );
            title( 'Dispersion Curves for Torsional Modes');

            figure(2);
            plot( f(start_it:end),real(2.*pi./k_f(start_it:end)),
'Color',[m(jt)/m(end),0,0]);
            grid on; hold on;
            axis([f(1) f(end) 1000 6000]);
            set(gca,'YTick',[0,1,2,3,4,5,6]*1000)
            xlabel( 'Frequency (MHz)' );
            ylabel( 'Group Velocity d \omega / dk (ms^-^1)' );
            title( 'Dispersion Curves for Torsional Modes');
        end

    end

end

figure(1);
plot( [f(1),f(end)], [cp1,cp1],'k','linewidth',2);

figure(2);
plot( [f(1),f(end)], [cp1,cp1],'k','linewidth',2);

figure(3);
for it = 1:length(m)
    plot( (b-a)*10^3, fcutoff(it,:)*10^(-6), '-o', 'Color',
[0,0,it/length(m)], 'linewidth', 3 );
    hold on;
```

```
end
grid on;
axis tight;
xlabel( 'Pipe Thickness (mm) [Mean Radius = 50.5mm]' ,'FontSize',10);
ylabel( 'Cut-off Frequency (MHz)','FontSize',10);
title( 'Cut-off Frequency against Pipe Thickness for Constant Mean
Radius.','FontSize',10 );
```

D.3 torsional_3.m

```
% This script plots the dispersional curves for torsional modes for a
given pipe configuration.
%The system is assumed to be lossless, attenuation is not present, and
the pipe is assumed to be a
% single-layer steel pipe.
%
% Written by Bahareh Zaghari, bz2e11@soton.ac.uk.

clear;clc;close all;

%% Declaring common constants and arrays.

cl = 6290; % Longitudinal wave velocity (ms^(-1))
cs = 3260; % Shear wave velocity (ms^(-1))
cp1 = cs;
n = 0; % Circumferential order (unitless)
m = 0:2;%Counter variable
f = 10:1e4:4e5; % Frequency domain (Hz).
scales = [1.25,1.5,2,2.5,3,4,5,6,7];
a = zeros( 1, 1+length(scales) );
b = zeros( 1, 1+length(scales) );
a(1) = 0.01;  %Internal pipe radius (m).
b(1) = 0.011; %External pipe radius (m).

for jt = 1:length(scales)
    a(jt+1) = a(1)*scales(jt);
    b(jt+1) = b(1)*scales(jt);
end

fcutoff = zeros( length(m), length(b) );

%%

for kt = 1:length(b)

    root_ests(1,:) = [1,1];
    for it = 1:length(m)
        new_roots = Sign_Change_Root_Finder( m(it), a(kt), b(kt) );
        root_ests( it, : ) = new_roots( it, : );
    end

    for jt = 1:length(m)
```

```
        beta = muller_old( @FuncToRoot, [ root_ests(jt,1),
0.5*(root_ests(jt,1) + root_ests(jt,2) ), root_ests(jt,2) ], 10^(-5),
10000, n, a(kt), b(kt) );
        k = zeros( 1, length(f) );
        k_f = k;
        omega = k;
        cp = k;

        %Cutoff Frequency
        fcutoff(jt,kt) = cs*(beta)/2/pi

        start_it = 1;
        while( fcutoff(jt,kt) > f(start_it) && start_it < length(f) )
            start_it = start_it + 1;
        end

        for it = start_it:length(f)
            k(it) = sqrt( ( 4*pi^2*f(it).^2  / cs^2 ) - beta^2 );
            k_f(it) = 4*pi^2*f(it)/k(it)/cs^2;
            omega(it) = 2*pi*f(it);
            cp(it) = omega(it)/k(it);
        end

        if( kt == 1 )
            figure(1);
            plot(
f(start_it:end),real(cp(start_it:end)),'Color',[m(jt)/m(end),0,0],'line
width',3 );
            grid on; hold on;
            axis([f(1) f(end) 0 15000 ]);
            set(gca,'YTick',[0,3,6,9,12,15]*1000)
            xlabel( 'Frequency (MHz)' );
            ylabel( 'Phase Velocity \omega / k (ms^-^1)' );
            title( 'Dispersion Curves for Torsional Modes' );

            figure(2);
            plot( f(start_it:end),real(2.*pi./k_f(start_it:end)),
'Color',[m(jt)/m(end),0,0],'linewidth',3 );
            grid on; hold on;
            axis([f(1) f(end) 1000 6000]);
            set(gca,'YTick',[0,1,2,3,4,5,6]*1000)
            xlabel( 'Frequency (MHz)' );
            ylabel( 'Group Velocity d \omega / dk (ms^-^1)' );
            title( 'Dispersion Curves for Torsional Modes' );
        end

    end

end

figure(1);
plot( [f(1),f(end)], [cp1,cp1],'k','linewidth',3);

figure(2);
plot( [f(1),f(end)], [cp1,cp1],'k','linewidth',3);
```

```
figure(3);
for it = 1:length(m)
    plot( (b-a)*10^3, fcutoff(it,:)*10^(-6), '-o', 'Color',
[0,0,it/length(m)], 'linewidth', 3 );
    hold on;
end
grid on;
axis tight;
xlabel( 'Scale Factor' ,'FontSize',11);
ylabel( 'Cut-off Frequency (MHz)','FontSize',11 );
title( 'Cut-off Frequency against Scale Factor. [ Outer Radii/Inner
Radii = 1.1]','FontSize',12 );
```

Appendix E

Equipment specifications

Function generator

Hp 33120A, 15MHz Function/arbitrary waveforms generator. Built-in 12-bit 40 MSa/s arbitrary waveform capability.

Oscilloscope

LeCroy 9304C, QUAD 200MHz, 100MS/s, 50 Kpts/ch.

Signal amplifier

ORTEC Precision ac Amplifier 9452.

Filter

Filter model 3202. KROHN-HITE CORPORATION. 20 Hz to 2 MHz.

Appendix F

MATLAB Scripts

F.1 MainProgram.m

```
%% Main Program();

%
%   This program is coded by Rambo Yuan at 1st June 2012 and modified
by
%   Bahareh Zaghari (bz2e11@soton.ac.uk)at 1st August 2012.
%
%   This program is used for the oblique transmittance experiment by
using
%   the LeCroy 9304C oscilloscope, HP 33120A Waveform Generator and
Step Motor.
%   The transmittance spectrum of the object is investigate from output
signals.
%   Before running this code, please make sure that The LeCroy 9304C is
%   connected with the computer using NI's GPIB interface;
%
%   Important Note:
%   1. The program use Ch1 and Ch3 to recieve the output signal from
%   transducer in different Volt_Div. Hence, TA and TB are used to
sweep
%   the signals in Ch1 and Ch3 respectively. Take care Waitsweep() and
%   Readsignal() defaultly recognise TA and TB as the chosen signal.

clc;
clear;
%% Global Constant;

FreqMax=4e6;    % Concerned frequency up to 1MHz;
Est_FreqStep=1e3;   % Estimate frequency steps 1KHz;
Est_Fs=1e8;      % Estimate Sampling Frequency 100MS/s, Related to
TDIV(20us);

%% Global Parmeters;


NFFT=2^nextpow2(Est_Fs/Est_FreqStep);
Act_FreqStep=Est_Fs/NFFT;
Fr=0:Act_FreqStep:FreqMax;
FreqNum=length(Fr);



%% Initialization : Find the Instruments and verfify it.
% Find and test the Oscilloscope;
Osc = gpib('ni', 0, 4);  %connect to GPIB
```

```
set(Osc, 'InputBufferSize', 1000000); % Set the buffer(I/O Buffer:
256), after 1000000buffer size instrument starts analysing.
set(Osc, 'Timeout', 3.0);%Time out is for internal clock. from 25nsec
to 20sec.
fopen(Osc);
% query(Osc, '*rst')
query(Osc, '*idn?')
fprintf(Osc, 'buzz beep');

% Presetting the Oscilloscope and the waveforms;
fprintf(Osc, 'cfmt off,word,hex\n');          %comm_format;select the
format for sending data
fprintf(Osc, 'chdr off\n');                   %comm_header;controls
formating the query responces
% fprintf(Osc, 'trse edge,sr,ex,ht,off\n');     % Set trigger type;
% fprintf(Osc, 'ex:trsl pos\n');                % Set trigger type;
fprintf(Osc, 'wait');

fprintf(Osc, 'c1:tra on\n');        % open the c1;
fprintf(Osc, 'c3:tra on\n');        % open the c3;


 fprintf(Osc, 'tdiv 0.5ms\n');      % Set the timebase to be 50 us for
one grid;
% fprintf(Osc, 'trdl -270e-6s\n');  % Set the time delay to be -230 us;
 fprintf(Osc, 'c1:vdiv 0.1v\n');   % Set the Volt_Div of C1;
% fprintf(Osc, 'c1:ofst 0\n');      % Set the Volt_Offset of C1;
fprintf(Osc, 'wait');

fprintf(Osc, 'ta:tra on\n');      % open the ta;
fprintf(Osc, 'ta:def eqn,''avgs(c1)'', maxpts,1000000,sweeps,400\n'); %
set ta;
% fprintf(Osc, 'ta:vpos 0\n');
% fprintf(Osc, 'ta:hpos 5\n');
% fprintf(Osc, 'ta:vmag 1\n');
% fprintf(Osc, 'ta:hmag 1\n');
fprintf(Osc, 'wait');

% fprintf(Osc, 'tb:tra on\n');      % open the ta;
% fprintf(Osc, 'tb:def eqn,''avgs(c3)'', maxpts,1000000,sweeps,100\n');
% set ta;
fprintf(Osc, 'wait');

%% Calibration the transducer's signal and reading the data;
input('Press Enter when you get ready for the signal calibration?');
[Mag_c3,PPV_c3,Lvl_c3]=Presetsignalc3(Osc);
Waitsweepc3(Osc);
[Ref_Xt_c3,Ref_Yt_c3,Ref_Par_c3]=Readsignalc3(Osc,Mag_c3,PPV_c3);


[Mag,PPV,Lvl]=Presetsignal(Osc);
Waitsweep(Osc);
[Ref_Xt,Ref_Yt,Ref_Par]=Readsignal(Osc,Mag,PPV);
Ref_Yw=Signalprocess(Ref_Xt,Ref_Yt,Ref_Par,NFFT,FreqNum,FreqMax,Act_Fre
qStep);
```

```
Ref_Yt_INV = Ref_Yt';
Ref_Xt_INV = Ref_Xt';

%%
%Calculate SNR

% s = std(Ref_Yt);
% mean = mean(Ref_Yt);
% SNR = mean/s;


%%
fclose(Osc);
```

F.2 Presetsignal.m

```
function [Mag,PPV,val]=Presetsignal(Osc)
%
%   This program is coded by Rambo Yuan at 1st June 2012 and modified
by
%   Bahareh Zaghari (bz2e11@soton.ac.uk)at 1st August 2012.
%
%%
Lvl=[2e-3 5e-3 1e-2 2e-2 5e-2 0.1 0.2 0.5 1.0 2.0];
str=query(Osc, 'c1:pava? pkpk');%return current parameters .mask test
values
val=regexpi(str,'[UF]','match','once'); % detect the overflow of volt;
%%% NOTE: 'once' is very important here. If the command lacks it, the
%%% return value will be a 'cell' type, otherwise be 'string' type;

if val==''
    val=regexpi(str, '([0-9e.+-]+)','match','once');
else
   % fprintf(Osc, 'c1:vdiv 0.5v\n');   % Set the Volt_Div of c1;
    fprintf(Osc, 'wait');
    str=query(Osc, 'c1:pava? pkpk');
    val=regexpi(str, '([0-9e.+-]+)','match','once');
end

PPV=str2double(val);         % Get the Peak to Peak Volt;
Li=find(8.*Lvl > PPV);       % Find the best volt/div for the signal;
val=Lvl(Li(1));
% str=strcat(['c1:vdiv ' num2str(val) 'v\n']);
% fprintf(Osc, str);
fprintf(Osc, 'wait');
% fprintf(Osc, 'ta:vmag 1\n');

Mag=8*val/PPV;
```

F.3 Presetsignalc1.m

```
function [Mag,PPV,val]=Presetsignalc1(Osc)
%
%   This program is coded by Rambo Yuan at 1st June 2012 and modified
by
%   Bahareh Zaghari (bz2e11@soton.ac.uk)at 1st August 2012.
%
%%
Lvl=[2e-3 5e-3 1e-2 2e-2 5e-2 0.1 0.2 0.5 1.0 2.0];
str=query(Osc, 'c1:pava? pkpk');%return current parameters .mask test
values
val=regexpi(str,'[UF]','match','once'); % detect the overflow of volt;
%%% NOTE: 'once' is very important here. If the command lacks it, the
%%% return value will be a 'cell' type, otherwise be 'string' type;

if val==''
    val=regexpi(str, '([0-9e.+-]+)','match','once');
else
    fprintf(Osc, 'c1:vdiv 0.5v\n');   % Set the Volt_Div of c3;
    fprintf(Osc, 'wait');
    str=query(Osc, 'c1:pava? pkpk');
    val=regexpi(str, '([0-9e.+-]+)','match','once');
end

PPV=str2double(val);         % Get the Peak to Peak Volt;
Li=find(8.*Lvl > PPV);       % Find the best volt/div for the signal;
val=Lvl(Li(1));
str=strcat(['c1:vdiv ' num2str(val) 'v\n']);
fprintf(Osc, str);
fprintf(Osc, 'wait');
fprintf(Osc, 'ta:vmag 1\n');

Mag=8*val/PPV;
```

F.4 Presetsignalc3.m

```
function [Mag,PPV,val]=Presetsignalc3(Osc)
%
%   This program is coded by Rambo Yuan at 1st June 2012 and modified
by
%   Bahareh Zaghari (bz2e11@soton.ac.uk)at 1st August 2012.
%
%%
Lvl=[2e-3 5e-3 1e-2 2e-2 5e-2 0.1 0.2 0.5 1.0 2.0];
str=query(Osc, 'c3:pava? pkpk');%return current parameters .mask test
values
val=regexpi(str,'[UF]','match','once'); % detect the overflow of volt;
%%% NOTE: 'once' is very important here. If the command lacks it, the
%%% return value will be a 'cell' type, otherwise be 'string' type;

if val==''
    val=regexpi(str, '([0-9e.+-]+)','match','once');
else
```

```
%     fprintf(Osc, 'c3:vdiv 1v\n');   % Set the Volt_Div of c3;
    fprintf(Osc, 'wait');
    str=query(Osc, 'c3:pava? pkpk');
    val=regexpi(str, '([0-9e.+-]+)','match','once');
end

PPV=str2double(val);        % Get the Peak to Peak Volt;
Li=find(8.*Lvl > PPV);      % Find the best volt/div for the signal;
val=Lvl(Li(1));
% str=strcat(['c3:vdiv ' num2str(val) 'v\n']);
% fprintf(Osc, str);
fprintf(Osc, 'wait');
%fprintf(Osc, 'ta:vmag 1\n');

Mag=8*val/PPV;
```

F.5 Readsignal.m

```
function [Xtag,Ytag,Par]=Readsignal(Osc,Mag,PPV)
%
%   This program is coded by Rambo Yuan at 1st June 2012 and modified
by
%   Bahareh Zaghari (bz2e11@soton.ac.uk)at 1st August 2012.
%
%%
Mag_Coef=0.85;
Tag='ta:';

% Magnify the tag to best resolution;
str=strcat(['ta:vmag ' num2str(Mag*Mag_Coef)]);
fprintf(Osc, str);
fprintf(Osc, 'wait');

% Read the parameter of Tag;
Cmd={'insp? ''last_valid_pnt''';
    'insp? ''vertical_gain''';
    'insp? ''vertical_offset''';
    'insp? ''horiz_interval''';
    'insp? ''horiz_offset'''};
Par=zeros(5,1);
% Par(1): Num of points for the waveform;
% Par(2): Vertical gain;
% Par(3): Vertical offset;
% Par(4): Horiz interval, also the sampling period time (Ts);
% Par(5): Horiz offset, the time delay from the trigger to the first
point;

for i=1:5
    str=char(strcat(Tag,Cmd(i)));
    str=query(Osc, str);
    str=regexpi(str, ':\s+([0-9e.+-]+)\s+"','tokens','once');
    if strcmp(str,'')
        disp('Warning: (Readsignal) Failure to obtain a parmeter!');
    end
    Par(i)=str2double(str);
```

```
end

% Check the Buffersize and set the loading number of points;
if Par(1)*4>get(Osc, 'InputBufferSize')
    disp('Warning: (Readsignal) The waveform data have overflow the
BufferSize!');
    fclose(Osc);
    return;
end
str=strcat('wfsu sp,0,np,',num2str(Par(1)),',fp,0,sn,0');
fprintf(Osc,str);           % waveform_setup;
disp(strcat('Num of Pnts for Signal:', num2str(Par(1))));

% Read the Tag's waveform data;
str=strcat(Tag,'wf? dat1');
data = query(Osc, str);
% data2 = fgets(Osc); % If the data is overflow the Buffersize;

% Transfer the Hex words to floats;
Ytag=zeros(1,Par(1));
for i=1:Par(1)
    t=hex2dec(data(4*(i-1)+1 : 4*i));
    if t>32767; t=t-65536; end
    Ytag(i)=t;
end
Ytag=Ytag.*Par(2)-Par(3);
Xtag=(1:Par(1)).*Par(4)+Par(5);

%%% Check the Pk 2 Pk Value;
P2P=max(Ytag)-min(Ytag);

if abs(P2P-PPV)/PPV > 0.05
    disp('Warning: (Readsignal) Tolerance is exceeded during reading
the waveform!')
end

% Plot the input waveform;
figure(1);
subplot(2,2,1:2);
grid on;
box on;
hold on;
plot(Xtag,Ytag,'Linewidth',2);

xlabel('Time delay from trigger (s)');
ylabel('Amplitude (V)');
```

F.6 Readsignalc3.m

```
function [Xtag,Ytag,Par]=Readsignalc3(Osc,Mag,PPV)
%
%   This program is coded by Rambo Yuan at 1st June 2012 and modified
by
%   Bahareh Zaghari (bz2e11@soton.ac.uk)at 1st August 2012.
```

```
%
%%
Mag_Coef=0.95;
Tag='tb:';

% Magnify the tag to best resolution;
str=strcat(['tb:vmag ' num2str(Mag*Mag_Coef)]);
fprintf(Osc, str);
fprintf(Osc, 'wait');

% Read the parameter of Tag;
Cmd={'insp? ''last_valid_pnt''';
    'insp? ''vertical_gain''';
    'insp? ''vertical_offset''';
    'insp? ''horiz_interval''';
    'insp? ''horiz_offset'''};
Par=zeros(5,1);
% Par(1): Num of points for the waveform;
% Par(2): Vertical gain;
% Par(3): Vertical offset;
% Par(4): Horiz interval, also the sampling period time (Ts);
% Par(5): Horiz offset, the time delay from the trigger to the first
point;

for i=1:5
    str=char(strcat(Tag,Cmd(i)));
    str=query(Osc, str);
    str=regexpi(str, ':\s+([0-9e.+-]+)\s+"','tokens','once');
    if strcmp(str,'')
        disp('Warning: (Readsignal) Failure to obtain a parmeter!');
    end
    Par(i)=str2double(str);
end

% Check the Buffersize and set the loading number of points;
if Par(1)*4>get(Osc, 'InputBufferSize')
    disp('Warning: (Readsignal) The waveform data have overflow the
BufferSize!');
    fclose(Osc);
    return;
end
str=strcat('wfsu sp,0,np,',num2str(Par(1)),',fp,0,sn,0');
fprintf(Osc,str);           % waveform_setup;
disp(strcat('Num of Pnts for Signal:', num2str(Par(1))));

% Read the Tag's waveform data;
str=strcat(Tag,'wf? dat1');
data = query(Osc, str);
% data2 = fgets(Osc); % If the data is overflow the Buffersize;

% Transfer the Hex words to floats;
Ytag=zeros(1,Par(1));
for i=1:Par(1)
    t=hex2dec(data(4*(i-1)+1 : 4*i));
    if t>32767; t=t-65536; end
    Ytag(i)=t;
```

```
end
Ytag=Ytag.*Par(2)-Par(3);
Xtag=(1:Par(1)).*Par(4)+Par(5);

%%% Check the Pk 2 Pk Value;
P2P=max(Ytag)-min(Ytag);

if abs(P2P-PPV)/PPV > 0.05
    disp('Warning: (Readsignal) Tolerance is exceeded during reading
the waveform!')
end

% Plot the input waveform;
figure(1);
hold on;
subplot(subplot(2,2,3:4));
grid on;
box on;
hold on;
plot(Xtag,Ytag,'Linewidth',2);

xlabel('Time delay from trigger (s)');
ylabel('Amplitude (V)');
```

F.7 Signalprocess.m

```
function
[YwOut]=Signalprocess(Xt,Yt,Par,NFFT,FreqNum,FreqMax,Act_FreqStep)
%
%   This program is coded by Rambo Yuan at 1st June 2012 and modified
by
%   Bahareh Zaghari (bz2e11@soton.ac.uk)at 1st August 2012.
%
%%
%%%% Explan Par:
% Par(1): Num of points for the signal;
% Par(2): Vertical gain;
% Par(3): Vertical offset;
% Par(4): Horiz interval, also the sampling period time (Ts);
% Par(5): Horiz offset, the time delay from the trigger to the first
point;

% Clear the Volt offset of the signal;
% PartYt=Yt(Xt>3.5e-4);
AvgY=mean(Yt);
Yt=Yt-AvgY;

% Add a tukey window on the signal to prevent Spectrum Leakage;
Trst_Pnts=500;      % Transition points of the window from 0 to 1;
NumSig=Par(1);       % Num of points for the signal;
TkWin=tukeywin(NumSig,2*Trst_Pnts/NumSig)';
Yt=Yt.*TkWin;

% Discrete Fast Fourier Transform;
```

```
Fs=1./Par(4);
Sw = fft(Yt,NFFT)/NumSig;
Yw=2*abs(Sw(1:NFFT/2+1));      % Single-sided amplitude spectrum
Fr = Fs/2*linspace(0,1,NFFT/2+1);

% Check the Act_FreqStep is same with current Frequency interval;
if (Fr(2)-Fr(1)-Act_FreqStep)/Act_FreqStep > 0.01
    disp('Warning: (SignalProcess) Frequency Step is not correct!');
end;

% Check whether there is a Spectrum Leakage to higher frequency band;
SumAmpl=sum(Yw);
HighBand=sum(Yw(Fr > FreqMax));
if HighBand > 0.05*SumAmpl
    disp('Warning: (SignalProcess) Significant Spectrum Leakage
happened!');
end

% Output the result for desired frequency range;
YwOut=Yw(1:FreqNum);
% Plot single-sided amplitude spectrum.
figure(2);

hold on;
box on;
plot(Fr,Yw,'Linewidth',2);
xlabel('Frequency (Hz)');
ylabel('Amplitude |Y(f)|');
xlim([0 FreqMax]);
```

F.8 Waitsweep.m

```
function [Chk]=Waitsweep(Osc)
%
%   This program is coded by Rambo Yuan at 1st June 2012 and modified
by
%   Bahareh Zaghari (bz2e11@soton.ac.uk)at 1st August 2012.
%
%%
query(Osc, 'inr?');     % clear the internal state register;
Chk=0;
Quant=quantizer([16 0]); % used for Waitsweep();
tic;
fprintf(Osc, 'clsw');
flag=1;
while flag
    str=query(Osc, 'inr?');
    str=regexpi(str, '([0-9]+)','match','once');
    tt=str2double(str);
    str=num2bin(Quant,tt);
    t=toc;
    if str(8)=='1'|| t>80;  flag=0;  end;
end
```

```
toc;
if str(8)~='1'
    Chk=1;
    disp('Warning: (Waitsweep) Wait terminated while sweep have not
finished!');
end;
```

F.9 Waitsweepc3.m

```
function [Chk]=Waitsweepc3(Osc)
%
%   This program is coded by Rambo Yuan at 1st June 2012 and modified
by
%   Bahareh Zaghari (bz2e11@soton.ac.uk)at 1st August 2012.
%
%%
query(Osc, 'inr?');     % clear the internal state register;
Chk=0;
Quant=quantizer([16 0]); % used for Waitsweep();
tic;
fprintf(Osc, 'clsw');
flag=1;
while flag
    str=query(Osc, 'inr?');
    str=regexpi(str, '([0-9]+)','match','once');
    tt=str2double(str);
    str=num2bin(Quant,tt);
    t=toc;
    if str(9)=='1'|| t>80;  flag=0;  end;
end
toc;
if str(9)~='1'
    Chk=1;
    disp('Warning: (Waitsweep) Wait terminated while sweep have not
finished!');
end;
```